Derivation and numerical solution of fully nonlinear and fully dispersive water wave model equations

Daulet Moldabayev

Thesis for the degree of philosophiae doctor (PhD)
at the University of Bergen

2017

Date of defence: 09.06.2017

Preface

This dissertation is submitted as a partial fulfillment of the requirements for the degree Doctor of Philosophy (PhD) at the Department of Mathematics, University of Bergen. The research was supported by the Research Council of Norway on grant no. 213474/F20 for the project "Nonlinear PDE in Spaces of Analytic Functions". The doctoral study was supervised by Prof. Henrik Kalisch.

The evaluation committee has consisted of Guttorm Alendal (University of Bergen, Bergen, Norway), Dmitry Pelinovsky (McMaster University, Hamilton, Ontario, Canada) and Angel Durán (Universidad de Valladolid, Valladolid, Spain).

This dissertation pursues several aims. The first one is to contribute to the understanding of implicit details in derivation of nonlinear dispersive water wave models. The main focus is on the Hamiltonian theory for the surface water wave problem. The second is to research the nature of solutions to model equations. Numerical investigation of the relations between different bifurcation curves and travelling-wave solutions confirms some established theoretical knowledge and puts forward evidences that are not fully understood analytically. The third aim is to present a method for numerical solution of water wave equations. This method, being relatively simple in implementation, allows to circumvent the problem of turning points on bifurcation curves and also to compute travelling-wave solutions that satisfy certain conditions such as waves having troughs at zero level.

Acknowledgements

First of all I would like to thank Henrik Kalisch and Magnus Svärd who carried out the selection process of candidates for the PhD position. I am sincerely thankful to Professor Henrik Kalisch, my main supervisor, for sharing knowledge and guiding me, for his enthusiasm, support and encouragement. The thesis would not have been possible without you.

In the course of the doctorate studies, I have had fruitful collaboration with Olivier Verdier, Evgueni Dinvay, Denys Dutykh, Ben Segal and others. I would like to thank them for productive discussions, advices on research questions and some inspiring ideas we came up with.

As a PhD Candidate I have been lucky to meet my colleagues and fellow students at the Department of Mathematics. They have always provided a friendly and supportive environment. I appreciate everything we have experienced during the time of our studies. I am also thankful to the administration of the department for supporting me along the way.

I would like to express my gratitude to my family for their continuous support and encouragement over the years of my studies. I am also thankful for all of my teachers and professors from schools and universities I studied at.

I am heartily grateful for my wife Assem. Your love, support and understanding are the source of my strength and motivation.

Outline

This thesis is organized in the following way. Part I contains general theoretical background on nonlinear dispersive water wave models, their derivation and description of methods used to solve the equations involved. Some properties of solutions to the equations and a summary of research results are also given in the first part. Part 2 consists of the research papers that present scientific results in detail.

List of research papers included in Part II

Paper A:
Moldabayev, D., Kalisch, H., Dutykh, D.: *The Whitham equation as a model for surface water waves*, Phys. D: Nonlinear phenomena, **309**, pp. 99–107 (2015), http://dx.doi.org/10.1016/j.physd.2015.07.010.

Paper B:
Dinvay, E., Moldabayev, D., Dutykh, D., Kalisch, H.: *The Whitham equation with surface tension*, Nonlinear Dynamics, **88**, No. 2, pp.1125–1138, (2017), http://dx.doi.org/10.1007/s11071-016-3299-7.

Paper C:
Kalisch, H., Moldabayev, D., Verdier, O.: *A numerical study of nonlinear dispersive wave models with SpecTraVVave*, Electronic Journal of Differential Equations, **2017**, No. 62, pp. 1–23 (2017), http://ejde.math.txstate.edu

Paper D:
Benjamin Segal, Daulet Moldabayev, Henrik Kalisch, Bernard Deconinck: *Explicit solutions for a long-wave model with constant vorticity*, accepted for publication in the European Journal of Mechanics - B/Fluids.

Contents

Part I

General background

Introduction

The water wave theory is a classical part of Fluid Mechanics. It has a long scientific history with a great number of mathematical results [10, 32]. The first studies in this field were done by Stokes in 1847 [34]. He developed some approximations to periodic waves and proposed conjectures about their behavior on deep water. Today these waves are known as Stokes waves.

The problem of water waves concerns the two-dimensional flow of an inviscid, incompressible fluid, bounded above by a free surface and below by a rigid horizontal bottom. In this situation, the flow is described by Euler equations with appropriate boundary conditions [13]. By solving these equations, one obtains a complete understanding of the flow dynamics. However, for some applications the dynamics of the free surface is of particular interest. Nonlinear dispersive wave equations, such as the Korteweg–de Vries equation [22], allow to approximate the description of the free surface evolution without having to provide a complete solution of the fluid flow below the surface. Different questions related to these equations are actively researched. The existence of traveling and solitary waves solutions [15], well posedness of these equations [21, 24, 25] are two examples.

In this work, nonlinear dispersive water wave equations are analyzed from a number of points: their accuracy in approximating the solutions of Euler equations, derivation from Hamiltonian formulation of the water wave problem, numerical solution of these equations, stability of their solutions and investigation of their bifurcation curves.

The Part I of this thesis consists of three chapters. Chapter 1 is devoted to mathematical formulation of the surface water-wave problem. We revise the Eulerian formulation of the problem, the Linear water-wave theory and the boundary conditions applied. The second chapter describes a method for deriving nonlinear dispersive water-wave equations. The main focus here is on the Hamiltonian formulation of the problem and different scaling regimes. A numerical method for solving the water-wave equations is also presented in Chapter 2. Chapter 3 gives a brief summary of the research results obtained in the course of the doctoral studies. Part II contains the research papers, published and submitted for publication, which were written for this PhD project.

Chapter 1

Theory on the problem of surface water waves

1.1 Euler equations

The mathematical description of the surface water wave problem begins with analyzing Navier-Stokes equations

$$\frac{D\overrightarrow{U}}{Dt} = \frac{\partial \overrightarrow{U}}{\partial t} + (\overrightarrow{U} \cdot \nabla)\overrightarrow{U} = -\frac{1}{\rho}\nabla P + \overrightarrow{g} + \nu \nabla^2 \overrightarrow{U}. \tag{1.1}$$

where $\overrightarrow{U}$ is the velocity field, ρ is the density, $\overrightarrow{g}$ acceleration due to gravity, P is the fluid pressure and ν denotes the kinematic viscosity. It should be noted that the fluid is density ρ is assumed to be constant. The law of mass conservation enables one to derive the continuity equation

$$\frac{D\rho}{Dt} + \rho \nabla \cdot \overrightarrow{U} = 0, \qquad \xrightarrow{\rho=\text{const.}} \qquad \nabla \cdot \overrightarrow{U} = 0, \tag{1.2}$$

the latter is often addressed to as incompressibility condition [13]. Rotation of the fluid flow is modelled by taking curl of the velocity field

$$\nabla \times \overrightarrow{U} = \overrightarrow{\Omega}. \tag{1.3}$$

The parameter $\overrightarrow{\Omega}$ is called vorticity. In this setting, absence of vorticity, i.e. $\overrightarrow{\Omega} = 0$, means that there is no rotation, and the flow is called irrotational.

Close observation of the equations governing the fluid flow show that in the case of incompressible and inviscid ($\nu = 0$) fluid, the vorticity does not change in time. If one takes the curl of equations (1.1), given listed assumptions and that $\nabla \times \nabla P = 0$, then it is possible to find that $\frac{D\overrightarrow{\Omega}}{Dt} = 0$. Hence, the initial fluid rotation is preserved without changes in the course of the flow.

The Euler equations appear in case of inviscid fluid flow as a simplified version of the Navier-Stokes equations (1.1). Conditions on boundaries of the flow domain give additional equations that constitute the Euler system for surface water wave problem [23]. The system is derived as follows.

We consider an open rectangular channel with flat bottom. The bottom is placed along the x-axis at the level $z = -h_0$, with z being the vertical axis. Waves propagate in the x-direction. The fluid surface is described by the relation $z = \eta(x, t)$. Figure

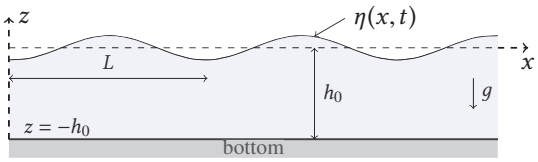

Figure 1.1: The domain of the fluid flow: longitudinal cross-section of a rectangular channel, η is the free surface, L is the wavelength, h_0 is the undisturbed depth, g is the gravity.

1.1 describes the geometric setup of the flow domain. It is assumed that there is no variation in along the y-axis and the that channel infinitely long. Hence, the domain can be expressed as $\mathcal{D}(t) = \{(x,z) \in R^2 \mid x \in R,\ -h0 \le z \le \eta(x,t),\}$.

If we denote the components of the velocity field as $\overrightarrow{U} = (U,V,W)$, then the Euler equations are written as

$$\begin{aligned} U_t + UU_x + WU_z &= -\frac{P_x}{\rho}, \\ W_t + UW_x + WW_z &= \frac{P_z}{\rho} - g, \end{aligned} \tag{1.4}$$

and the relation (1.2) has the form

$$U_x + W_z = 0. \tag{1.5}$$

It is assumed that the fluid vorticity is equal to the constant Ω_0, and the relation (1.3) reads

$$W_x - U_z = -\Omega_0. \tag{1.6}$$

If we assume that the flow is irrotational, i.e. $\Omega_0 = 0$, then we can express the relation (1.3) as $\nabla \times (\nabla\phi) = 0$. The function ϕ is called the velocity potential and $\nabla\phi = (U,W)^T$. For the velocity potential ϕ, the incompressibility condition (1.5) results in the Laplace equation

$$\phi_{xx} + \phi_{zz} = 0 \quad \text{in } -h_0 < z < \eta(x,t). \tag{1.7}$$

By integrating the Euler equations (1.4) with the condition $\Omega_0 = 0$ in (1.6), one arrives to the Bernoulli equation

$$\phi_t + \frac{1}{2}(\phi_x^2 + \phi_z^2) + \frac{P}{\rho} + gz = C(t) + \mathcal{C}. \tag{1.8}$$

The variable $C(t)$ can be eliminated by defining a new velocity potential

$$\Phi = \phi - \int_0^t C(s)ds.$$

Now we focus our attention on the bottom and the free surface boundary conditions. These conditions are natural to such a problem setup. It is required that the fluid cannot penetrate the bottom. This condition written as

$$\phi_{zz} = 0 \quad \text{on } z = -h_0. \tag{1.9}$$

It is also required that fluid particles cannot leave the free surface. This is the kinematic condition (1.10). The pressure at the free surface has to be equal to the atmospheric pressure if the surface tension is neglected. This is called the dynamic and is derived from the Bernoulli equation in the form written in (1.11).

$$\eta_t + \phi_x \eta_x - \phi_z = 0 \quad \text{on } z = \eta(x,t) \tag{1.10}$$

$$\phi_t + \frac{1}{2}\left(\phi_x^2 + \phi_z^2\right) + \eta = 0 \quad \text{on } z = \eta(x,t). \tag{1.11}$$

The atmospheric pressure is assumed to be zero, since it is very small in comparison with the fluid pressure.

Above we have assumed that the flow was irrotational. If we consider that the flow is rotational, i.e. $\Omega_0 \neq 0$, the water wave problem is expressed in terms of the stream-function ψ. The stream-functions defines the velocity field as $(U,W) = (\psi_z, -\psi_x)$. To this end, the equation (1.6) implies that

$$\Delta\psi = \Omega_0. \tag{1.12}$$

For this case, we also assume that the flow is steady and the velocity field not dependent on time. This simplifies the Euler equations (1.4) - the time derivatives there can be removed. The Bernoulli equation for this case is written as

$$\frac{1}{2}(\psi_x^2 + \psi_z^2) + \frac{P}{\rho} + gz = \mathcal{Y}(\psi), \tag{1.13}$$

where $\mathcal{Y}(\psi)$ is constant along streamlines. In analogy with the equation (1.7), the the stream-function satisfies the Laplace equation:

$$\psi_{xx} + \psi_{zz} = \Omega_0 \quad \text{in } -h_0 < z < \eta(x). \tag{1.14}$$

The condition at the bottom reads

$$\psi_{zz} = 0 \quad \text{on } z = -h_0, \tag{1.15}$$

and at the free surface:

$$\psi_z \eta_x + \psi_x = 0 \quad \text{on } z = \eta(x), \tag{1.16}$$

$$\frac{1}{2}(\psi_x^2 + \psi_z^2) + gz = \Gamma \quad \text{on } z = \eta(x), \tag{1.17}$$

where $\Gamma = \mathcal{Y}(\psi)|_{z=\eta}$ is constant.

1.2 Linear theory

Let us review the parameters that describe the fluid flow in the surface water wave problem. In Figure 1.1, the surface elevation is represented by $\eta(x,t)$, the wavelength L defines the distance between two successive troughs. The wave amplitude is denoted by a, which may be defined as the distance from the zero level $z = 0$ to the wave crest. The phase speed c is defined as

$$c = \frac{L}{T}, \tag{1.18}$$

where the parameter T denotes the wave period. The free surface $\eta(x,t)$ can be represented in terms of a cosine function:

$$\eta(x,t) = a\cos(kx - \omega t), \tag{1.19}$$

with $k = 2\pi/L$ and $\omega = 2\pi/T$ being the wavenumber and the radian frequency. To this end, the wavespeed c can also be written as

$$c = \frac{\omega}{k}. \tag{1.20}$$

The linear water wave theory is a special case of the theory described in section 1.1. We assume that the flow is irrotational and the relation a/L is small. This results in the fact that the velocity field components become small and the nonlinear terms in the Euler equations can be neglected [23]. In this setting, the free surface is described by $z = 0$ and not by $z = \eta$. Thus the linear water wave problem may be written as follows:

$$\phi_{xx} + \phi_{zz} = 0 \quad \text{in } -h_0 < z < 0, \tag{1.21}$$
$$\phi_z = 0 \quad \text{on } z = -h_0, \tag{1.22}$$
$$\phi_z = \eta_t \quad \text{on } z = 0, \tag{1.23}$$
$$\phi_t = -g\eta \quad \text{on } z = 0. \tag{1.24}$$

The solution to this system is derived by combining (1.19) and the the kinematic boundary conditions (1.22)-(1.23), and written as

$$\begin{aligned} \eta(x,t) &= a\cos(kx - \omega t), \\ \phi &= \frac{a\omega}{k}\frac{\cosh(k(z+h_0))}{\sinh(kh_0)}\sin(kx - \omega t). \end{aligned} \tag{1.25}$$

Using ϕ, we find the velocity field components:

$$\begin{aligned} U = \phi_x &= a\omega\frac{\cosh(k(z+h_0))}{\sinh(kh_0)}\cos(kx - \omega t), \\ W = \phi_z &= a\omega\frac{\sinh(k(z+h_0))}{\sinh(kh_0)}\sin(kx - \omega t). \end{aligned}$$

In the linear theory, the dispersion relation is the relation $\omega = \omega(k)$. It characterizes the dependency between the wavelength L, wavespeed c and wavenumber k. For the problem decribed in (1.21)-(1.24), the dispersion relation is written as

$$\omega = \sqrt{gk\tanh(kh_0)}, \tag{1.26}$$

hence, the wavespeed reads:

$$c = \frac{\omega}{k} = \sqrt{\frac{g}{2\pi}L\tanh(kh_0)}. \tag{1.27}$$

It can be noted that the wavespeed is a function of wavelength. Therefore the linear surface wave problem is a dispersive model, since waves of different wavelengths propagate with different speeds.

To obtain a full picture of the problem, one may derive the pressure P using the Bernoulli equation and the dispersion relation (1.26):

$$P = -\rho g z + \rho g a \frac{\cosh(k(z+h_0))}{\cosh(kh_0)} \cos(kx - \omega t). \tag{1.28}$$

The linear theory enables one to find the streamlines and particles paths as well.

In the case when the fluid depth is much smaller than the wavelength the dispersion relation for the linear theory (1.26) reduces to

$$\omega = \sqrt{g h_0 k^2}, \tag{1.29}$$

and the wavespeed becomes a constant $c = c_0$, where $c_0 = \sqrt{g h_0}$. This is due to the fact that in long-wave approximation, i.e. $h0/L << 1$, $\tanh(kh_0) \to kh_0$.

This case is addressed to as Shallow-water theory. It is also assumed that the flow is uniform and the vertical velocity is zero. Thus, for the problem domain illustrated in Figure 1.1, if we denote uniform horizontal velocity by $u(x,t)$, Euler equations (1.4) become

$$u_t + u u_x = \frac{P_x}{\rho}, 0 \quad = \frac{-P_z}{\rho} - g, \tag{1.30}$$

where all terms with vertical velocity W are disregarded.

Chapter 2

Derivation of water wave equations and their numerical solution

2.1 Hamiltonian theory

From the previous chapter we know that the surface water wave problem is described by the Euler equations with appropriate boundary conditions at the bottom and at the free surface. There are also some of model equations that describe only the dynamics of the free surface. This is of advantage in the cases when the solution of the flow below the surface is not of interest. In a general form, these models are written as

$$\eta_t + [f(\eta)]_x + \mathcal{L}\eta_x = 0, \tag{2.1}$$

where $\eta(x,t)$ is surface elevation, $\mathcal{L}$ is a self-adjoint operator, and f is a real-valued nonlinear function. Such equations are derived in an inconsistent way in the fluid mechanics for wave problems. For example, the derivation of the Whitham equation, introduced by Whitham in [36], is also somewhat ad-hoc. In nondimensional form the Whitham equation is written as

$$\eta_t + \frac{3}{2}\eta\eta_x + K\eta_x = 0, \qquad \widehat{K\eta}(k) = \sqrt{\frac{\tanh(k)}{k}}, \tag{2.2}$$

where the operation $\widehat{\cdot}$ stands for taking the Fourier transform. This section briefly describes the Hamiltonian formulation of surface water wave problem and derivation of model equations from Hamiltonian function under different scaling regimes. For simplicity, we will consider the case where surface tension is disregarded.

By taking the depth h_0 as a unit of distance, and the parameter $\sqrt{h_0/g}$ as a unit of time, we can write the water wave problem in nondimensional form:

$$\begin{aligned} \phi_{xx} + \phi_{zz} &= 0 \quad \text{in } -1 < z < \eta(x,t), \\ \phi_{zz} &= 0 \quad \text{on } z = -1, \\ \left.\begin{aligned} \eta_t + \phi_x\eta_x - \phi_z &= 0 \\ \phi_t + \tfrac{1}{2}\left(\phi_x^2 + \phi_z^2\right) + \eta &= 0 \end{aligned}\right\} &\text{on } z = \eta(x,t). \end{aligned} \tag{2.3}$$

where $\phi(x,z,t)$ is the velocity potential and $\eta(x,t)$ describes the surface elevation. The assumptions on flow properties are the same as in section 1.1 and the domain for problem is $\{(x,z) \in R^2 \mid x \in R,\ -1 < z < \eta(x,t)\}$.

The total energy of the system (2.3) is the sum of kinetic energy and potential energy. The potential energy must be zero if there is no wave motion at the surface. To this end, the Hamiltonian function for the problem can be written as

$$H = \int_{\mathbb{R}} \int_0^{\eta} z \, dz dx + \int_{\mathbb{R}} \int_{-1}^{\eta} \frac{1}{2} |\nabla \phi|^2 \, dz dx. \tag{2.4}$$

Analysis described in [9, 32, 37] provides us with the following representation of the Hamiltonian function:

$$H = \frac{1}{2} \int_{\mathbb{R}} \left[\eta^2 + \Phi G(\eta) \Phi \right] dx, \tag{2.5}$$

where $\Phi(x,t) = \phi(x, \eta(x,t), t)$ and $G(\eta)$ is a Dirichlet-Neumann operator such that

$$G(\eta)\Phi = \sum_{j=0}^{\infty} G_j(\eta)\Phi,$$

as described in [30]. In this case the terms $G_0(\eta)$ and $G_1(\eta)$ are written as

$$G_0(\eta) = D\tanh(D) \quad \text{and} \quad G_1(\eta) = D\eta D - D\tanh(D)\eta D\tanh(D),$$

with the operator $D = -i\partial_x$. The analysis is to linear terms in η, hence, the terms $G_j(\eta)$, $j \geq 2$ are not be considered further. We introduce the operator $\mathcal{K}(\eta)$ such that

$$G(\eta) = D\mathcal{K}(\eta)D,$$

and the expansion

$$\mathcal{K}(\eta) = \sum_{j=0}^{\infty} \mathcal{K}_j(\eta), \qquad \mathcal{K}_j(\eta) = D^{-1} G_j(\eta) D^{-1}$$

is valid around zero. One should notice that $\mathcal{K}_0 = \frac{\tanh D}{D}$, $\mathcal{K}_1 = \eta - \tanh D(\eta \tanh D)$. In such terms, the Hamiltonian (2.5) can be expressed as

$$H = \frac{1}{2} \int_{\mathbb{R}} \left[\eta^2 + u\mathcal{K}(\eta)u \right] dx, \tag{2.6}$$

where $u = \Phi_x$ is the dependent variable. Then the water wave problem can be represented as the Hamiltonian system

$$\eta_t = -\partial_x \frac{\delta H}{\delta u}, \qquad u_t = -\partial_x \frac{\delta H}{\delta \eta}.$$

This system has a symmetric structure map $J_{\eta,u}$:

$$J_{\eta,u} = \begin{pmatrix} 0 & -\partial_x \\ -\partial_x & 0 \end{pmatrix}. \tag{2.7}$$

Further, we consider the wave problem with characteristic nondimensional wavelength λ and a characteristic nondimensional amplitude α. Different approximations in the this problem are obtained by considering the amplitude α to be a function of wave

number $\mu = 1/\lambda$. Different scaling regimes are defined by the behavior of $\alpha = \alpha(\mu)$ at small μ. In the long-wave approximation $\eta = O(\alpha)$, $u = O(\alpha)$ and $D = -i\partial x = O(\mu)$.

Under different scaling regimes, one can take approximations of the operator $\mathcal{K}$ in Hamiltonian function (2.6). This leads to derivation of systems that approximate (2.3). For example, the Whitham system is written as follows:

$$\eta_t = -\partial_x \frac{\delta H}{\delta u} = -\frac{\tanh D}{D} u_x - (\eta u)_x + O(\mu^3\alpha^2), \tag{2.8}$$

$$u_t = -\partial_x \frac{\delta H}{\delta \eta} = -\eta_x - u u_x + O(\mu^3\alpha^2). \tag{2.9}$$

These systems describe water waves that propagate in both directions - right and left. It is possible to separate the right-going and left-going parts of the waves and obtain single equations dedicated to each one of them. We will demonstrate the argument taking the Whitham system as an example.

Consider linearized version of (2.8)-(2.9):

$$\eta_t + \frac{\tanh D}{D} u_x = 0, \tag{2.10}$$

$$u_t + \eta_x = 0. \tag{2.11}$$

Taking solutions of this system in the form

$$\eta(x,t) = Ae^{i\xi x - i\omega t}, \qquad u(x,t) = Be^{i\xi x - i\omega t}$$

prompts the matrix equation

$$\begin{pmatrix} -\omega & \tanh\xi \\ \xi & -\omega \end{pmatrix} \begin{pmatrix} A \\ B \end{pmatrix} = \begin{pmatrix} 0 \\ 0 \end{pmatrix}.$$

For the latter equation to have a nontrivial solution, the determinant of the matrix must be equal to zero: $\omega^2 - \xi \tanh\xi = 0$. Defining the wavespeed as $c = \omega(\xi)/\xi$ one obtains the dispersion relation for the Whitham equation:

$$c^2(\xi) = \frac{\tanh\xi}{\xi} \quad \Longrightarrow \quad c(\xi) = \pm\sqrt{\frac{\tanh\xi}{\xi}}.$$

Positive wavespeed $c > 0$ corresponds to right-going solutions the system (2.10)-(2.11), left-going solutions have $c < 0$.

The transformation of variables allows us to separate these solutions:

$$r = \frac{1}{2}(\eta + Ku), \qquad s = \frac{1}{2}(\eta - Ku), \tag{2.12}$$

where K is an invertible function of the operator D that is chosen specifically for different model equations. However, the possibility to find suitable K that r and s is not guaranteed. The original functions are represented as

$$\eta = r + s, \qquad u = K^{-1}(r - s). \tag{2.13}$$

In terms of r and s Hamiltonian system (2.1) takes the form

$$r_t = -\partial_x \left(\frac{K}{2} \frac{\delta H}{\delta r} \right), \tag{2.14}$$

$$s_t = \partial_x \left(\frac{K}{2} \frac{\delta H}{\delta s} \right). \tag{2.15}$$

The shallow-water scaling regime can be obtained by taking $\alpha = O(1)$ and $\mu \to 0$. If we assume that left-going waves can be discarded $s = o(1)$, the equation (2.14) leads to the shallow- water equation

$$r_t + \frac{3}{2} r r_x + r_x = o(\mu).$$

If we let $\alpha = O(\mu^2)$, $\mu \to 0$ and $s = o(\mu^2)$, we obtain the Boussinesq scaling regime, which allows us to derive the KdV equation

$$r_t + r_x + \frac{3}{2} r r_x - \frac{1}{6} r_{xxx} = o(\mu^5).$$

2.2 Numerical method for solving nonlinear dispersive water wave equations

This sections describes a numerical method, which is designed to compute traveling-wave solutions for water wave equations of a general form

$$\eta_t + [f(\eta)]_x + \mathcal{L}\eta_x = 0,$$

where $\mathcal{L}$ is a self-adjoint operator, and f is a real-valued function. For example, for the KdV equation $\mathcal{L} = I + \frac{1}{6}\partial_x^2$ and $f(\eta) = \frac{3}{4}\eta^2$. The operator $\mathcal{L}$ is considered to be a Fourier multiplier operator

$$\widehat{\mathcal{L}\eta}(k) = \gamma(k)\widehat{\eta}(k).$$

In case of the Whitham equation, $\mathcal{L}$ is given by convolution with the integral kernel K_{h_0} in the form

$$\mathcal{L}\eta(x) = \int_{-\infty}^{\infty} K_{h_0}(y)\eta(x-y)\,\mathrm{d}y, \qquad \widehat{K_{h_0}}(k) = \gamma(k) = \sqrt{\frac{g\tanh(h_0 k)}{k}}. \tag{2.16}$$

The theory of Stokes waves lies basis of the current method.

2.2.1 Cosine collocation method

The traveling-wave solutions to the equation (2.2) are found in the following form:

$$\eta(x,t) = \phi(x - ct).$$

The equation then becomes integrable

$$\phi' + [f(\phi)]' + \mathcal{L}\phi' = 0, \tag{2.17}$$

$$-c\phi + f(\phi) + \mathcal{L}\phi = B, \tag{2.18}$$

where B is a constant of integration.

We assume that $f \in C^2(R)$, $f(0) = 0$ and $f'(0) = 0$. The method is designed for computing even periodic traveling-wave solutions. In some cases, it can be proved that solutions of (2.18) are be even, but in general case it is not known [6]. This assumption helps to make the numerical method applicable to many equations without special configuration. This also enables us to use cosine collocation method and reduce the number of unknowns by 2 – only one-half of the solutions needs to be computed, the other half is constructed by symmetry.

We project the equation (2.18) on a subspace of $L^2(0, 2\pi)$, namely on

$$\mathcal{S}_N = \operatorname{span}_{\mathbb{R}}\{\cos(lx) \mid 0 \le l \le N-1\}. \tag{2.19}$$

The collocation points $x_n = \pi\frac{2n-1}{2N}$, $n = 1, \dots, N$ discretize the domain. If the full wavelength of solutions is $L \neq 2\pi$, the x-variable is scaled:

$$x' = \frac{L}{2\pi}x,$$

and new collocation points x'_n and wavenumbers κ_l given by

$$x'_n = \frac{L}{2}\frac{2n-1}{2N}, \qquad \kappa_l = \frac{2\pi}{L}l.$$

Our aim is to find a function $\phi_N \in \mathcal{S}_N$ satisfying the equations

$$-c\phi_N(x'_n) + f(\phi_N)(x'_n) + \mathcal{L}^N\phi_N(x'_n) = 0, \tag{2.20}$$

at collocation points x'_n. The function ϕ_N is the discrete version of ϕ:

$$\phi_N(x') = \sum_{l=0}^{N-1} \omega(\kappa_l)\Phi_N(\kappa_l)\cos(\kappa_l x'),$$

$$\omega(\kappa_l) = \begin{cases} \sqrt{1/N}, & \kappa_l = 0, \\ \sqrt{2/N}, & \kappa_l > 0, \end{cases}$$

$$\Phi_N(\kappa_l) = \omega(\kappa_l)\sum_{n=1}^{N} \phi_N(x'_n)\cos(\kappa_l x'_n),$$

where $\kappa_l = 0, \frac{2\pi}{L}, \dots, \frac{2\pi}{L}(N-1)$. The values $\Phi_N(\cdot)$ are the discrete cosine coefficients. The term $\mathcal{L}^N\phi_N$ is evaluated using the matrix $\mathcal{L}^N(i,j)$ given as

$$\mathcal{L}^N\phi_N(x'_i) = \sum_{j=1}^{N} \mathcal{L}^N(i,j)\phi_N(x'_j),$$

$$\mathcal{L}^N(i,j) = \sum_{l=0}^{N-1} \omega^2(\kappa_l)\gamma(\kappa_l)\cos(\kappa_l x'_i)\cos(\kappa_l x'_j),$$

where $\gamma(\cdot)$ is the Fourier multiplier function of the operator $\mathcal{L}$.

The equation (2.20) is evaluated at each point x'_n. This may be written $F(\phi_N) = 0$, where F is a nonlinear system of N equations and N unknowns. This system is solved

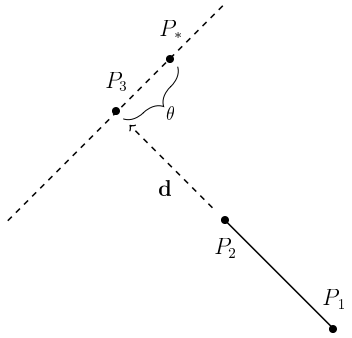

Figure 2.1: Navigation on the bifurcation curve.

by an iterative method such as Newton's method. The wavespeed c has to be fixed in F to compute a particular solution. If a turning point appears on the bifurcation curve for the equation under study, this approach will not work as there will be two solutions ϕ_N for the same wavespeed c. This situation is described in [16].

In the current method, the amplitude a and the wavespeed c of a solution are defined as functions of a parameter θ: $a = a(\theta)$, $c = c(\theta)$. Such an approach enables one to follow turning points on the bifurcation curve.

As the Figure Figure 2.1 shows, we use two points on the bifurcation curve, $P_1 = (c_1, a_1)$ and $P_2 = (c_2, a_2)$, to define a direction vector $\mathrm{d} = (d^c, d^a)$:

$$\mathrm{d}: \quad d^c = c_2 - c_1, \qquad d^a = a_2 - a_1.$$

Then the point $P_3 = (c_3, a_3)$ is fixed at a small distance s from the point P_2 in the direction d:

$$P_3: \quad c_3 = c_2 + s \cdot d^c, \qquad a_3 = a_2 + s \cdot d^a.$$

We take P_3 as an initial guess for computing the next solution $P_* = (c_*, a_*)$. The point P_* lies in the direction of the vector $\mathrm{d}_\perp = (d^c_\perp, d^a_\perp)$ orthogonal to the vector d:

$$\begin{aligned} \mathrm{d}_\perp: \quad & d^c_\perp = -d^a, \qquad d^a_\perp = d^c, \\ P_*: \quad & c_* = c_3 + \theta d^c_\perp \qquad a_* = a_3 + \theta d^a_\perp. \end{aligned}$$

The variable θ is computed the system

$$F\begin{pmatrix} \phi_N(x_1) \\ \vdots \\ \phi_N(x_N) \\ B \\ \theta \end{pmatrix} = \begin{pmatrix} (-c + \mathcal{L}_N)\phi_N(x_1) + f(\phi_N(x_1)) - B \\ \vdots \\ (-c + \mathcal{L}_N)\phi_N(x_N) + f(\phi_N(x_N)) - B \\ \Omega(\phi_N, c, a, B) \\ \phi_N(x_1) - \phi_N(x_N) - a \end{pmatrix} = \begin{pmatrix} 0 \\ \vdots \\ 0 \\ 0 \\ 0 \end{pmatrix}. \tag{2.21}$$

We require the computed solution to have waveheight a by setting

$$\phi_N(x_1) - \phi_N(x_N) - a = 0.$$

Nb. of grid points	$\log_{10}(\|\eta_{\text{exact}}-\eta\|_{L^\infty})$	$\log_{10}(\|\eta_{\text{exact}}-\eta\|_{L^2})$	Ratio of L^2-errors
32	−1.389	−2.092	
64	−3.705	−4.549	286.8
128	−8.809	−9.508	90935.0
256	−15.353	−16.144	4329670.9
512	−15.353	−16.087	0.9

Table 2.1: Estimates of error between the exact and computed solitary wave solutions for the KdV equation. $L/2 = 30$, waveheight $a = 1.2651$

The equation $\Omega(\phi_N, c, a, B) = 0$ allows to enforce different conditions on the computed solution. For example, the function

$$\Omega(\phi_N, c, a, B) = \phi_N(x_1) + \cdots + \phi_N(x_N),$$

requires a computed solution to have the mean of over a period equal to zero;

$$\Omega(\phi_N, c, a, B) = B,$$

sets the problem in the homogeneous form ($B = 0$);

$$\Omega(\phi_N, c, a, B) = \phi_N(x_N). \tag{2.22}$$

enables to compute traveling-wave solutions that approximate solitary waves. Solitary wave solutions are treated as traveling waves having long wavelength and trough at zero. We test the latter condition for the KdV equation:

$$\eta_t + \eta_x + \frac{3}{2}\eta\eta_x + \frac{1}{6}\eta_{xxx} = 0,$$

which has exact solitary solutions in the form

$$\eta_{\text{exact}}(x,t) = a\,\text{sech}^2\left(\sqrt{\tfrac{3a}{4}}(x-ct)\right), \qquad c = 1 + a/2.$$

The computations suggest that the method features exponential convergence to the exact solitary wave solution. The method is implemented in the Python language [18, 31] and distributed as the SpecTraVVave solver [28].

Chapter 3

Summary of results

This chapter provides an overview of the results achieved in the course of research work.

3.1 The Whitham equation as a model for surface water waves

In this paper, the Hamiltonian theory for surface water waves is used to derive asymptotically both the Whitham equation and a system of Whitham type, which allows for wave propagation in two directions. Moreover, the performance of the Whitham equation as a model for time-dependent surface water waves is compared with well-established models such as the KdV, BBM and Padé (2,2) equations. Numerical solutions of the Euler equations with boundary conditions on the free-surface are taken for the point of reference.

3.1.1 Derivation of evolution systems of Whitham type.

Investigation of amplitude–wavelength relation for solitary waves of the Whitham equation yields the scaling regime

$$\mathcal{W}(\kappa, \nu) = \frac{a}{h_0} e^{\kappa (l/h_0)^\nu} \sim 1, \tag{3.1}$$

where values for κ and ν are computed numerically. This regime is central for deriving the Whitham type system and the Whitham equation from the Hamiltonian function H for surface water wave problem:

$$H = \int_{\mathbb{R}} \int_0^\eta z \, dz dx + \int_{\mathbb{R}} \int_{-1}^\eta \frac{1}{2} |\nabla \phi|^2 \, dz dx. \tag{3.2}$$

We follow the method detailed in the chapter 2.1 and re-write as

$$H = \frac{1}{2} \int_{\mathbb{R}} \left[\eta^2 + u \mathcal{K}(\eta) u \right] dx, \tag{3.3}$$

where $u = \Phi_x$ is the dependent variable, $\Phi(x,t) = \phi(x, \eta(x,t), t)$, $K = \sqrt{\frac{\tanh D}{D}}$. The water wave problem is then written as a Hamiltonian system

$$\eta_t = -\partial_x \frac{\delta H}{\delta u}, \qquad u_t = -\partial_x \frac{\delta H}{\delta \eta}.$$

Derivation of the Whitham type system is based on the scaling regime (3.1) and the Hamiltonian (3.3). We introduce a parameter $\mu = \frac{h_0}{l}$ and assume the amplitude-depth ratio to be the following $a/h_0 = e^{-\kappa/\mu^\nu}$. Thus we the regime $\mathcal{W}(\kappa, \nu) = 1$ is embedded. Further, we expand the operator $\mathcal{K}(\eta)$ in the Hamiltonian function (3.3) and disregard terms of order $O(\mu^2 e^{-\kappa/\mu^\nu})$, but not of order $O(e^{-\kappa/\mu^\nu})$. The truncated Hamiltonian in dimensional variables may be written as

$$H = \frac{1}{2}\int_{\mathbb{R}} \left[\eta^2 + u\mathcal{K}_0^N(\eta)u + u\eta u\right] dxdz. \tag{3.4}$$

The operators $\mathcal{K}_0$ and $\mathcal{K}_0^N$ are equal up to the order of approximation and therefore the Whitham system is can be obtained from the Hamiltonian (3.4) as follows:

$$\eta_t = -\partial_x \frac{\delta H}{\delta u} = -\mathcal{K}_0 u_x - (\eta u)_x, \tag{3.5}$$

$$u_t = -\partial_x \frac{\delta H}{\delta \eta} = -\eta_x - u u_x. \tag{3.6}$$

It is also possible to derive a higher-order system by discarding terms of order $O(\mu^4 e^{-\kappa/\mu^\nu})$, but not of order $O(\mu^2 e^{-\kappa/\mu^\nu})$:

$$\eta_t = -\mathcal{K}_0 u_x - (\eta u)_x - (\eta u_x)_{xx},$$
$$u_t = -\eta_x - u u_x + u_x u_{xx}.$$

3.1.2 Derivation of evolution equations of Whitham type.

To derive the Whitham equation for one-directional wave prepagation we consider the linearized version of the Whitham system (3.5)-(3.6), which is written as follows:

$$\eta_t = -\mathcal{K}_0 u_x, \tag{3.7}$$

$$u_t = -\eta_x. \tag{3.8}$$

If one considers η and u to be of the form $\eta(x,t) = Ae^{(i\xi x - i\omega t)}$, $u(x,t) = Be^{(i\xi x - i\omega t)}$, it will lead to the relation $\omega^2 - \frac{\tanh\xi}{\xi}\xi^2 = 0$, which gives the existence of a nontrivial solution of the linearized system. By defining $c = \omega/\xi$, one obtains the dispersion relation $c = \pm\sqrt{\frac{\tanh\xi}{\xi}}$. Right-going wave solutions are featured with $c > 0$ and, hence, the equation (3.8) provides us with the relation $\eta = Ku$. Thus we define functions r and s to separate the right-going and left-going parts of solutions:

$$r = \frac{1}{2}(\eta + Ku), \qquad s = \frac{1}{2}(\eta - Ku).$$

Using similar analysis of Hamiltonian function as the one described above, we arrive to the Whitham equation:

$$r_t = -Kr_x - \frac{3}{2}rr_x,$$

and it's higher-order version

$$r_t = -Kr_x - \frac{3}{2}rr_x - \frac{13}{12}r_x r_{xx} - \frac{5}{12}rr_{xxx}.$$

3.1.3 Numerical results.

Approximation of solutions of the Euler equations with free-surface boundary conditions was analyzed for nondimensional versions of the Whitham equation, the KdV equation, BBM equation and the Padé (2,2) model. Equations were solved numerically using a standard pseudo-spectral method (see [16, 17]), a fourth-order evolution integrator algorithm was used for computation of solutions' development in time [12]. Comparison was performed for initial conditions with both positive and negative surface elevation, and different amplitude-wavelength settings.

Numerical experiments show that the Whitham equation outperforms other models except for the case of long waves with positive main part. In this case, the KdV and BBM equations give better results than the Whitham equation. The Padé (2,2) model performs better than the KdV and BBM equations, the Whitham equation is more accurate for shorter waves and negative disturbances.

3.2 The Whitham equation with surface tension

This paper generalizes the results of the previous paper to the case where surface tension is present. The equation under study is

$$\eta_t + W\eta_x + \frac{3}{2}\eta\eta_x = 0, \quad W\eta_x = w(-i\partial_x)\eta_x = \left(\mathcal{F}^{-1}w\right) * \eta_x, \tag{3.9}$$

where the convolution kernel of the operator w is given in terms of the Fourier transform by

$$w(\xi) = \sqrt{(1+\varkappa\xi^2)\frac{\tanh(\xi)}{\xi}}. \tag{3.10}$$

The parameter $\varkappa$, which is the inverse of the Bond number, embeds the surface tension into the model.

The system of equations for the water wave problem in presence of surface tension is written as follows:

$$\phi_{xx} + \phi_{zz} = 0 \quad \text{in } -1 < z < \eta(x,t), \tag{3.11}$$

$$\phi_{zz} = 0 \quad \text{on } z = -1, \tag{3.12}$$

$$\left.\begin{aligned} \eta_t + \phi_x\eta_x - \phi_z &= 0 \\ \phi_t + \tfrac{1}{2}\left(\phi_x^2 + \phi_z^2\right) + \eta - \varkappa\eta_{xx}\left(1+\eta_x^2\right)^{-3/2} &= 0 \end{aligned}\right\} \text{on } z = \eta(x,t). \tag{3.13}$$

Hamiltonian function for this case is

$$H = \int_{\mathbb{R}}\int_0^{\eta} z\,dzdx + \int_{\mathbb{R}}\int_{-1}^{\eta} \tfrac{1}{2}|\nabla\phi|^2\,dzdx + \varkappa\int_{\mathbb{R}} \frac{\eta_x^2}{1+\sqrt{1+\eta_x^2}}dx.$$

The function H can be represented in a more convenient way as

$$H = \int_{\mathbb{R}} \left[\tfrac{1}{2}\eta^2 + \tfrac{1}{2}\Phi G(\eta)\Phi + \varkappa\frac{\eta_x^2}{1+\sqrt{1+\eta_x^2}}\right] dx, \tag{3.14}$$

where $\Phi(x,t) = \varphi(x,\eta(x,t),t)$ is the trace of the potential at the free surface, and $G(\eta)$ is a Dirichlet-Neumann operator, which has a power series form [30]. Using analogous reasoning as in the previous paper, we transform the Hamiltonian (3.14) to be

$$H = \int_{\mathbb{R}} \left[\tfrac{1}{2}\eta^2 + \tfrac{1}{2} u \mathcal{K}(\eta) u + \varkappa \tfrac{\eta_x^2}{1+\sqrt{1+\eta_x^2}} \right] dx. \tag{3.15}$$

However, in this case, one should notice that the dependent variable $u = \Phi_x$ has a different structure: $u = \varphi_x + \eta_x \varphi_z = \varphi_\tau \sqrt{1+\eta_x^2}$, where φ_τ is the tangential velocity component to the surface.

We split the Hamiltonian (3.15) into gravity and capillary terms as follows

$$H = H_g + H_c + O(\mu^2\alpha^4), \tag{3.16}$$

$$H_g = \frac{1}{2}\int_{\mathbb{R}} \left[\eta^2 + u \tfrac{\tanh D}{D} u + \eta u^2 - u \tanh D(\eta \tanh Du) \right] dx, \tag{3.17}$$

$$H_c = \varkappa \int_{\mathbb{R}} \tfrac{\eta_x^2 dx}{1+\sqrt{1+\eta_x^2}} = \frac{\varkappa}{2}\int_{\mathbb{R}} \eta_x^2 dx + O(\mu^4\alpha^4), \tag{3.18}$$

where D, μ and α are as in [27]. Following the methods detailed in [7, 8], we represent the system (3.11)-(3.13) in terms of η and u from the Hamiltonian equations:

$$\eta_t = -\partial_x \frac{\delta H}{\delta u}, \qquad u_t = -\partial_x \frac{\delta H}{\delta \eta}. \tag{3.19}$$

This will eventually lead us to the Whitham system with surface tension

$$\eta_t = -\frac{\tanh D}{D} u_x - (\eta u)_x + O(\mu^3\alpha^2),$$
$$u_t = -\eta_x - u u_x + \varkappa \eta_{xxx} + O(\mu^3\alpha^2).$$

Employing the reasoning developed in [27], we obtain the dispersion relation

$$c^2(\xi) = (1 + \varkappa\xi^2)\frac{\tanh\xi}{\xi},$$

and the variables that correspond to the right-going and left-going wave solutions

$$r = \frac{1}{2}(\eta + Ku), \quad s = \frac{1}{2}(\eta - Ku), \quad \text{where} \quad K = \sqrt{\frac{1}{1+\varkappa D^2} \cdot \frac{\tanh D}{D}}. \tag{3.20}$$

Further, we represent the Hamiltonian (3.15) in terms of r and s and analyze the consequent Hamiltonian system

$$r_t + \partial_x \left(\frac{K}{2} \frac{\delta H}{\delta r} \right) = 0, \qquad s_t - \partial_x \left(\frac{K}{2} \frac{\delta H}{\delta s} \right) = 0, \tag{3.21}$$

using different approximations and scaling regimes. The first equation of this system allows us to derive several models such as the shallow-water, KdV, BBM and Whitham equations. The Padé (2,2) model and the Kawahara equation can also be derived from (3.21).

In this paper, several numerical experiments were carried to compare the accuracy of the Whitham equation with surface tension with the KdV equation ($\varkappa = 1/2$) and Kawahara equation ($\varkappa = 1/3$). Analysis was done for amplitudes and wavelengths corresponding to different Stokes numbers. Positive and negative initial surface elevations were also analyzed. Numerical solutions for full Euler equations were taken for reference.

The experiments show that the Whitham equation has better accuracy than the KdV and Kawahara models. The only case where this does not hold is with a wave of depression and Stokes number close to one.

3.3 A numerical study of nonlinear dispersive wave models with SpecTraVVave

The Paper C describes the SpecTraVVave solver for computing approximations to traveling-wave solutions of nonlinear dispersive wave equations of the form

$$u_t + [f(u)]_x + \mathcal{L}u_x = 0, \tag{3.22}$$

where $u(x,t)$ is surface elevation, $\mathcal{L}$ is a self-adjoint operator, and f is a real-valued function. The numerical algorithm behind the solver is based on continuation method along the waveheight-velocity bifurcation curve detailed in [16]. We developed a convenient navigation technique along the bifurcation curve that allows us to circumvent issues related to turning points. Another advantage of our method is that it allows to impose different conditions on solutions of the equations such as "zero mean" and "trough at zero" to approximate solitary-wave solutions. The solver is programmed in Python language [18, 31]. Tests on convergence of solutions computed by the algorithm to the exact solitary wave solutions of the KdV equation were positive. SpecTraVVave is then used to experiment with the Whitham, modified Benjamin–Ono and the Benjamin equations in order to obtain more understanding about their solutions.

3.3.1 Termination of the waveheight-velocity bifurcation curve of the Whitham equation.

The SpecTraVVave solver is used to compute waveheight-velocity bifurcation curve of the Whitham equation

$$u_t + \frac{3}{2}uu_x + Ku_x = 0, \qquad \widehat{Ku}(k) = \sqrt{\frac{\tanh(k)}{k}}. \tag{3.23}$$

We compute traveling-wave solutions of this equation in the following form:

$$u(x,t) = \phi(x - ct).$$

In terms of ϕ the equation obtains an integrable form, which is written as

$$\phi' + \frac{3}{2}\phi\phi' + K\phi' = 0 \quad \Longrightarrow \quad -c\phi + \frac{3}{4}\phi^2 + K\phi = B. \tag{3.24}$$

where we set $B = 0$. The following questions were investigated and given answers to:

a) Where does the bifurcation curve terminate?

b) Where on the bifurcation curve do solutions change their stability?

c) Is there any role that the turning point on the bifurcation curve plays?

We focus the reader's attention on the following findings:

1. Traveling-wave solution with minimum velocity corresponds to the turning point of the bifurcation curve;

2. Traveling-wave solution with maximum L^2-norm corresponds to the point of change of stability;

3. Cusped traveling-wave solution corresponds to the point of termination of the bifurcation curve.

Justification of the second proposition is based on analysis developed by Boussinesq and used in [2, 4, 5, 29]. We define the functionals V and E:

$$V(\phi) = \frac{1}{2}\int_{-\infty}^{+\infty} \phi^2 \,\mathrm{d}\zeta, \qquad E(\phi) = \int_{-\infty}^{+\infty} \left\{\tfrac{1}{2}\phi^3 - \phi K\phi\right\} \mathrm{d}\zeta,$$

and rewrite equation (3.24) in terms of variational derivatives of E and V as

$$E'(\phi) - cV'(\phi) = 0. \tag{3.25}$$

Stability of wave solutions are related to convexity of the function $d(c) = E(\phi) - cV(\phi)$. Stable solutions have velocities c for which $d''(c) > 0$, unstable solutions are featured with velocities c such that $d''(c) < 0$. The derivative of $d(c)$ in view of (3.25) gives

$$d'(c) = -V(\phi) = -\frac{1}{2}\int_{-\infty}^{+\infty} \phi^2 \,\mathrm{d}\zeta = -\frac{1}{2}\|\phi\|_{L^2}^2. \tag{3.26}$$

It turns out that $d''(c)$ changes sign in the neighborhood of the solution ϕ_{L^2} with maximum L^2-norm. Solutions, which are placed around ϕ_{L^2} on the amplitude-velocity bifurcation curve, are tested in a 4th-order evolution integrator and the proposition has been confirmed.

One can write the integrated equation given in (3.24) as

$$\left(\frac{c}{\sqrt{3}} - \frac{\sqrt{3}}{2}\phi\right)^2 = \frac{1}{3}c^2 - K\phi. \tag{3.27}$$

The inequality $\phi < \frac{3}{2}c$, that may be derived from the latter equation, imposes the condition that any continuous solution ϕ must be smooth. However, if $\phi = \frac{3}{2}c$ this argument does not work. Hence, one may conclude that a cusped solution has a maximum value of $\frac{3}{2}c$.

The cusped-wave solution mentioned in the third proposition satisfies the relation

$$\frac{c}{\sup_x \phi(x)} = \frac{3}{2}$$

with a good accuracy. This provides a numerical evidence to the proposition and justifies it in view of the argument given above. This conclusion has been proved analytically in [14].

3.3.2 Interaction of solitary wave solutions of modified Benjamin–Ono equation

We use the SpecTraVVave solver to compute accurate approximations to solitary-wave solutions of the modified Benjamin–Ono

$$u_t + u^2 u_x + u_x - \mathcal{H}u_{xx} = 0,$$

Two computed solutions, one higher than the other, are set into a time integrator and their interaction is studied.

Numerical experiment shows that during interaction the solitary-wave solutions combine into one. This may be seen as if the higher wave annihilated the smaller one. Further growth of the resulting wave leads to a blow-up process such as the one described in [20] and proved in [26]. Absence of complete interaction of the solitary-wave solutions prompts us to conclude that the modified Benjamin–Ono equation may not be integrable.

3.3.3 Effect of competing dispersion in the Benjamin equation

The purpose of the work described in this section is studying the effects of competing dispersion operators on periodic traveling waves. We employ the SpecTraVVave to compute bifurcation branches of the Benjamin equation

$$u_t + u_x + uu_x - \mathcal{H}u_{xx} - \tau u_{xxx} = 0, \tag{3.28}$$

with τ being a parameter that models surface tension [3], [19], [35]. Fixing the parameter $\tau = 0.1$, leads us to the dispersion relation

$$c(k) = 1 - |k| + 0.1k^2. \tag{3.29}$$

For $c = 0.525$ the dispersion relation has two corresponding wavenumbers $k_3 = 0.5$ and $k_2 = 19/2$. This results in two bifurcation curves originating from one point, but for solutions with different wavelengths $L_3 = 4\pi$ and $L_2 = 4\pi/19$. We also compute the bifurcation branch for $c = 1$, i.e. $k_1 = 10$ and $L_1 = \pi/5$.

The bifurcation branches corresponding to L_3 and L_2 contain solutions related to capillary and gravity regimes. The branches originate in one point, but tend to different directions without further interaction. However, the branches for solutions with wavelengths L_1 and L_3 have two common points. As the amplitude increases, the branch L_3 crosses the branch L_1, then it grows further and terminates at a point on the branch L_1. During the process of this interaction the solutions of the branch L_3 develop new fundamental wavelength and change from 4π to $\pi/5$.

Similar phenomena for the Whitham equation with surface tension were reported in [33].

3.4 Explicit solutions for a long-wave model with constant vorticity

This paper presents a method for finding exact solutions to the nonlinear differential equation

$$\left(Q + \frac{\omega_0}{2}u^2\right)^2 \left(\frac{du}{dx}\right)^2 = -3\left(\frac{\omega_0^2}{12}u^4 + gu^3 - (2R - \omega_0 Q)u^2 + 2Su - Q^2\right). \tag{3.30}$$

The equation models steady surface water waves in presence of background shear flow. It is shown that the equation (3.30) admits solutions given in parametric forms of the Weierstrass P, zeta and sigma functions. Explicit solutions to the equation (3.30) are compared to numerical results obtained in [1] for the same equation.

My contribution to this paper was finding that the exact solutions of (3.30) are very close in shape to regular wave profiles from full Euler equations computed by Teles da Silva and Peregrine in [11]. In case of overhanging waves such an agreement could not be achieved due to the parametric representation of solutions of (1).

I also studied the pressure distribution and streamlines below the surface. It was found that pressure profiles differ depending on the direction of wave propagation - upstream and downstream. In the first case, the flow under the surface develops critical layers with recirculating flow and non-monotone pressure profiles. In the second case, the flow produces irregular pressure profiles due to the loss of long-wave approximation.

Bibliography

[1] ALI, A., AND KALISCH, H. On the formulation of mass, momentum and energy conservation in the kdv equation. Acta Applicandae Mathematicae 133, 1 (2014), 113–131, doi: 10.1007/s10440-013-9861-0. 3.4

[2] BENJAMIN, T. B. The stability of solitary waves. Proceedings of the Royal Society of London A: Mathematical, Physical and Engineering Sciences 328, 1573 (1972), 153–183, doi: 10.1098/rspa.1972.0074. 3.3.1

[3] BENJAMIN, T. B. A new kind of solitary wave. Journal of Fluid Mechanics 245 (1992), 401–411, doi: 10.1017/S002211209200051X. 3.3.3

[4] BONA, J. L., SOUGANIDIS, P. E., AND STRAUSS, W. A. Stability and instability of solitary waves of korteweg-de vries type. Proceedings of the Royal Society of London A: Mathematical, Physical and Engineering Sciences 411, 1841 (1987), 395–412, doi: 10.1098/rspa.1987.0073. 3.3.1

[5] BRIDGES, T. J. Superharmonic instability, homoclinic torus bifurcation and water-wave breaking. Journal of Fluid Mechanics 505 (2004), 153–162, doi: 10.1017/S0022112004008432. 3.3.1

[6] CHEN, H., AND BONA, J. L. Existence and asymptotic properties of solitary-wave solutions of benjamin-type equations. Adv. Differential Equations 3, 1 (1998), 51–84. 2.2.1

[7] CRAIG, W., AND GROVES, M. D. Hamiltonian long-wave approximations to the water-wave problem. Wave Motion 19, 4 (1994), 367–389, doi: 10.1016/0165-2125(94)90003-5. 3.2

[8] CRAIG, W., GUYENNE, P., AND KALISCH, H. Hamiltonian long-wave expansions for free surfaces and interfaces. Communications on Pure and Applied Mathematics 58, 12 (2005), 1587–1641, doi: 10.1002/cpa.20098. 3.2

[9] CRAIG, W., AND SULEM, C. Numerical simulation of gravity waves. Journal of Computational Physics 108, 1 (1993), 73– – 83, doi: 10.1006/jcph.1993.1164. 2.1

[10] CRAIK, A. D. The origins of water wave theory. Annual Review of Fluid Mechanics 36, 1 (2004), 1–28, doi: 10.1146/annurev.fluid.36.050802.122118. I

[11] DA SILVA, A. F. T., AND PEREGRINE, D. H. Steep, steady surface waves on water of finite depth with constant vorticity. Journal of Fluid Mechanics 195 (1988), 281–302, doi: 10.1017/S0022112088002423. 3.4

[12] DE FRUTOS, J., AND SANZ-SERNA, J. M. An easily implementable fourth-order method for the time integration of wave problems. Journal of Computational Physics 103, 1 (1992), 160–168, doi: 10.1016/0021-9991(92)90331-R. 3.1.3

[13] DEAN, R., AND DALRYMPLE, R. Water Wave Mechanics for Engineers and Scientists. Advanced series on ocean engineering. World Scientific, 1991. I, 1.1

[14] EHRNSTRÖM, M., AND WAHLÉN, E. On whitham's conjecture of a highest cusped wave for a nonlocal dispersive equation. arXiv:1602.05384. 3.3.1

[15] EHRNSTRÖM, M., GROVES, M. D., AND WAHLÉN, E. On the existence and stability of solitary-wave solutions to a class of evolution equations of whitham type. Nonlinearity 25, 10 (2012), 2903–2936. I

[16] EHRNSTRÖM, M., AND KALISCH, H. Global bifurcation for the whitham equation. Math. Mod. Nat. Phenomena 8 (2013), 13–30, doi: 10.1051/mmnp/20138502. 2.2.1, 3.1.3, 3.3

[17] FORNBERG, B., AND WHITHAM, G. B. A numerical and theoretical study of certain nonlinear wave phenomena. Philosophical Transactions of the Royal Society of London A: Mathematical, Physical and Engineering Sciences 289, 1361 (1978), 373–404, doi: 10.1098/rsta.1978.0064. 3.1.3

[18] FÜHRER, C., SOLEM, J. E., AND VERDIER, O. Computing with Python: An introduction to Python for science and engineering. Pearson, 2014. 2.2.1, 3.3

[19] KALISCH, H. Derivation and comparison of model equations for interfacial capillary-gravity waves in deep water. Mathematics and Computers in Simulation 74, 2–3 (2007), 168–178, doi: 10.1016/j.matcom.2006.10.008. 3.3.3

[20] KALISCH, H., AND BONA, J. L. Models for internal waves in deep water. Discrete and Continuous Dynamical Systems 6 (2000), 1–20. 3.3.2

[21] KLEIN, C., AND SAUT, J.-C. A numerical approach to blow-up issues for dispersive perturbations of burgers' equation. Physica D 295 (2015), 46–65. I

[22] KORTEWEG, D. D. J., AND DE VRIES, D. G. Xli. on the change of form of long waves advancing in a rectangular canal, and on a new type of long stationary waves. Philosophical Magazine Series 5 39, 240 (1895), 422–443, doi: 10.1080/14786449508620739. I

[23] KUNDU, P., COHEN, I., AND DOWLING, D. Fluid Mechanics. Academic Press, 2012. 1.1, 1.2

[24] LANNES, D. The Water Waves Problem, in: Mathematical Surveys and Monographs, vol. 188. Amer. Math. Soc., Providence, 2013. I

[25] LANNES, D., AND SAUT, J.-C. Remarks on the full dispersion kadomtsev-petviashvli equation. Kinet. Relat. Models 6 (2013), 989–1009. I

[26] MARTEL, Y., AND PILOD, D. Construction of a minimal mass blow up solution of the modified benjamin–ono equation. Mathematische Annalen (2016), 1–93, doi: 10.1007/s00208-016-1497-8. 3.3.2

[27] MOLDABAYEV, D., KALISCH, H., AND DUTYKH, D. The whitham equation as a model for surface water waves. Physica D: Nonlinear Phenomena 309 (2015), 99–107, doi: 10.1016/j.physd.2015.07.010. 3.2, 3.2

[28] MOLDABAYEV, D., VERDIER, O., AND KALISCH, H. Spectravvave. available at https://github.com/olivierverdier/SpecTraVVave. 2.2.1

[29] NGUYEN, N. T., AND KALISCH, H. Orbital stability of negative solitary waves. Mathematics and Computers in Simulation 80, 1 (2009), 139–150, doi: 10.1016/j.matcom.2009.06.010. 3.3.1

[30] NICHOLLS, D. P., AND REITICH, F. A new approach to analyticity of dirichlet-neumann operators. Proceedings of the Royal Society of Edinburgh: Section A Mathematics 131, 6 (2001), 1411–1433, doi: 10.1017/S0308210500001463. 2.1, 3.2

[31] PÉREZ, F., AND GRANGER, B. E. Ipython: a system for interactive scientific computing. Computing in Science and Engineering 9, 3 (2007), 21–29, doi: 10.1109/MCSE.2007.53. 2.2.1, 3.3

[32] PETROV, A. A. Variational statement of the problem of liquid motion in a container of finite dimensions. Journal of Applied Mathematics and Mechanics 28, 4 (1964), 917– 922, doi: 10.1016/0021-8928(64)90077-2. I, 2.1

[33] REMONATO, F., AND KALISCH, H. Numerical bifurcation for the capillary whitham equation. Physica D: Nonlinear Phenomena (2016), –, doi: 10.1016/j.physd.2016.11.003. 3.3.3

[34] STOKES, G. G. On the Theory of Oscillatory Waves, vol. 1 of Cambridge Library Collection - Mathematics. Cambridge University Press, 2009, p. 197–229. I

[35] WALSH, S. Steady stratified periodic gravity waves with surface tension i: Local bifurcation. Discrete and Continuous Dynamical Systems 34, 8 (2014), 3241–3285, doi: 10.3934/dcds.2014.34.3241. 3.3.3

[36] WHITHAM, G. B. Linear and Nonlinear Waves. Wiley, New York, 1974. 2.1

[37] ZAKHAROV, V. E. Stability of periodic waves of finite amplitude on the surface of a deep fluid. J. Appl. Mech. Tech. Phys. 9 (1968), 190–194. 2.1

Part II

Scientific results

A

Paper A

The Whitham equation as a model for surface water waves

Daulet Moldabayev, Henrik Kalisch, Denys Dutyh

Physica D: Nonlinear phenomena **309**, pp.99–107, (2015)
http://dx.doi.org/10.1016/j.physd.2015.07.010

Physica D 309 (2015) 99–107

Contents lists available at ScienceDirect

Physica D

journal homepage: www.elsevier.com/locate/physd

The Whitham Equation as a model for surface water waves

Daulet Moldabayev [a], Henrik Kalisch [a,*], Denys Dutykh [b]

[a] Department of Mathematics, University of Bergen, Postbox 7800, 5020 Bergen, Norway
[b] LAMA, UMR5127, CNRS - Université Savoie Mont Blanc, 73376 Le Bourget-du-Lac Cedex, France

HIGHLIGHTS

- Definition of Whitham scaling regime.
- Derivation of a Hamiltonian Whitham system.
- Asymptotic derivation of the Whitham equation.
- Comparison of Whitham, KdV, BBM and Padé models with inviscid free surface dynamics.

ARTICLE INFO

Article history:
Received 16 October 2014
Received in revised form
9 June 2015
Accepted 24 July 2015
Available online 31 July 2015
Communicated by J. Bronski

Keywords:
Nonlocal equations
Nonlinear dispersive equations
Hamiltonian models
Solitary waves
Surface waves

ABSTRACT

The Whitham equation was proposed as an alternate model equation for the simplified description of unidirectional wave motion at the surface of an inviscid fluid. As the Whitham equation incorporates the full linear dispersion relation of the water wave problem, it is thought to provide a more faithful description of shorter waves of small amplitude than traditional long wave models such as the KdV equation.

In this work, we identify a scaling regime in which the Whitham equation can be derived from the Hamiltonian theory of surface water waves. A Hamiltonian system of Whitham type allowing for two-way wave propagation is also derived. The Whitham equation is integrated numerically, and it is shown that the equation gives a close approximation of inviscid free surface dynamics as described by the Euler equations. The performance of the Whitham equation as a model for free surface dynamics is also compared to different free surface models: the KdV equation, the BBM equation, and the Padé (2,2) model. It is found that in a wide parameter range of amplitudes and wavelengths, the Whitham equation performs on par with or better than the three considered models.

1. Introduction

In its simplest form, the water-wave problem concerns the flow of an incompressible inviscid fluid with a free surface over a horizontal impenetrable bed. In this situation, the fluid flow is described by the Euler equations with appropriate boundary conditions, and the dynamics of the free surface are of particular interest in the solution of this problem.

There are a number of model equations which allow the approximate description of the evolution of the free surface without having to provide a complete solution of the fluid flow below the surface. In the present contribution, interest is focused on the derivation and evaluation of a nonlocal water-wave model known as the Whitham equation. The equation is written as

$$\eta_t + \frac{3}{2}\frac{c_0}{h_0}\eta\eta_x + K_{h_0} * \eta_x = 0, \tag{1}$$

where the convolution kernel K_{h_0} is given in terms of the Fourier transform by

$$\mathcal{F}K_{h_0}(\xi) = \sqrt{\frac{g\tanh(h_0\xi)}{\xi}}, \tag{2}$$

g is the gravitational acceleration, h_0 is the undisturbed depth of the fluid, and $c_0 = \sqrt{gh_0}$ is the corresponding long-wave speed. The convolution can be thought of as a Fourier multiplier operator, and (2) represents the Fourier symbol of the operator.

The Whitham equation was proposed by Whitham [1] as an alternative to the well known Korteweg–de Vries (KdV) equation

$$\eta_t + c_0\eta_x + \frac{3}{2}\frac{c_0}{h_0}\eta\eta_x + \frac{1}{6}c_0h_0^2\eta_{xxx} = 0. \tag{3}$$

* Corresponding author.
E-mail addresses: daulet.moldabayev@math.uib.no (D. Moldabayev), henrik.kalisch@math.uib.no (H. Kalisch), Denys.Dutykh@univ-savoie.fr (D. Dutykh).

http://dx.doi.org/10.1016/j.physd.2015.07.010

The validity of the KdV equation as a model for surface water waves can be described as follows. Suppose a wave field with a prominent amplitude a and characteristic wavelength l is to be studied. The KdV equation is known to produce a good approximation of the evolution of the waves if the amplitude of the waves is small and the wavelength is large when compared to the undisturbed depth, and if in addition, the two non-dimensional quantities a/h_0 and h_0^2/l^2 are of similar size. The latter requirement can be written in terms of the Stokes number as

$$\mathcal{S} = \frac{al^2}{h_0^3} \sim 1.$$

While the KdV equation is a good model for surface waves if $\mathcal{S} \sim 1$, one notorious problem with the KdV equation is that it does not model accurately the dynamics of shorter waves. Recognizing this shortcoming of the KdV equation, Whitham proposed to use the same nonlinearity as the KdV equation, but couple it with a linear term which mimics the linear dispersion relation of the full water-wave problem. Thus, at least in theory, the Whitham equation can be expected to yield a description of the dynamics of shorter waves which is closer to the solutions of the more fundamental Euler equations which govern the flow.

The Whitham equation has been studied from a number of vantage points during recent years. In particular, the existence of traveling and solitary waves has been established in [2,3]. Well posedness of a similar equation was investigated in [4–6], and a model with variable depth has been studied numerically in [7]. Moreover, it has been shown in [8,9] that periodic solutions of the Whitham equation feature modulational instability for short enough waves in a similar way as small-amplitude periodic wave solutions of the water-wave problem. However, even though the equation is routinely mentioned in texts on nonlinear waves [10,11], it appears that the performance of the Whitham equation in the description of surface water waves has not been investigated so far.

The purpose of the present article is to give an asymptotic derivation of the Whitham equation as a model for surface water waves, and to confirm Whitham's expectation that the equation is a fair model for the description of time-dependent surface water waves. For the purpose of the derivation, we introduce an exponential scaling regime in which the Whitham equation can be derived asymptotically from an approximate Hamiltonian principle for surface water waves. In order to motivate the use of this scaling, note that the KdV equation has the property that wide classes of initial data decompose into a number of solitary waves and small-amplitude dispersive residue [12]. For the KdV equations, solitary-wave solutions are known in closed form, and are given by

$$\eta = \frac{a}{h_0}\,\mathrm{sech}^2\left(\sqrt{\frac{3a}{4h_0^3}}(x-ct)\right) \tag{4}$$

for a certain wave celerity c. These waves clearly comply with the amplitude–wavelength relation $a/h_0 \sim h_0^2/l^2$ which was mentioned above. It appears that the Whitham equation – as indeed do many other nonlinear dispersive equations – also has the property that broad classes of initial data rapidly decompose into ordered trains of solitary waves (see Fig. 1). Quantifying the amplitude–wavelength relation for these solitary waves yields an asymptotic regime which is expected to be relevant to the validity of the Whitham equation as a water wave model.

As the curve fit in the right panel of Fig. 1 shows, the relationship between wavelength and amplitude of the Whitham solitary waves can be approximately described by the relation $\frac{a}{h_0} \sim e^{-\kappa(l/h_0)^\nu}$ for certain values of κ and ν. Since the Whitham solitary waves are not known in exact form, the values of κ and ν have to be found numerically. Then one may define a Whitham scaling regime

$$\mathcal{W}(\kappa,\nu) = \frac{a}{h_0}e^{\kappa(l/h_0)^\nu} \sim 1, \tag{5}$$

and it will be shown in Sections 2 and 3 that this scaling can be used advantageously in the derivation of the Whitham equation. The derivation proceeds by examining the Hamiltonian formulation of the water-wave problem due to Zakharov, Craig and Sulem [13,14], and by restricting to wave motion which is predominantly in the direction of increasing values of x. The approach is similar to the method of [15], but relies on the new relation (5).

First, in Section 2, a Whitham system is derived which allows for two-way propagation of waves. The Whitham equation is found in Section 3. Finally, in Section 4, a comparison of modeling properties of the KdV and Whitham equations is given. The comparison also includes the regularized long-wave equation

$$\eta_t + c_0\,\eta_x + \frac{3}{2}\frac{c_0}{h_0}\,\eta\,\eta_x - \frac{1}{6}h_0^2\,\eta_{xxt} = 0, \tag{6}$$

which was put forward in [16] and studied in depth in [17], and which is also known as the BBM or PBBM equation. The linearized dispersion relation of this equation is not an exact match to the dispersion relation of the full water-wave problem, but it is much closer than the KdV equation, and it might also be expected that this equation may be able to model shorter waves more successfully than the KdV equation. In order to obtain an even better match of the linear dispersion relation, one may make use of Padé expansions. In the context of simplified evolutions equations, this approach was pioneered in [18]. For uni-directional models, this approach was advocated in [19], and in particular, the equation based on the Padé (2,2) approximation was studied in depth. In dimensional variables, this model takes the form

$$\eta_t + c_0\,\eta_x + \frac{3}{2}\frac{c_0}{h_0}\,\eta\,\eta_x - \frac{3}{20}c_0h_0^2\,\eta_{xxx} - \frac{19}{60}h_0^2\,\eta_{xxt} = 0. \tag{7}$$

The dispersion relations for the KdV, BBM and Padé (2,2) models are respectively

$$c(k) = c_0 - \frac{1}{6}c_0h_0^2k^2 \quad \text{(KdV)},$$

$$c(k) = c_0\frac{1}{1+\frac{1}{6}h_0^2k^2} \quad \text{(BBM)},$$

$$c(k) = c_0\frac{1+\frac{3}{20}h_0^2k^2}{1+\frac{19}{60}h_0^2k^2} \quad \text{(Padé (2,2))}.$$

These approximate dispersion relations are compared to the full dispersion relation in Fig. 2. It appears clearly that the Padé (2,2) approximation remains much closer to the full dispersion relation than the dispersion relations based on either the linear KdV or linear BBM equations. As will be seen in Section 4, solutions of both the Whitham and Padé (2,2) equations give closer approximations to solutions of the full Euler equations than either the KdV or BBM equations in most cases investigated. However, the Whitham equation still keeps a slight edge over the Padé model.

2. Derivation of evolution systems of Whitham type

The surface water-wave problem is generally described by the Euler equations with slip conditions at the bottom, and kinematic and dynamic boundary conditions at the free surface. Assuming weak transverse effects, the unknowns are the surface elevation $\eta(x,t)$, the horizontal and vertical fluid velocities $u_1(x,z,t)$ and $u_2(x,z,t)$, respectively, and the pressure $P(x,z,t)$. If the assumption of irrotational flow is made, then a velocity potential $\phi(x,z,t)$ can be used. In order to nondimensionalize the problem, the undisturbed depth h_0 is taken as a unit of distance, and the

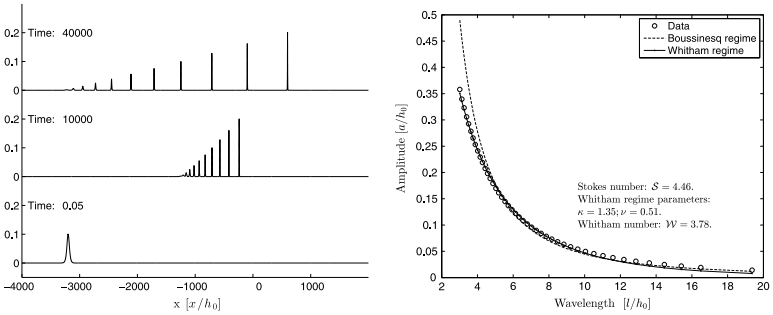

Fig. 1. Left panel: Formation of solitary waves of the Whitham equation from Gaussian initial data. Right panel: Curve fit for the Whitham regime and for the Boussinesq regime to amplitude/wavelength data from Whitham solitary waves. The wavelength is defined as $l = \frac{1}{a}\int_{-\infty}^{\infty} \eta(x)dx$.

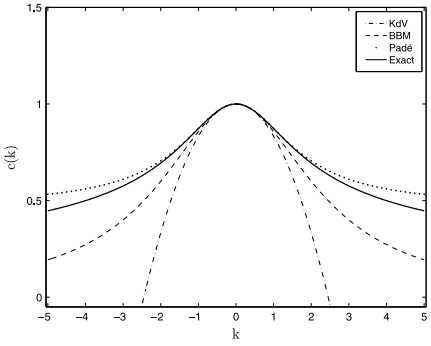

Fig. 2. Approximate models to the exact dispersion relation of the full water-wave problem.

parameter $\sqrt{h_0/g}$ as a unit of time. For the remainder of this article, all variables appearing in the water-wave problem are considered as being non-dimensional. The problem is posed on a domain $\{(x,z)^T \in \mathbb{R}^2 | -1 < z < \eta(x,t)\}$ which extends to infinity in the positive and negative x-direction. Due to the incompressibility of the fluid, the potential then satisfies Laplace's equation in this domain. The fact that the fluid cannot penetrate the bottom is expressed by a homogeneous Neumann boundary condition at the flat bottom. Thus we have

$$\begin{aligned} &\phi_{xx} + \phi_{zz} = 0 \ \text{ in } \ -1 < z < \eta(x,t) \\ &\phi_z = 0 \qquad\quad \text{on } z = -1. \end{aligned}$$

The pressure is eliminated with the help of the Bernoulli equation, and the free-surface boundary conditions are formulated in terms of the potential and the surface excursion by

$$\left.\begin{aligned} &\eta_t + \phi_x\eta_x - \phi_z = 0, \\ &\phi_t + \frac{1}{2}\left(\phi_x^2 + \phi_z^2\right) + \eta = 0, \end{aligned}\right\} \text{ on } z = \eta(x,t).$$

The total energy of the system is given by the sum of kinetic energy and potential energy, and normalized such that the potential energy is zero when no wave motion is present at the surface. Accordingly the Hamiltonian function for this problem is

$$H = \int_{\mathbb{R}}\int_0^{\eta} z\, dzdx + \int_{\mathbb{R}}\int_{-1}^{\eta} \frac{1}{2}|\nabla\phi|^2\, dzdx. \tag{8}$$

Defining the trace of the potential at the free surface as $\Phi(x,t) = \phi(x,\eta(x,t),t)$, one may integrate in z in the first integral and use the divergence theorem on the second integral in order to arrive at the formulation

$$H = \frac{1}{2}\int_{\mathbb{R}} \left[\eta^2 + \Phi G(\eta)\Phi\right] dx. \tag{9}$$

This is the Hamiltonian formulation of the water wave problem as found in [13,20,14], and written in terms of the Dirichlet–Neumann operator $G(\eta)$. As shown in [21], the Dirichlet–Neumann operator can be expanded in a series of the form

$$G(\eta)\Phi = \sum_{j=0}^{\infty} G_j(\eta)\Phi. \tag{10}$$

In order to proceed, we need to understand the first few terms in this series. As shown in [15,13], the first two terms in this series can be written with the help of the operator $D = -i\partial_x$ as

$$G_0(\eta) = D\tanh(D), \qquad G_1(\eta) = D\eta D - D\tanh(D)\eta D\tanh(D).$$

Note that it can be shown that the terms $G_j(\eta)$ for $j \geq 2$ are of quadratic or higher-order in η, and will therefore not be needed in the current analysis.

It will be convenient for the present purpose to formulate the Hamiltonian in terms of the dependent variable $u = \Phi_x$. To this end, we define the operator $\mathcal{K}(\eta)$ by

$$G(\eta) = D\mathcal{K}(\eta)D.$$

As was the case with $G(\eta)$, the operator $\mathcal{K}(\eta)$ can be expanded in a Taylor series around zero as

$$\mathcal{K}(\eta)\xi = \sum_{j=0}^{\infty} \mathcal{K}_j(\eta)\xi, \qquad \mathcal{K}_j(\eta) = D^{-1}G_j(\eta)D^{-1}. \tag{11}$$

In particular, note that $\mathcal{K}_0 = \frac{\tanh D}{D}$. In non-dimensional variables, we write the operator with the integral kernel K_{h_0} as $K = \sqrt{\frac{\tanh D}{D}}$, so that we have $\mathcal{K}_0 = K^2$. The Hamiltonian is then expressed as

$$H = \frac{1}{2}\int_{\mathbb{R}} \left[\eta^2 + u\mathcal{K}(\eta)u\right] dx. \tag{12}$$

The water-wave problem can then be written as a Hamiltonian system using the variational derivatives of H and posing the Hamiltonian equations

$$\eta_t = -\partial_x\frac{\delta H}{\delta u}, \qquad u_t = -\partial_x\frac{\delta H}{\delta \eta}. \tag{13}$$

This system is not in canonical form as the associated structure map $J_{\eta,u}$ is symmetric:

$$J_{\eta,u} = \begin{pmatrix} 0 & -\partial_x \\ -\partial_x & 0 \end{pmatrix}.$$

We now proceed to derive a system of equations which is similar to the Whitham equation (1), but allows bi-directional wave propagation. This system will be a stepping stone on the way to a derivation of (1), but may also be of independent interest. Consider a wavefield having a characteristic wavelength l and a characteristic amplitude a. Taking into account the nondimensionalization, the two scalar parameters $\lambda = l/h_0$ and $\alpha = a/h_0$ appear. In order to introduce the long-wave and small amplitude approximation into the non-dimensional problem, we use the scaling $\tilde{x} = \frac{1}{\lambda}x$, and $\eta = \alpha\tilde{\eta}$. This induces the transformation $\tilde{D} = \lambda D = -\lambda i\partial x$. If the energy is nondimensionalized in accord with the nondimensionalization mentioned earlier, then the natural scaling for the Hamiltonian is $\tilde{H} = \alpha^2 H$. In addition, the unknown u is scaled as $u = \alpha\tilde{u}$. The scaled Hamiltonian (12) is then written as

$$\begin{aligned}\tilde{H} = {} & \frac{1}{2}\int_{\mathbb{R}} \tilde{\eta}^2\,dx + \frac{1}{2}\int_{\mathbb{R}} \tilde{u}\left[1 - \frac{1}{3}\lambda^{-2}\tilde{D}^2 + \cdots\right]\tilde{u}\,dx \\ & + \frac{\alpha}{2}\int_{\mathbb{R}} \tilde{\eta}\tilde{u}^2\,dx - \frac{\alpha}{2}\int_{\mathbb{R}} \tilde{u}\left[\lambda^{-1}\tilde{D} - \frac{1}{3}\lambda^{-3}\tilde{D}^3 + \cdots\right] \\ & \times \tilde{\eta}\left[\lambda^{-1}\tilde{D} - \frac{1}{3}\lambda^{-3}\tilde{D}^3 + \cdots\right]\tilde{u}\,dx.\end{aligned}$$

Let us now introduce the small parameter $\mu = \frac{1}{\lambda}$, and assume for simplicity that $\alpha = e^{-\kappa/\mu^\nu}$, which corresponds to the case where $W(\kappa, \nu) = 1$. Then the Hamiltonian can be written in the following form:

$$\begin{aligned}\tilde{H} = {} & \frac{1}{2}\int_{\mathbb{R}} \tilde{\eta}^2\,dx + \frac{1}{2}\int_{\mathbb{R}} \tilde{u}\left[1 - \frac{1}{3}\mu^2\tilde{D}^2 + \cdots\right]\tilde{u}\,dx \\ & + \frac{e^{-\kappa/\mu^\nu}}{2}\int_{\mathbb{R}} \tilde{\eta}\tilde{u}^2\,dx - \frac{e^{-\kappa/\mu^\nu}}{2}\int_{\mathbb{R}} \tilde{u}\left[\mu\tilde{D} - \frac{1}{3}\mu^3\tilde{D}^3 + \cdots\right] \\ & \times \tilde{\eta}\left[\mu\tilde{D} - \frac{1}{3}\mu^3\tilde{D}^3 + \cdots\right]\tilde{u}\,dx.\end{aligned}$$

Disregarding terms of order $\mathcal{O}(\mu^2 e^{-\kappa/\mu^\nu})$, but not of order $\mathcal{O}(e^{-\kappa/\mu^\nu})$ yields the expansion

$$\begin{aligned}\tilde{H} = {} & \frac{1}{2}\int_{\mathbb{R}} \tilde{\eta}^2\,dx + \frac{1}{2}\int_{\mathbb{R}} \tilde{u}\left[1 - \frac{1}{3}\mu^2\tilde{D}^2 + \cdots\right]\tilde{u}\,dx \\ & + \frac{e^{-\kappa/\mu^\nu}}{2}\int_{\mathbb{R}} \tilde{\eta}\tilde{u}^2\,dx. \qquad (14)\end{aligned}$$

Note that by taking μ small enough, an arbitrary number of terms of algebraic order in μ may be kept in the asymptotic series, so that the truncated version of the Hamiltonian in dimensional variables may be written as

$$H = \frac{1}{2}\int_{\mathbb{R}} \left[\eta^2 + u\mathcal{K}_0^N(\eta)u + u\eta u\right]dxdz. \qquad (15)$$

However, the difference between $\mathcal{K}_0$ and $\mathcal{K}_0^N$ is below the order of approximation, so that it is possible to formally define the truncated Hamiltonian with $\mathcal{K}_0$ instead of $\mathcal{K}_0^N$.
Hence, the Whitham system is obtained from the Hamiltonian (15) as follows:

$$\eta_t = -\partial_x\frac{\delta H}{\delta u} = -\mathcal{K}_0 u_x - (\eta u)_x, \qquad (16)$$

$$u_t = -\partial_x\frac{\delta H}{\delta \eta} = -\eta_x - uu_x. \qquad (17)$$

One may also derive a higher-order equation by keeping terms of order $\mathcal{O}(\mu^2 e^{-\kappa/\mu^\nu})$, but discarding terms of order $\mathcal{O}(\mu^4 e^{-\kappa/\mu^\nu})$. In this case we find the system

$$\begin{aligned}\eta_t &= -\mathcal{K}_0 u_x - (\eta u)_x - (\eta u_x)_{xx}, \\ u_t &= -\eta_x - uu_x + u_x u_{xx}.\end{aligned}$$

3. Derivation of evolution equations of Whitham type

In order to derive the Whitham equation for uni-directional wave propagation, it is important to understand how solutions of the Whitham system (16)–(17) can be restricted to either left or right-going waves. As it will turn out, if η and u are such that $\eta = Ku$, then this pair of functions represents a solution of (16)–(17) which is propagating to the right. Indeed, let us analyze the relation between η and u in the linearized Whitham system

$$\eta_t = -\mathcal{K}_0 u_x, \qquad (18)$$

$$u_t = -\eta_x. \qquad (19)$$

Considering a solution of the system (18)–(19) in the form

$$\eta(x,t) = Ae^{(i\xi x - i\omega t)}, \qquad u(x,t) = Be^{(i\xi x - i\omega t)}, \qquad (20)$$

gives rise to the matrix equation

$$\begin{pmatrix} -\omega & \frac{\tanh\xi}{\xi}\xi \\ \xi & -\omega \end{pmatrix}\begin{pmatrix} A \\ B \end{pmatrix} = \begin{pmatrix} 0 \\ 0 \end{pmatrix}. \qquad (21)$$

If existence of a nontrivial solution of this system is to be guaranteed, the determinant of the matrix has to be zero, so that we have $\omega^2 - \frac{\tanh\xi}{\xi}\xi^2 = 0$. Defining the phase speed as $c = \omega/\xi$, we obtain the dispersion relation

$$c = \pm\sqrt{\frac{\tanh\xi}{\xi}}. \qquad (22)$$

The choice of $c > 0$ corresponds to right-going wave solutions of the system (18)–(19), and the relation between η and u can be deduced from (19). Accordingly, it is expedient to separate solutions into a right-going part r and a left-going part s which are defined by

$$r = \frac{1}{2}(\eta + Ku), \qquad s = \frac{1}{2}(\eta - Ku).$$

According to the transformation theory detailed in [22], if the unknowns r and s are used instead of η and u, the structure map changes to

$$J_{r,s} = \left(\frac{\partial F}{\partial(\eta,u)}\right)J_{\eta,u}\left(\frac{\partial F}{\partial(\eta,u)}\right)^T = \begin{pmatrix} -\frac{1}{2}\partial_x K & 0 \\ 0 & \frac{1}{2}\partial_x K \end{pmatrix}. \qquad (23)$$

We now use the same scaling for both dependent and independent variables as before. Thus we have $r = \alpha\tilde{r}$ and $s = \alpha\tilde{s}$. The Hamiltonian is written in terms of $\tilde{r}$ and $\tilde{s}$ as

$$\begin{aligned}\tilde{H} = {} & \frac{1}{2}\int_{\mathbb{R}} (\tilde{r}+\tilde{s})^2\,dx \\ & + \frac{1}{2}\int_{\mathbb{R}} \tilde{K}^{-1}(\tilde{r}-\tilde{s})\left[1 - \frac{1}{3}\mu^2\tilde{D}^2 + \cdots\right]\tilde{K}^{-1}(\tilde{r}-\tilde{s})\,dx \\ & + \frac{\alpha}{2}\int_{\mathbb{R}} (\tilde{r}+\tilde{s})\left(\tilde{K}^{-1}(\tilde{r}-\tilde{s})\right)^2\,dx \\ & - \frac{\alpha}{2}\int_{\mathbb{R}} \tilde{K}^{-1}(\tilde{r}-\tilde{s})\left[\mu\tilde{D} - \frac{1}{3}\mu^3\tilde{D}^3 + \cdots\right](\tilde{r}+\tilde{s}) \\ & \times \left[\mu\tilde{D} - \frac{1}{3}\mu^3\tilde{D}^3 + \cdots\right]\tilde{K}^{-1}(\tilde{r}-\tilde{s})\,dx.\end{aligned}$$

Following the transformation rules, the structure map transforms to $J_{\tilde{r},\tilde{s}} = 1/\alpha^2 J_{r,s}$. In addition, the time scaling $t = \lambda\tilde{t}$ is employed. Since the focus is on right-going solutions, the equation to be considered is

$$\lambda\tilde{r}_{\tilde{t}} = -\frac{1}{2\alpha^2}\lambda\partial_{\tilde{x}}\tilde{K}\left[\frac{\delta(\alpha^2\tilde{H})}{\delta\tilde{r}}\right]. \tag{24}$$

So far, this equation is exact. If we now assume that s is of the order of $\mathcal{O}(\mu^2 e^{-\kappa/\mu^\nu})$, then the equation for $\tilde{r}$ is

$$\begin{aligned}\tilde{r}_{\tilde{t}} = &-\frac{1}{2}\partial_{\tilde{x}}\left[1-\frac{1}{6}\mu^2\tilde{D}^2+\cdots\right]\left\{2\tilde{r}+\frac{\alpha}{2}\left(\left[1+\frac{1}{6}\mu^2\tilde{D}^2+\cdots\right]\tilde{r}\right)^2\right.\\ &+\alpha\left[1+\frac{1}{6}\mu^2\tilde{D}^2+\cdots\right]\left(\tilde{r}\left[1+\frac{1}{6}\mu^2\tilde{D}^2+\cdots\right]\tilde{r}\right)\\ &-\frac{\alpha}{2}\left(\left[\mu\tilde{D}-\frac{1}{3}\mu^3\tilde{D}^3+\cdots\right]\left[1+\frac{1}{6}\mu^2\tilde{D}^2+\cdots\right]\tilde{r}\right)^2\\ &-\alpha\left[\mu\tilde{D}-\frac{1}{3}\mu^3\tilde{D}^3+\cdots\right]\left[1+\frac{1}{6}\mu^2\tilde{D}^2+\cdots\right]\\ &\left.\times\left(\tilde{r}\left[\mu\tilde{D}-\frac{1}{3}\mu^3\tilde{D}^3+\cdots\right]\left[1+\frac{1}{6}\mu^2\tilde{D}^2+\cdots\right]\tilde{r}\right)\right\}\\ &+\mathcal{O}(\alpha\mu^2).\end{aligned}$$

As in the case of the Whitham system, we use $\alpha = \mathcal{O}(e^{-\kappa/\mu^\nu})$, and disregard terms of order $\mathcal{O}(\mu^2 e^{-\kappa/\mu^\nu})$, but not of order $\mathcal{O}(e^{-\kappa/\mu^\nu})$. This procedure yields the Whitham equation (1) which is written in nondimensional variables as

$$r_t = -Kr_x - \frac{3}{2}rr_x.$$

As was the case for the system found in the previous section, it is also possible here to include terms of order $\mathcal{O}(\mu^2 e^{-\kappa/\mu^\nu})$, resulting in the higher-order equation

$$r_t = -Kr_x - \frac{3}{2}rr_x - \frac{13}{12}r_x r_{xx} - \frac{5}{12}rr_{xxx}.$$

4. Numerical results

In this section, the performance of the Whitham equation as a model for surface water waves is compared to the KdV equation (3), the BBM equation (6), and the Padé (2,2) equation (7). For this purpose initial data are imposed, the Whitham, KdV, BBM, and Padé equations are solved numerically, and the solutions are compared to numerical solutions of the full Euler equations with free-surface boundary conditions. We continue to work in normalized variables, such as stated in the beginning of Section 2.

The numerical treatment of the three model equations is by a standard pseudo-spectral scheme, such as explained in [23,24] for example. For the time stepping, an efficient fourth-order implicit method developed in [25] is used. The numerical treatment of the free-surface problem for the Euler equations is based on a conformal mapping of the fluid domain into a rectangle. In the time-dependent case, this method has roots in the work of Ovsyannikov [26], and was later used in [27–30]. The particular method used for the numerical experiments reported here is a pseudo-spectral scheme which is detailed in [31].

Initial conditions for the Euler equations are chosen in such a way that the solutions are expected to be right moving. This is achieved by posing an initial surface disturbance $\eta_0(x)$ together with the trace of the potential $\Phi(x) = \int_0^x \eta_0(x')\,dx'$. In order to normalize the data, we choose $\eta_0(x)$ in such a way that the average of $\eta_0(x)$ over the computational domain is zero. The experiments are performed with several different amplitudes α and wavelengths λ (for the purpose of this section, we define the wavelength λ as the distance between the two points x_1 and x_2 at which $\eta_0(x_1) = \eta_0(x_2) = \alpha/2$). Both positive and negative initial disturbances are considered. While disturbances with positive main part have been studied widely, an initial wave of depression is somewhat more exotic, but nevertheless important, as shown for instance in [32]. A summary of the experiments' settings is given in Table 1. Experiments run with an initial wave of elevation are labeled as *positive*, and experiments run with an initial wave of depression are labeled as *negative*. The domain for the computations is $-L \le x \le L$, with $L = 50$. The function initial data in the *positive* cases is given by

Table 1
Summary of the Stokes number, nondimensional amplitude and nondimensional wavelength of the initial data used in the numerical experiments.

Experiment	Stokes number	α	λ
A	0.2	0.1	$\sqrt{2}$
B	0.2	0.2	1
C	1	0.1	$\sqrt{10}$
D	1	0.2	$\sqrt{5}$
E	5	0.1	$\sqrt{50}$
F	5	0.2	5

$$\eta_0(x) = \alpha\,\mathrm{sech}^2(f(\lambda)x) - C, \tag{25}$$

where

$$f(\lambda) = \frac{2}{\lambda}\log\left(\frac{1+\sqrt{1/2}}{\sqrt{1/2}}\right), \quad \text{and} \quad C = \frac{1}{L}\frac{\alpha}{f(\lambda)}\tanh\left(\frac{L}{f(\lambda)}\right)$$

and C and $f(\lambda)$ are chosen so that $\int_{-L}^{L}\eta_0(x)dx = 0$, and the wavelength λ is the distance between the two points x_1 and x_2 at which $\eta_0(x_1) = \eta_0(x_2) = a/2$. The velocity potential in this case is given by

$$\Phi(x) = \frac{\alpha}{f(\lambda)}\tanh(f(\lambda)x) - Cx. \tag{26}$$

In the *negative* case, the initial data are given by

$$\eta_0(x) = -\alpha\,\mathrm{sech}^2(f(\lambda)x) + C.$$

The definitions for $f(\lambda)$ and C are the same, and the velocity potential is

$$\Phi(x) = -\frac{\alpha}{f(\lambda)}\tanh(f(\lambda)x) + Cx.$$

In Figs. 3 and 4, the time evolution of a wave with an initial narrow peak and one with an initial narrow depression at the center is shown. The amplitude is $\alpha = 0.2$, and the wavelength is $\lambda = \sqrt{5}$. In Fig. 3, the time evolution according to the Euler, Whitham, KdV and BBM equations are shown, and in Fig. 4, the time evolution according to the Euler, Whitham, and Padé (2,2) equations are shown.

It appears in Fig. 3 that the KdV equation produces a significant number of spurious oscillations, the BBM equation also produces a fair number of spurious oscillations, and the Whitham equation produces fewer small oscillations than Euler equations. Moreover, while the highest peak in the upper panels in Fig. 3 is underpredicted by the KdV and BBM equation, the Whitham equation produces peaks which are slightly too high. In the case of an initial depression, the Whitham equation also produces some peaks which are too high, but on the other hand, the KdV and the BBM equations introduce phase errors in the main oscillations. As is visible in Fig. 4, the Padé (2,2) equation reproduces the leading wave fairly accurately, but overpredicts the trailing oscillations in the case of a positive disturbance, and underpredicts the trailing oscillations in the case of a negative initial disturbance. Nevertheless, since the Padé (2,2) does not introduce a phase error, the overall performance is better than that of the KdV and BBM equations.

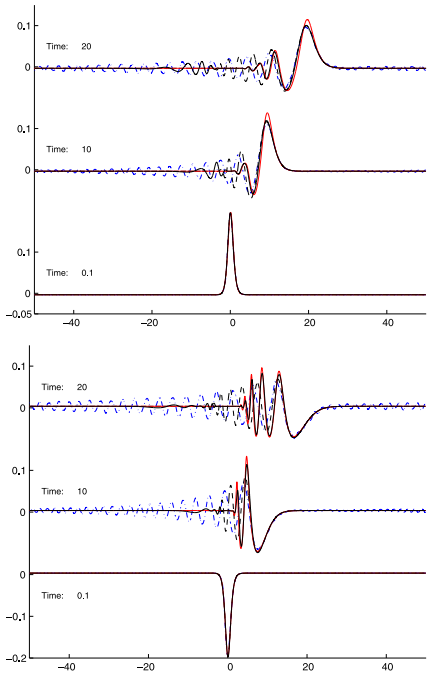

Fig. 3. Wave profiles at three different times: – Euler (black line), -.- KdV, - - BBM, – Whitham (red line). Experiment D: $\mathcal{S} = 1$, $\alpha = 0.2$, $\lambda = \sqrt{5}$. Upper panel: positive case; lower panel: negative case. Horizontal axis: x/h_0, vertical axis: z/h_0. Snapshots are given at nondimensional time $t/\sqrt{h_0/g}$.

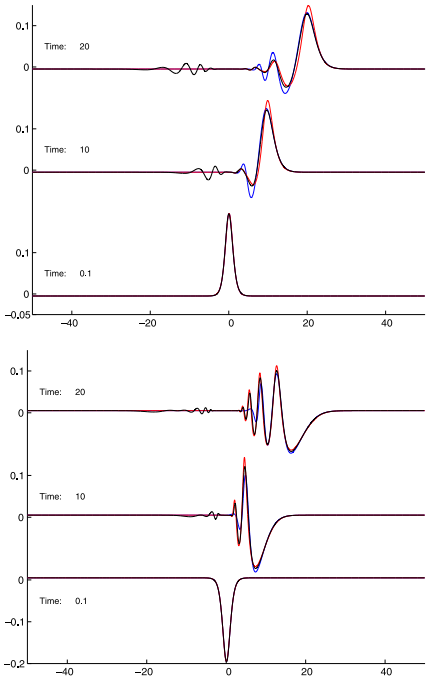

Fig. 4. Wave profiles at three different times: – Euler (black line), – Padé (blue line), – Whitham (red line). Experiment D: $\mathcal{S} = 1$, $\alpha = 0.2$, $\lambda = \sqrt{5}$. Upper panel: positive case; lower panel: negative case. Horizontal axis: x/h_0, vertical axis: z/h_0. Snapshots are given at nondimensional time $t/\sqrt{h_0/g}$.

In order to compare the performance of the four approximate equations in a more quantitative manner, the discrepancies between solutions of the model equations and the prediction due to solving the Euler equations are measured in an integral norm. In the center right panels of Figs. 5 and 6, the computations from Figs. 3 and 4 are summarized by plotting the normalized L^2-error between the KdV, BBM, Padé and Whitham, respectively, and the Euler solutions as a function of non-dimensional time. Using this quantitative measure of comparison, it appears that the Whitham equation gives the best overall rendition of the free surface dynamics predicted by the Euler equations.

In the center left panels of Figs. 5 and 6, a similar computation with $\mathcal{S} = 1$, but smaller amplitude is analyzed. Also in these cases, it appears that the Whitham equation gives a good approximation to the corresponding Euler solutions, and in particular, a much better approximation than either the KdV or the BBM equation. The Padé equation also does better than both KdV and BBM equations, but not better than the Whitham equation.

Figs. 5 and 6 show comparisons in several other cases of both positive and negative initial amplitude, and Stokes numbers $\mathcal{S} = 0.2$, $\mathcal{S} = 1$ and $\mathcal{S} = 5$. In most cases, the normalized L^2-error between the Whitham and Euler solutions is similar or smaller than the errors between the Euler solutions and the other three model equations. However, the Padé equation generally outperforms both the KdV and the BBM equation by some measure.

The only case in this study in which the KdV, BBM and Padé equations outperform the Whitham equation is in the case of very long positive initial disturbances. The case when $\mathcal{S} = 5$ is shown in the lower panels of Fig. 5. However, even in this case, the Whitham equation yields approximations of the Euler solutions which are similar or better than in the case of smaller wavelengths. In addition, in the case of negative initial data, the performance of the Whitham equation is on par with the KdV, BBM and Padé equations in the case when $\mathcal{S} = 5$ (lower panels of Fig. 5).

5. Conclusion

In this article, the Whitham equation (1) has been studied as an approximate model equation for wave motion at the surface of a perfect fluid. Numerical integration of the equation suggests that broad classes of initial data decompose into individual solitary waves. The wavelength–amplitude ratio of these approximate solitary waves has been studied, and it was found that this ratio can be described by an exponential relation of the form $\frac{a}{h_0} \sim e^{-\kappa(l/h_0)^\nu}$. Using this scaling in the Hamiltonian formulation of the water-wave problem, a system of evolution equations has been derived which contains the exact dispersion relation of the water-wave problem in its linear part. Restricting to one-way propagation, the Whitham equation emerged as a model which combines the usual quadratic nonlinearity with one branch of the exact dispersion relation of the water-wave problem. The performance of the Whitham equation in the approximation of

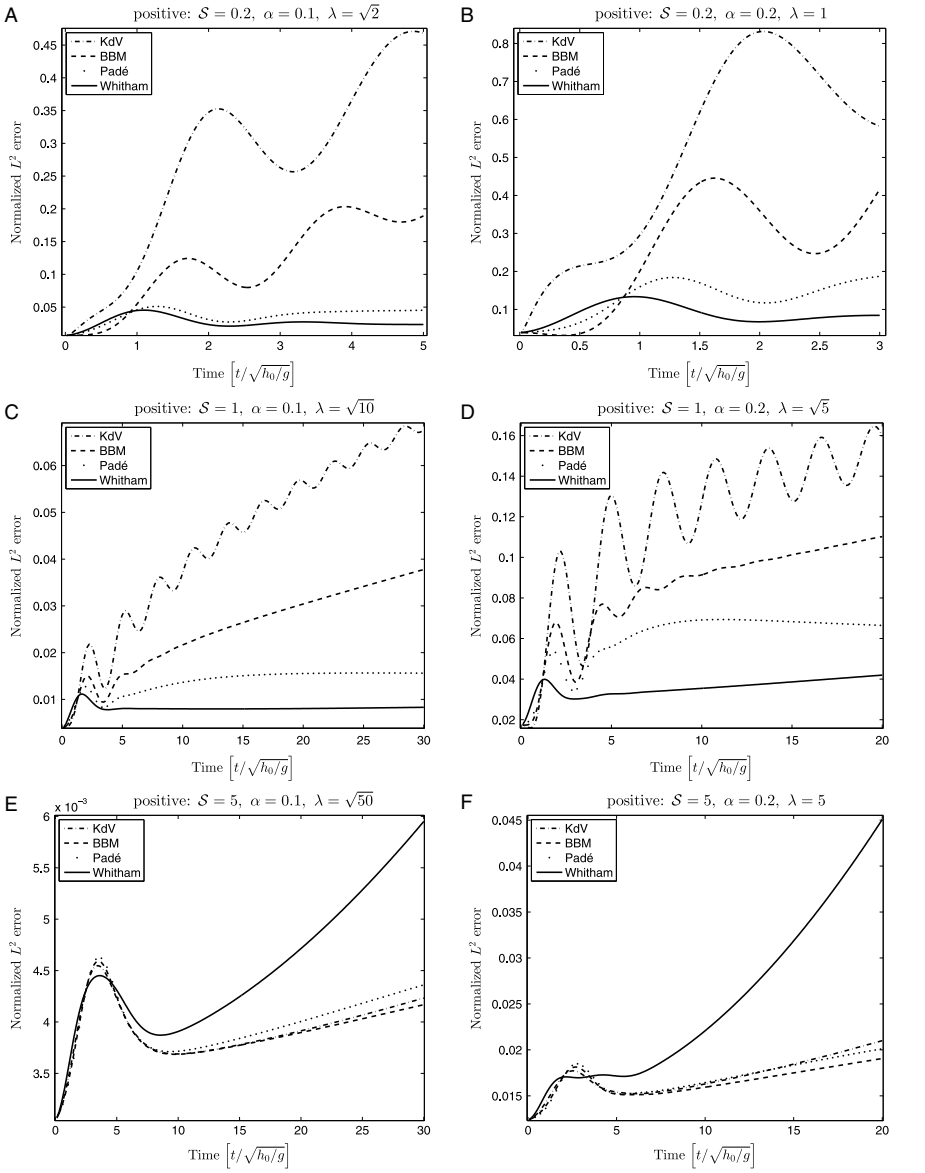

Fig. 5. L^2 errors in approximation of solutions to full Euler equations by different model equations: cases A and B ($\mathcal{S} = 0.2$), cases C and D ($\mathcal{S} = 1$), cases E and F ($\mathcal{S} = 5$), positive.

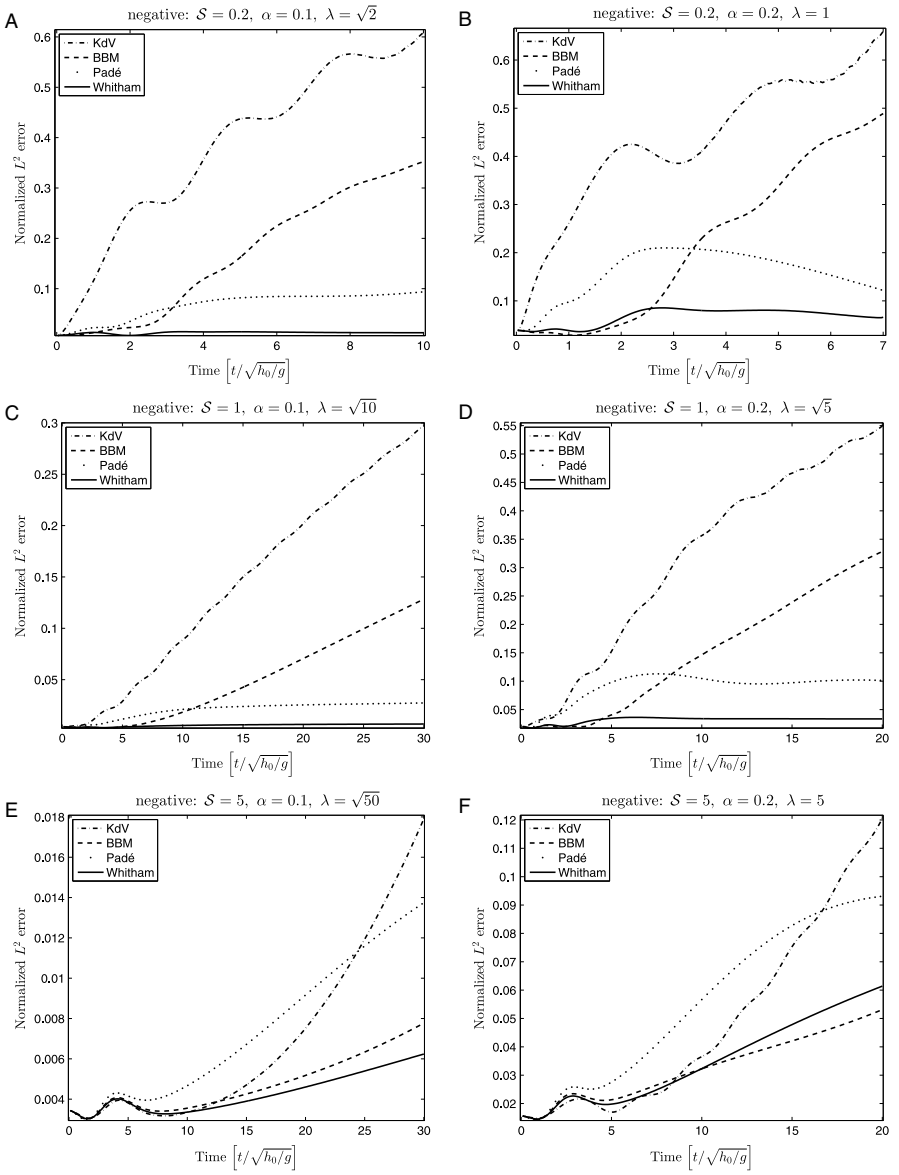

Fig. 6. L^2 errors in approximation of solutions to full Euler equations by different model equations: cases A and B ($\mathcal{S} = 0.2$), cases C and D ($\mathcal{S} = 1$), cases E and F ($\mathcal{S} = 5$), negative.

solutions of the Euler equations free-surface boundary conditions was analyzed, and compared to the performance of the KdV and BBM equations, and to the Padé (2,2) model. It was found that the Whitham equation gives a more faithful representation of the solutions of the Euler equations than either the KdV or the BBM equations, except in the case of very long waves with positive main part. In this last case, the KdV and BBM equations have the upper hand over the Whitham equation. The Padé (2,2) model also outperforms the KdV and BBM equations, but does not quite as well as the Whitham equation for shorter waves and negative disturbances. However, in the case of very long waves with positive main part, the Padé model stays on par with the KdV and BBM equations.

Acknowledgment

This research was supported by the Research Council of Norway (213474/F20).

References

[1] G.B. Whitham, Variational methods and applications to water waves, Proc. R. Soc. Lond. Ser. A 299 (1967) 6–25.
[2] M. Ehrnström, M.D. Groves, E. Wahlén, Solitary waves of the Whitham equation - a variational approach to a class of nonlocal evolution equations and existence of solitary waves of the Whitham equation, Nonlinearity 25 (2012) 2903–2936.
[3] M. Ehrnström, H. Kalisch, Traveling waves for the Whitham equation, Differential Integral Equations 22 (2009) 1193–1210.
[4] D. Lannes, The Water Waves Problem, in: Mathematical Surveys and Monographs, vol. 188, Amer. Math. Soc, Providence, 2013.
[5] D. Lannes, J.-C. Saut, Remarks on the full dispersion Kadomtsev-Petviashvli equation, Kinet. Relat. Models 6 (2013) 989–1009.
[6] C. Klein, J.-C. Saut, A numerical approach to blow-up issues for dispersive perturbations of Burgers' equation, Physica D 295 (2015) 46–65.
[7] P. Aceves-Sánchez, A.A. Minzoni, P. Panayotaros, Numerical study of a nonlocal model for water-waves with variable depth, Wave Motion 50 (2013) 80–93.
[8] V.M. Hur, M.A. Johnson, Modulational instability in the Whitham equation of water waves, Stud. Appl. Math. 134 (1) (2015) 120–143.
[9] N. Sanford, K. Kodama, J.D. Carter, H. Kalisch, Stability of traveling wave solutions to the Whitham equation, Phys. Lett. A 378 (2014) 2100–2107.
[10] P.G. Drazin, R.S. Johnson, Solitons: an introduction, in: Cambridge Texts in Applied Mathematics, Cambridge University Press, Cambridge, 1989.
[11] G.B. Whitham, Linear and Nonlinear Waves, Wiley, New York, 1974.
[12] M. Ablowitz, H. Segur, Solitons and the inverse scattering transform, in: SIAM Studies in Applied Mathematics, vol. 4, SIAM, Philadelphia, 1981.
[13] W. Craig, C. Sulem, Numerical simulation of gravity waves, J. Comput. Phys. 108 (1993) 73–83.
[14] V.E. Zakharov, Stability of periodic waves of finite amplitude on the surface of a deep fluid, J. Appl. Mech. Tech. Phys. 9 (1968) 190–194.
[15] W. Craig, M.D. Groves, Hamiltonian long-wave approximations to the water-wave problem, Wave Motion 19 (1994) 367–389.
[16] D.H. Peregrine, Calculations of the development of an undular bore, J. Fluid Mech. 25 (1966) 321–330.
[17] T.B. Benjamin, J.L. Bona, J.J. Mahony, Model equations for long waves in nonlinear dispersive systems, Philos. Trans. R. Soc. Lond., Ser. A 272 (1972) 47–78.
[18] J.M. Witting, A unified model for the evolution of nonlinear water waves, J. Comput. Phys. 56 (1984) 203–236.
[19] R. Fetecau, D. Levy, Approximate model equations for water waves, Commun. Math. Sci. 3 (2) (2005) 159–170.
[20] A.A. Petrov, Variational statement of the problem of liquid motion in a container of finite dimensions, Prikl. Math. Mekh. 28 (1964) 917–922.
[21] D.P. Nicholls, F. Reitich, A new approach to analyticity of Dirichlet-Neumann operators, Proc. Roy. Soc. Edinburgh Sect. A 131 (2001) 1411–1433.
[22] W. Craig, P. Guyenne, H. Kalisch, Hamiltonian long-wave expansions for free surfaces and interfaces, Comm. Pure Appl. Math. 58 (2005) 1587–1641.
[23] M. Ehrnström, H. Kalisch, Global bifurcation for the Whitham equation, Math. Mod. Nat. Phenomena 8 (2013) 13–30.
[24] B. Fornberg, G.B. Whitham, A numerical and theoretical study of certain nonlinear wave phenomena, Phil. Trans. Roy. Soc. A 289 (1978) 373–404.
[25] J. De Frutos, J.M. Sanz-Serna, An easily implementable fourth-order method for the time integration of wave problems, J. Comput. Phys. 103 (1992) 160–168.
[26] L.V. Ovsyannikov, To the shallow water theory foundation, Arch. Mech. 26 (1974) 407–422.
[27] A.I. Dyachenko, E.A. Kuznetsov, M.D. Spector, V.E. Zakharov, Analytical description of the free surface dynamics of an ideal fluid (canonical formalism and conformal mapping), Phys. Lett. A 221 (1996) 73–79.
[28] Y.A. Li, J.M. Hyman, W. Choi, A numerical study of the exact evolution equations for surface waves in water of finite depth, Stud. Appl. Math. 113 (2004) 303–324.
[29] W. Choi, R. Camassa, Exact evolution equations for surface waves, J. Eng. Mech. 125 (1999) 756–760.
[30] P. Milewski, J.-M. Vanden-Broeck, Z. Wang, Dynamics of steep two-dimensional gravity-capillary solitary waves, J. Fluid Mech. 664 (2010) 466–477.
[31] D. Mitsotakis, D. Dutykh, J.D. Carter, On the nonlinear dynamics of the traveling-wave solutions of the Serre equations (2014) submitted for publication, http://arxiv.org/abs/1404.6725.
[32] J.L. Hammack, H. Segur, The Korteweg–de Vries equation and water waves. Part 2. Comparison with experiments, J. Fluid Mech. 65 (1974) 289–314.

Paper C

A numerical study of nonlinear dispersive wave models with SpecTraV-Vave

Henrik Kalisch, Daulet Moldabayev, Olivier Verdier

Electronic Journal of Differential Equations **2017**, No. 62, pp. 1–23, (2017)
http://ejde.math.txstate.edu or http://ejde.math.unt.edu

C

Electronic Journal of Differential Equations, Vol. 2017 (2017), No. 62, pp. 1–23.
ISSN: 1072-6691. URL: http://ejde.math.txstate.edu or http://ejde.math.unt.edu

A NUMERICAL STUDY OF NONLINEAR DISPERSIVE WAVE MODELS WITH SPECTRAVVAVE

HENRIK KALISCH, DAULET MOLDABAYEV, OLIVIER VERDIER

Communicated by Jerry Bona

Abstract. In nonlinear dispersive evolution equations, the competing effects of nonlinearity and dispersion make a number of interesting phenomena possible. In the current work, the focus is on the numerical approximation of traveling-wave solutions of such equations. We describe our efforts to write a dedicated Python code which is able to compute traveling-wave solutions of nonlinear dispersive equations in a very general form.

The SpecTraVVave code uses a continuation method coupled with a spectral projection to compute approximations of steady symmetric solutions of this equation. The code is used in a number of situations to gain an understanding of traveling-wave solutions. The first case is the Whitham equation, where numerical evidence points to the conclusion that the main bifurcation branch features three distinct points of interest, namely a turning point, a point of stability inversion, and a terminal point which corresponds to a cusped wave.

The second case is the so-called modified Benjamin-Ono equation where the interaction of two solitary waves is investigated. It is found that two solitary waves may interact in such a way that the smaller wave is annihilated. The third case concerns the Benjamin equation which features two competing dispersive operators. In this case, it is found that bifurcation curves of periodic traveling-wave solutions may cross and connect high up on the branch in the nonlinear regime.

1. Introduction

This article concerns traveling wave solutions for a class of nonlinear dispersive equations of the form

$$u_t + [f(u)]_x + \mathcal{L}u_x = 0, \tag{1.1}$$

where $\mathcal{L}$ is a self-adjoint operator, and f is a real-valued function with $f(0) = 0$ and $f'(0) = 0$, and which satisfies certain growth conditions. Equations of this form arise routinely in the study of wave problems in fluid mechanics and many other contexts. A prototype of such an equation is the KdV equation that appears if $\mathcal{L} = I + \frac{1}{6}\partial_x^2$ and $f(u) = \frac{3}{4}u^2$. In the current work, the operator $\mathcal{L}$ is considered to be given as a Fourier multiplier operator, such as for instance in the Benjamin–Ono equation, which arises in the study of interfacial waves. In this case, the Fourier

2010 *Mathematics Subject Classification.* 35C07, 35Q53, 45J05, 65M70.
Key words and phrases. Traveling Waves; nonlinear dispersive equations; bifurcation; solitary waves.

Submitted November 7, 2016. Published March 2, 2017.

multiplier operator is given by $\mathcal{L} = I - \mathcal{H}\partial_x$, where the Hilbert transform $\mathcal{H}$ is defined as

$$\mathcal{H}u(x) = \frac{1}{\pi}\,\mathrm{p.v.}\int_{-\infty}^{\infty}\frac{u(x-y)}{y}\,\mathrm{d}y, \quad \widehat{\mathcal{H}u}(k) = -\mathrm{i}\,\mathrm{sgn}(k)\widehat{u}(k). \tag{1.2}$$

We also study in detail traveling wave solutions of the Whitham equation, which appears when $\mathcal{L}$ is given by convolution with the integral kernel K_{h_0} in the form

$$\mathcal{L}u(x) = \int_{-\infty}^{\infty} K_{h_0}(y)u(x-y)\,\mathrm{d}y, \quad \widehat{K_{h_0}}(k) = \sqrt{\frac{g\tanh(h_0k)}{k}}, \tag{1.3}$$

and f is the same function as in the KdV equation.

The particular form of equation (1.1) exhibits the competing effects of dispersion and nonlinearity, which gives rise to a host of interesting phenomena. The most well known special phenomenon is the existence of solitary waves and of periodic traveling waves containing higher Fourier modes. Indeed, note that in the purely dispersive model $u_t + \mathcal{L}u_x = 0$, the only possible permanent progressive waves are simple sinusoidal waves, while in the nonlinear model (1.1) higher Fourier modes must be considered to obtain solutions.

The order of the operator $\mathcal{L}$ appearing in (1.1) has a major effect on the types of solutions that may be found. A higher-order operator, such as in the Korteweg–de Vries equation, acts as a smoothing operator because of its effect of spreading different frequency components out due to a strongly varying phase speed [35]. Lower-order operators such as the operator K_{h_0} in (1.3) appearing in the Whitham equation may allow solutions to develop singularities, such as derivative blow-up (see [29, 31]) and formation of cusps (see [25]).

On the other hand, highly nonlinear functions $f(u)$ may lead to L^∞-blow-up. For instance, the generalized KdV equation which is written in normalized form as

$$u_t + u^p u_x + u_x + u_{xxx} = 0, \tag{1.4}$$

features global existence of solutions for $p = 1, 2, 3$, but the solutions blow-up in the critical case $p = 4$ (the case $p \geq 5$ is open). In the case of the generalized Benjamin–Ono equation

$$u_t + u^p u_x + u_x - \mathcal{H}u_{xx} = 0,$$

where $\mathcal{H}$ is the Hilbert transform, numerical evidence points to singularity formation for $p > 2$ [11], but no proofs are available at this time.

To study different phenomena related to equations of the form (1.1) and their traveling wave solutions, a Python-based solver package SpecTraVVave was developed by the authors [41]. The general idea behind the solver is to use a numerical continuation method [36] implemented with a pseudo-spectral algorithm. Similar previous projects include AUTO [21] and Wavetrain [49]. AUTO is written in *C*, whereas Wavetrain is written in *Fortran*. Both programs are efficient and very general, as they are able to cover a wide range of problems involving bifurcation analyses. However, from a user's perspective, such a generality coupled with low level programming languages may lead to some difficulties in utilizing these programs efficiently.

SpecTraVVave is designed to provide researchers with a simple yet effective tool for investigating problems on traveling waves. The package is flexible, and its functionality can be easily expanded. The availability of the IPython notebook [45]

makes the solver very interactive, so that it should be easier for new users to get started.

To maximize ease of use, SpecTraVVave was designed to find even solutions of (1.1). Symmetry of steady solutions can be proved for some of the models in the form (1.1), but not for all [16]. Some of these equations also admit non-smooth solutions, for instance as termination points of a bifurcation branch. This happens for example for the Whitham equation, which features bifurcation curves which terminate in a solution with a cusp [25]. One of the goals of the present paper is to investigate the precise nature of the termination of the bifurcation curve.

The content of this article is structured as follows. A mathematical description of the numerical method of SpecTraVVave is given in Section 2. Section 3 presents results of different experiments carried out with the package. Concluding remarks are given in Section 4. A method for finding initial guesses for the solver is described in Section 5. Section 6 contains a schematic of program and a description of its workflow.

2. Spectral scheme and construction of nonlinear system.

2.1. **Cosine collocation method.** To compute traveling wave solutions to (1.1) the following ansatz is employed:

$$u(x,t) = \phi(x - ct).$$

Thus, the equation takes the form

$$\phi' + [f(\phi)]' + \mathcal{L}\phi' = 0,$$

which can be integrated to give

$$-c\phi + f(\phi) + \mathcal{L}\phi = B. \tag{2.1}$$

The constant B is a priori undetermined. One may set the B equal to zero as a way of normalizing the solutions. Another option is to impose an additional condition, for example that the integral of ϕ over one wavelength be zero. In this case, B will be found along with the solution ϕ.

We consider $\mathcal{L}$ as a Fourier multiplier operator with symbol $\alpha(k)$. We also assume that f is at least twice differentiable, and we have $f(0) = 0$ and $f'(0) = 0$. When computing traveling-wave solutions we focus on even periodic solutions. While it can be proved in some cases that solutions of (2.1) must be even, this is not known for a general operator $\mathcal{L}$. Nevertheless, we make this assumption here in order to make the numerical procedure as uniform as possible. For even periodic solutions, one may use a cosine collocation instead of a Fourier method. In particular, using the cosine functions as basis elements automatically removes the inherent symmetries due to reflective and translational symmetry. Moreover, the number of unknowns is reduced by a factor of 2, and the problem of the asymmetric arrangement of nodes in the FFT is circumvented. Of course, all these problems could also be dealt with a collocation method based on the Fourier basis, but the cosine basis does all of the above automatically. In addition, the Python cosine transform is based on an integrated algorithm, which relies on an optimized version of the discrete cosine transform (DCT).

The following description of computation scheme was presented in detail in [24], but we will briefly repeat it here for consistency of the manuscript. For the purpose of clarity, we will refer to full wavelength L of a solution as the (full) wavelength,

and half of fundamental wavelength will be called half-wavelength. Such a definition is required because the method computes a half of a solution profile, the other half is automatically constructed due to symmetry.

Traveling wave solutions to (2.1) are to be computed in the form of a linear combination of cosine functions of different wave-numbers, i.e., in the space

$$\mathcal{S}_N = \operatorname{span}_{\mathbb{R}}\{\cos(lx) : 0 \le l \le N-1\}. \tag{2.2}$$

This is a subspace of $L^2(0,2\pi)$, and the collocation points $x_n = \pi\frac{2n-1}{2N}$ for $n = 1,\dots,N$ are used to discretize the domain. If the required full wavelength of solutions is to be $L \neq 2\pi$, one can use a scaling on the x-variable. Defining the new variable

$$x' = \frac{L}{2\pi}x,$$

yields collocation points x'_n and wavenumbers κ_l defined by

$$x'_n = \frac{L}{2}\frac{2n-1}{2N}, \qquad \kappa_l = \frac{2\pi}{L}l.$$

We are seeking a function $\phi_N \in \mathcal{S}_N$ that satisfies the equations

$$-c\phi_N(x'_n) + f(\phi_N)(x'_n) + \mathcal{L}^N\phi_N(x'_n) = 0, \tag{2.3}$$

at the collocation points x'_n. The operator $\mathcal{L}^N$ is the discrete form of the operator $\mathcal{L}$, and ϕ_N is the discrete cosine representation of ϕ which is given by

$$\phi_N(x') = \sum_{l=0}^{N-1}\omega(\kappa_l)\Phi_N(\kappa_l)\cos(\kappa_l x'),$$

$$\omega(\kappa_l) = \begin{cases}\sqrt{1/N}, & \kappa_l = 0,\\ \sqrt{2/N}, & \kappa_l > 0,\end{cases}$$

$$\Phi_N(\kappa_l) = \omega(\kappa_l)\sum_{n=1}^{N}\phi_N(x'_n)\cos(\kappa_l x'_n),$$

where $\kappa_l = 0, \frac{2\pi}{L},\dots,\frac{2\pi}{L}(N-1)$ are the scaled wavenumbers, and $\Phi_N(\cdot)$ are the discrete cosine coefficients. As equation (2.3) is enforced at the collocation points x'_n, one may evaluate the term $\mathcal{L}^N\phi_N$ using the matrix $\mathcal{L}^N(i,j)$ defined by

$$\mathcal{L}^N\phi_N(x'_i) = \sum_{j=1}^{N}\mathcal{L}^N(i,j)\phi_N(x'_j),$$

$$\mathcal{L}^N(i,j) = \sum_{l=0}^{N-1}\omega^2(\kappa_l)\alpha(\kappa_l)\cos(\kappa_l x'_i)\cos(\kappa_l x'_j),$$

where $\alpha(\cdot)$ is the Fourier multiplier function of the operator $\mathcal{L}$.

2.2. **Construction of nonlinear system.** Equation (2.3) enforced at N collocation points yields a nonlinear system of N equations in N unknowns, which can be written in shorthand as

$$F(\phi_N) = 0.$$

This system can be solved by a standard iterative method, such as Newton's method. In this system, the value of phase speed c has to be fixed for computing one particular solution. Such an approach becomes impractical when a turning point on the bifurcation curve appears.

In SpecTraVVave a different approach is employed: both the amplitude a and the phase speed c of a solution are treated as functions of a parameter θ: $a = a(\theta)$, $c = c(\theta)$. The parameter θ is to be computed from the system (2.4). This construction makes it possible to follow turning points on the bifurcation branch with relative ease. Having computed two solutions, i.e., two points on the bifurcation curve $P_1 = (c_1, a_1)$ and $P_2 = (c_2, a_2)$, one may find a direction vector $\mathbf{d} = (d^c, d^a)$ of the line that contains these points:

$$\mathbf{d}: \quad d^c = c_2 - c_1, \quad d^a = a_2 - a_1.$$

Then the point $P_3 = (c_3, a_3)$ is fixed at some (small) distance s from the point P_2 in the direction $\mathbf{d}$.

$$P_3: \quad c_3 = c_2 + s \cdot d^c, \quad a_3 = a_2 + s \cdot d^a.$$

The point P_3 plays the role of the initial guess for velocity and amplitude when computing the next solution $P_* = (c_*, a_*)$. The solution point P_* is required to lay on the line with direction vector $\mathbf{d}_\perp = (d^c_\perp, d^a_\perp)$, which is orthogonal to the vector $\mathbf{d}$.

$$\begin{aligned} \mathbf{d}_\perp: \quad & d^c_\perp = -d^a, \quad d^a_\perp = d^c, \\ P_*: \quad & c_* = c_3 + \theta d^c_\perp, \quad a_* = a_3 + \theta d^a_\perp. \end{aligned}$$

A schematic sketch of finding a new solution P_* is given in Figure 1.

The variable θ is computed by Newton's method from the extended system

$$F\begin{pmatrix} \phi_N(x_1) \\ \vdots \\ \phi_N(x_N) \\ B \\ \theta \end{pmatrix} = \begin{pmatrix} (-c + \mathcal{L}_N)\phi_N(x_1) + f(\phi_N(x_1)) - B \\ \vdots \\ (-c + \mathcal{L}_N)\phi_N(x_N) + f(\phi_N(x_N)) - B \\ \Omega(\phi_N, c, a, B) \\ \phi_N(x_1) - \phi_N(x_N) - a \end{pmatrix} = \begin{pmatrix} 0 \\ \vdots \\ 0 \\ 0 \\ 0 \end{pmatrix}. \tag{2.4}$$

Here a nonhomogeneous problem ($B \neq 0$) is considered. The equation

$$\phi_N(x_1) - \phi_N(x_N) - a = 0,$$

makes the waveheight of the computed solution to be that of a. The equation

$$\Omega(\phi_N, c, a, B) = 0,$$

is called the *boundary condition*. It allows to enforce different specifications on the computed traveling wave solution. For example, if one sets

$$\Omega(\phi_N, c, a, B) = \phi_N(x_1) + \cdots + \phi_N(x_N),$$

then *the mean of the computed wave over a period will have to be equal to zero*. One may also experiment with

$$\Omega(\phi_N, c, a, B) = B,$$

to consider the homogeneous problem ($B = 0$). It can be also interesting to set

$$\Omega(\phi_N, c, a, B) = \phi_N(x_N). \tag{2.5}$$

This enables us to compute traveling wave solutions that mimic solitary wave solutions.

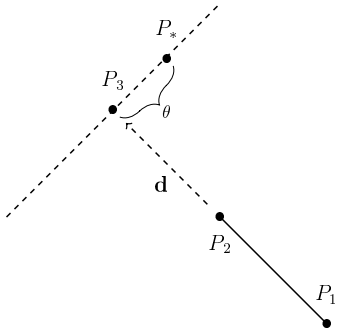

FIGURE 1. Navigation on the bifurcation curve.

2.3. **Convergence.** To test the numerical implementation of the discretization, the method is applied to a case where the solution is known. One such case is the KdV equation

$$u_t + u_x + \frac{3}{2}uu_x + \frac{1}{6}u_{xxx} = 0,$$

which has a known solution, given in the form

$$u_{\text{exact}}(x,t) = a\,\text{sech}^2\left(\sqrt{\frac{3a}{4}}(x-ct)\right),$$

with $c = 1 + a/2$. Using the boundary equation (2.5), SpecTraVVave is capable of computing approximations to solitary wave solutions of nonlinear wave equations. Solitary wave solutions are treated as traveling waves with sufficiently long wavelength that have the wave trough at zero. In case of the KdV equation solitary wave solutions have exponential decay, and therefore, considering the symmetry of solitary solutions, the half-wavelength of 30 is considered for the comparison. Approximation errors are summarized in Table 1.

grid points	$\log_{10}(\|u_{\text{exact}} - u\|_{L^\infty})$	$\log_{10}(\|u_{\text{exact}} - u\|_{L^2})$	Ratio of L^2-errors
32	−1.389	−2.092	
64	−3.705	−4.549	286.8
128	−8.809	−9.508	90935.0
256	−15.353	−16.144	4329670.9
512	−15.353	−16.087	0.9

TABLE 1. Estimates of error between the exact and computed solitary wave solutions for the KdV equation. Half-wavelength 30, waveheight $a = 1.2651$

3. Experiments with SpecTraVVave.

3.1. **Termination of waveheight-velocity bifurcation curve of the Whitham equation.** The waveheight-velocity bifurcation curve of the Whitham equation

$$u_t + \frac{3}{2}uu_x + Ku_x = 0, \quad \widehat{Ku}(k) = \sqrt{\frac{\tanh(k)}{k}}, \tag{3.1}$$

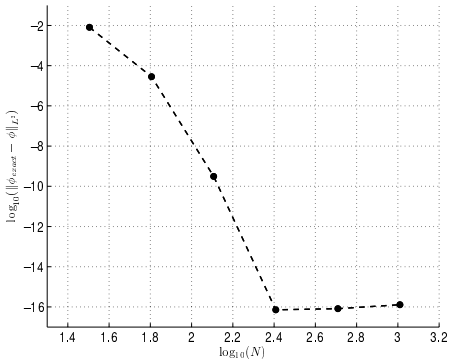

FIGURE 2. Graph of error estimates given in Table 1.

was studied numerically in [24]. An attempt was made to identify the termination point of the Whitham bifurcation curve. The investigation was limited by computational tools and complete results were not obtained. In particular, the authors could not confirm that traveling wave solutions do not exist past the point where the authors, based on pioneering work of Whitham [52] suspected a cusped solution. In this section a number of numerical results on nature of the bifurcation curve for the Whitham equation are presented. Solutions to (3.1) are computed in the form of traveling waves $u(x,t) = \phi(x - ct)$ and the homogeneous ($B = 0$) integrated version the equation is considered:

$$-c\phi + \frac{3}{4}\phi^2 + K\phi = 0. \tag{3.2}$$

Special attention is given to relation between stability of solutions and their wave-height and velocity parameters, i.e., their position on the bifurcation curve. The following questions are under study:

(a) Where does the bifurcation curve terminate?
(b) Where on the bifurcation curve do solutions change their stability?
(c) Is there any role that the turning point on the bifurcation curve plays?

The results presented here focus on 2π-periodic solutions to (3.2), i.e., solutions of system (2.4). Figure 3 presents Whitham bifurcation curves with numbers of grid points $N = 512$, $N = 1024$ and $N = 2048$. The current implementation of the SpecTraVVave package allows fixing the number of grid points N and a so-called doubling parameter $\mathcal{D}$, i.e., the number by which N is doubled as computations are made. This allows us to get sets of solutions with $N, 2N, \ldots, 2^{\mathcal{D}}N$ grid points. If $\mathcal{D} = 1$ then only two sets of solutions are computed and they are regarded as lower grid (lower resolution) and higher grid (higher resolution) solutions. While system (2.4) is processed by Newton solver, lower grid solutions are taken as initial guesses for higher grid solutions. All curves shown in this manuscript have been produced after tests with a number of resolutions were run, and the curves shown did not change significantly under further refinement.

Figure 4(a) presents the Whitham bifurcation curve computed by SpecTraVVave with $N = 1024$ and $\mathcal{D} = 1$. There are three solutions which deserve to be singled out:

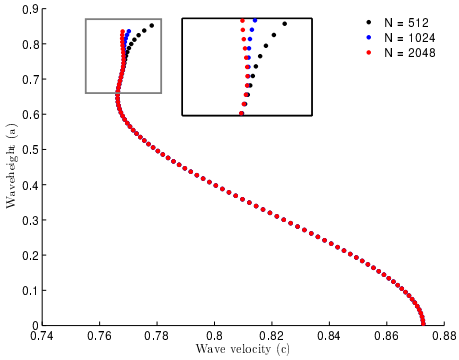

FIGURE 3. Whitham bifurcation curve in different grid resolutions.

(1) Traveling wave solution with minimum velocity (rhombus);
(2) Traveling wave solution with maximum L^2-norm (circle);
(3) Cusped traveling wave solution (square).

Profiles of the above listed solutions are given in Figure 5(a). The solution with minimum velocity corresponds to the turning point of the bifurcation curve. The solution with maximum L^2-norm is very close to the latter one, although it has a higher waveheight and a different velocity. The solution marked by a square is called here the *terminal solution*. As already mentioned, previous studies, such as [23, 24] did not provide any conclusive analysis on the part of the bifurcation curve past the turning point. In particular, it was not clear whether solutions ceased to exist at or after the turning point, or whether solutions were stable or unstable after the turning point.

Let us first focus on the stability of solutions. Note that SpecTraVVave has an evolution integrator routine, which enables one to check the stability of computed solutions. The current version of the package uses the fourth-order method developed in [20]. In addition one may use a more refined analysis, resting on the evaluation of invariant functionals. This analysis is based on the observation that the traveling waves can be thought of as solutions of a constrained minimization problem. This analysis is based on ideas developed by Boussinesq, first exploited in [8], and later used in [12, 14, 42], and many other works.

Let us define two functionals V and E:

$$V(\phi) = \frac{1}{2}\int_{-\infty}^{+\infty} \phi^2 \, \mathrm{d}\zeta, \quad E(\phi) = \int_{-\infty}^{+\infty} \left\{ \frac{1}{2}\phi^3 - \phi \, K\phi \right\} \mathrm{d}\zeta.$$

Equation (3.2) can be then written in terms of variational derivatives of E and V as

$$E'(\phi) - cV'(\phi) = 0. \tag{3.3}$$

It is known from [12] that under certain conditions, the stability of solitary wave solutions depends on convexity of the function $d(c) = E(\phi) - cV(\phi)$. Solutions with values of c for which $d''(c) > 0$ are stable solutions, and solutions with wave speeds for which $d''(c) < 0$ are unstable solutions.

The current numerical investigation can therefore be interpreted as an indication of the stability properties of traveling wave solutions of the Whitham equation. Note

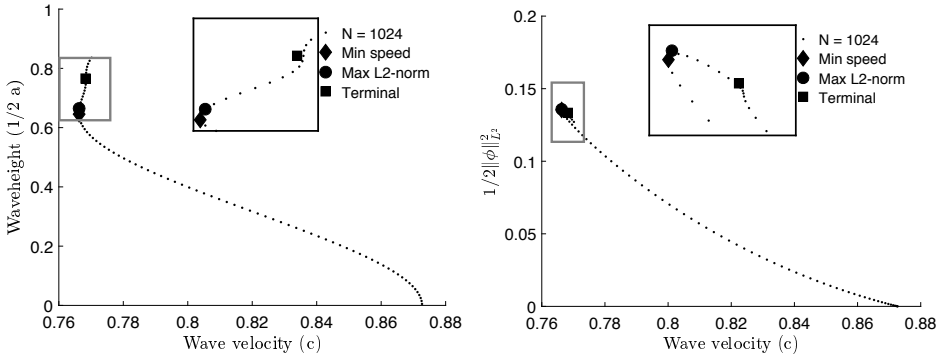

(a) Bifurcation curve in the wavespeed-wave-height parameter space

(b) Bifurcation curve in a wavespeed-L^2-norm diagram

FIGURE 4. Whitham bifurcation curves for 2π-periodic solutions.

that differentiation of $d(c)$ yields

$$d'(c) = \underbrace{E'(\phi) - cV'(\phi)}_{=0} - V(\phi).$$

Using (3.3) as indicated yields

$$d'(c) = -V(\phi) = -\frac{1}{2}\int_{-\infty}^{+\infty} \phi^2 \, \mathrm{d}\zeta = -\frac{1}{2}\|\phi\|_{L^2}^2.$$

Therefore, to understand the convexity of $d(c)$, it is sufficient to find points of maximum L^2-norm on the curve in the right panel of Figure 4. It is straightforward to see that $d''(c)$ changes sign in the neighbourhood of the maximum point of this curve, i.e., around the solution with maximum L^2-norm. In particular, $d''(c) > 0$, i.e., solutions are stable to the left of the maximum point, and $d''(c) < 0$, i.e., solutions are unstable to the right of the maximum point.

In addition, the solutions were tested with the evolution integrator to confirm their stability/instability in time. The solution with maximum L^2-norm and those on the left-hand side were always found to be stable in the time-dependent computations. Solutions on the right-hand side do not preserve their shape and thus are unstable. Examples are given in Figure 6. This analysis confirms that the point corresponding to the minumum wave speed (the turning point), and the point of stability inversion are two distinct points on the bifurcation curve. Moreover, the point of stability inversion is a little further up the branch from the turning point.

Next, we turn our attention to the analysis of the terminal point. There are two main questions. Does the branch terminate, and if so, does the terminal point on the branch correspond to a cusped traveling wave. First of all, note that the solution, which is computed by SpecTraVVave, past the terminal solution has two crests, no matter how small the stepping on the bifurcation branch is taken. (see Figure 5(b)). Secondly, as will be explained presently, the relation

$$\frac{c}{\sup_x \phi(x)} = \frac{3}{2}$$

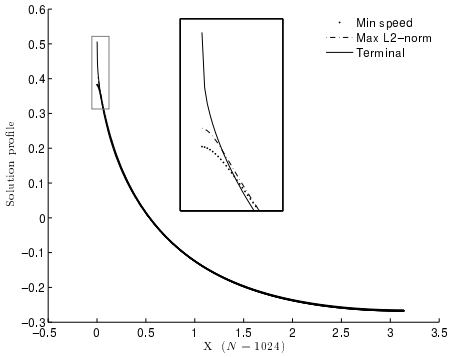

(a) Profiles of the solutions singled out in Figure 4 (a)

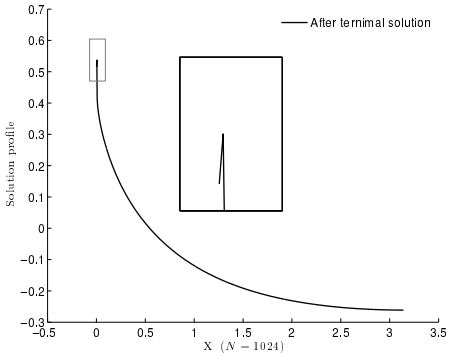

(b) Profile after terminal solution

FIGURE 5. Profiles of specific traveling wave solutions.

holds for the terminal solution with a good degree of approximation. For the most accurate runs, we obtain $c/\sup_{x\in\mathbb{R}}\phi(x) \approx 1.51$. To explain how this relation comes about note that the steady integrated form of the Whitham equation can be written as

$$\Big(\frac{c}{\sqrt{3}} - \frac{\sqrt{3}}{2}\phi\Big)^2 = \frac{1}{3}c^2 - K\phi. \tag{3.4}$$

It is clear that for any $\phi < 3c/2$, the relation (3.4) can be used in a bootstrap argument to show that any continuous solution must be in fact smooth. However for the case $\phi = 3c/2$ this bootstrap argument fails since the left-hand side vanishes. It can be concluded that a solutions containing a cusp will have a maximum value of $3c/2$.

As an additional check, the discrete cosine coefficients of the solutions were examined, and fitted to the following models:

$$\mathcal{E}(k) = \nu_1 e^{-\nu_2 k^n}, \quad \mathcal{P}(k) = \frac{\mu_1}{\mu_2 + \mu_3 k^m},$$

where ν_1, ν_2, μ_1, μ_2, μ_3, n and m are fitting parameters. A smooth function is known to have discrete cosine coefficients with exponential decay in k. On the other hand, if a function is not smooth, the discrete cosine coefficients feature polynomial decay. To identify the best fit, two parameters were used: L^2-norm of the residual and the Akaike information criterion (AIC) measure.

From the data given in the Table 2, one can deduce that for solutions with minimum speed and maximum L^2-norm exponential fit is better than polynomial. That is not the case for the terminal solution. Thus, the first two solutions are smooth and the terminal solution is nonsmooth. In fact, the polynomial fit is better than exponential for solutions that are between the maximum L^2-norm solution and the terminal solution.

The numerical evidence brought forward supports the conclusion that the Whitham bifurcation branch terminates at the terminal point indicated in Figure 3. Of course, as already mentioned, this conclusion has now also been reached using tools of mathematical analysis [25].

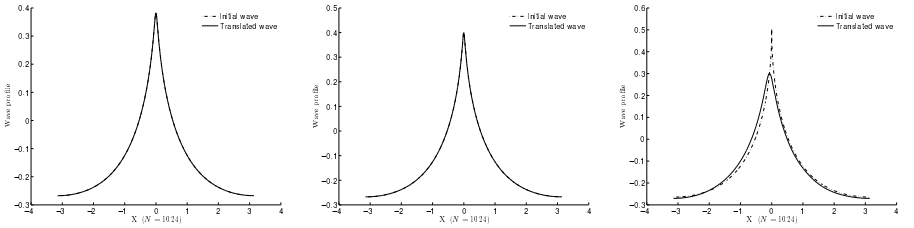

(a) Minimum speed solution (b) Maximum L^2-norm solution (c) Terminal solution

FIGURE 6. Evolution of specific solutions in time. Time range for each solution is three periods.

Model	Min speed solution $\mathcal{E}(k)$	$\mathcal{P}(k)$	Max L^2-norm solution $\mathcal{E}(k)$	$\mathcal{P}(k)$	Terminal solution $\mathcal{E}(k)$	$\mathcal{P}(k)$
Res. L^2-norm	5×10^{-5}	4×10^{-3}	7×10^{-5}	3×10^{-3}	6×10^{-3}	6×10^{-4}
AIC	-543	-321	-529	-333	-298	-416

TABLE 2. Results for measures of fit.

3.2. **Interaction of solitary wave solutions of modified Benjamin–Ono equation.** In this section, we utilize the SpecTraVVave package to obtain high-precision approximations to solitary-wave solutions of the modified Benjamin–Ono

$$u_t + u^2 u_x + u_x - \mathcal{H}u_{xx} = 0,$$

which is a special case of the generalized Benjamin–Ono equation, with $p = 2$. This case corresponds to the critical scaling, i.e., invariance of the energy norm under the natural invariant scaling.

The Benjamin–Ono equation was found by Benjamin [7] as a model for long small-amplitude interfacial waves in deep water. The validity of approximating the more physically correct configuration of a continuous density distribution by the two-layer approximation has recently been justified mathematically [17].

Solitary-wave solutions of the modified Benjamin–Ono equation with $p = 3$, $p = 4$ and $p = 5$ were approximated in [11] with a standard Newton scheme. The solutions in [11] were not very accurate, but since singularity formation of the evolution equations were under study, the accuracy of the solitary-wave approximation was not an important issue. The problem with the method of [11] and some other works was that the fft used there was not purged of possible symmetries (translational and reflective). In the current code, since a cosine formulation is chosen, these symmetries are automatically eliminated, and the resulting computations are able to to render more accurate approximations.

Solitary-wave solutions of these equation could be computed with higher accuracy using a type of Petviashvili method in [44], but here we employ the SpecTraVVave package using the boundary equation (2.5), and treating solitary waves as traveling waves with sufficiently long wavelength that have wave trough at zero. Once these high-accuracy solutions are found, they are aligned in an evolution code using a high-order time integrator, and the interaction of two waves is studied.

Two questions are investigated. First, the interaction is investigated for evidence of integrability. Second, we are looking for possible annihilation of one of the waves, such as may happen in some other evolution equations [19].

A possible approach to studying the question of complete integrability is analyzing the interaction of two solitary wave solutions of the equation, such as carried out in [32, 34] for other nonlocal equations. In Figure 7, snapshots of interaction of two solitary waves at different times are shown. The time difference between two consecutive snapshots is constant. As it may be observed, during the process of interaction, the two initial solitary waves combine into a single wave, and an additional oscillation is produced. This leads us to the conclusion that the interaction of solitary waves is not elastic and the modified Benjamin–Ono equation may not be integrable. In addition, it appears that the smaller wave disappears as most of its mass is acquired by the larger wave. Thus one may argue that the small wave is annihilated by the larger wave. It can also be observed that the larger wave starts growing, and it is likely that this growth will lead to finite-time blow-up. This question was not investigated further since blow-up phenomena have already been studied closely in [34]. Indeed, very recently, the finite-time blow-up has been proven mathematically in [39].

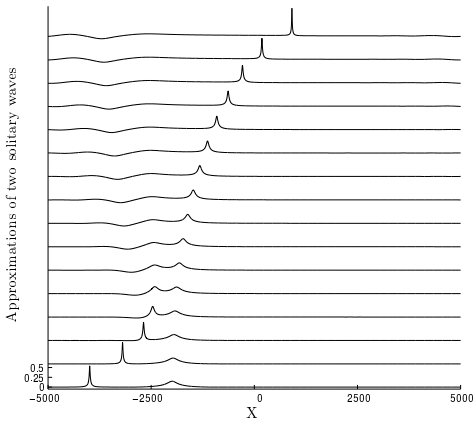

FIGURE 7. Interaction of two solitary waves of the modified Benjamin-Ono equation.

3.3. **Effect of competing dispersion in the Benjamin equation.** The Benjamin equation was found by Benjamin [9] as a model for two-layer flow in the case when the interface is subject to surface tension. The approximation may not be a good model for a stratified situation, but more applicable to the case where two fluids are separated by a sharp interface. The equation is

$$u_t + u_x + uu_x - \mathcal{H}u_{xx} - \tau u_{xxx} = 0, \tag{3.5}$$

where τ is a parameter similar to the inverse of the Bond number in free surface flow [9, 33, 50].

In this section, a study relating to the effects of competing dispersion operators on the shape of periodic traveling waves in the Benjamin equation is presented. An in-depth study of solitary waves was carried out in [22]. As will come to light, the

periodic case features some new phenomena, such as secondary bifurcations, connecting and crossing branches. For the purpose of this study, we fix the parameter $\tau = 0.1$, so that the dispersion relation for the linearized equation is

$$c(k) = 1 - |k| + 0.1k^2. \tag{3.6}$$

Traveling wave solutions with full wavelengths $L_1 = \pi/5$, $L_2 = 4\pi/19$ and $L_3 = 4\pi$ are computed for (3.5). The corresponding wavenumbers are $k_1 = 10$, $k_2 = 19/2$, and $k_3 = 0.5$, respectively. A plot of the dispersion relation (3.6) is given in Figure 8. Bifurcation branches of traveling wave solutions with the selected wavelengths are given in Figure 9.

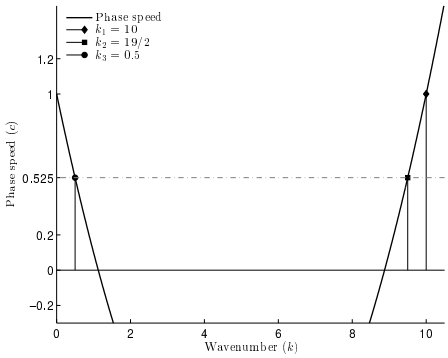

FIGURE 8. Dispersion relation (3.6)

The branch denoted by L_1 originates at the bifurcation point located at $c = 1$ and zero waveheight. The branches denoted by L_2 and L_3 originate from the same bifurcation point, located at $c = 0.525$ and zero waveheight. These two branches continue in different directions, due to differences in wavelength. In particular, the L_3 branch contains waves with shorter wavelengths, and falls into the capillary regime. On the other hand, the L_2 branch falls in the gravity regime. As the waveheight grows, solutions on the L_3 branch first cross the L_1 branch without

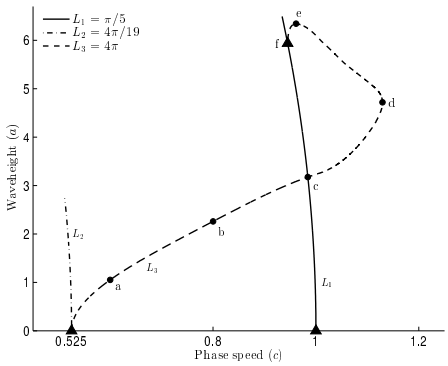

FIGURE 9. Bifurcation curves of (3.5) with different wavelengths, ▲ – points of bifurcation, • – selected solutions (see Figure 10).

connecting. Additional oscillations develop in the solutions until a new fundamental wavelength $\pi/5$ is reached, and the branch terminates as it connects to the L_1 branch. The situation is depicted in Figure 10. The point where the L_1 and L_3 branches meet is approximately $(c^*, a^*) = (0.945, 5.938)$. The corresponding profiles essentially overlap, as shown on Figure 11. This point can also be interpreted as a secondary bifurcation point of the L_1 branch, where solutions with wavelengths that are multiples of $\pi/5$ develop. We should note that similar phenomena concerning crossing and connecting branches were previously observed in [47] for the Whitham equation with surface tension which was introduced in [30].

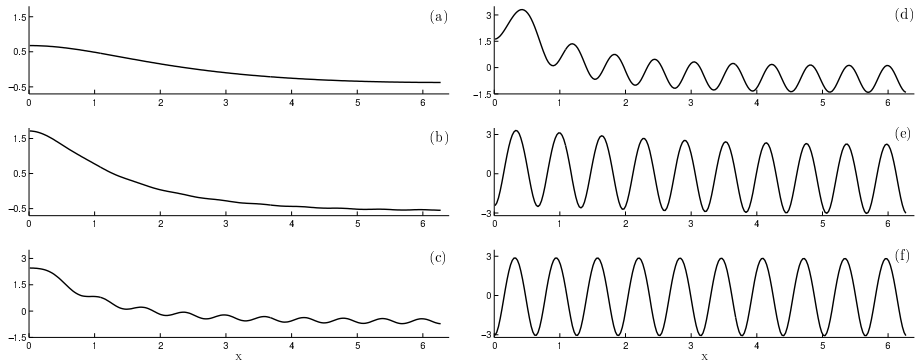

FIGURE 10. Selected solutions of (3.5). Labels preserved as shown in Figure 9.

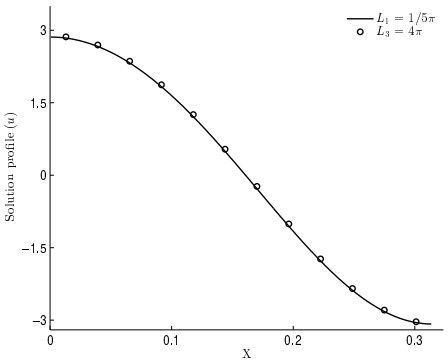

FIGURE 11. Solution profiles at the point (c^*, a^*) where the L_1 and L_3 branches meet (see Figure 9).

4. Conclusions and future work

The numerical algorithm of SpecTraVVave features ample flexibility for researching different aspects of nonlocal dispersive wave equations and their traveling wave

solutions. The solver package is simpler in use when compared with programs such as AUTO and Wavetrain, however it does not have the same level of generality. Moreover, AUTO and Wavetrain are programmed in low-level programming languages and will therefore run more efficiently. SpecTraVVave is implemented in an object-oriented fashion [27], which makes the program easily expandable. IPython provides means for interactive work with the package, and enables users to create convenient notebook-programs. A parametric approach in defining amplitude and phase speed makes it possible to follow turning points on bifurcation curves. Specification of different boundary conditions allows computing solutions with certain features, such as traveling waves with zero mean, or approximations to solitary waves.

In this work, the SpecTraVVave package has been put to use for the study of a number on nonlinear evolution equations: the Whitham equation, the modified Benjamin–Ono equation and the Benjamin equation. For the chosen set of parameters, experiments on the Whitham equation resulted in numerical confirmation of the conjecture on cusped solutions. It was also possible to identify the point of stability inversion of traveling wave solutions of the equation and the termination point of its bifurcation curve.

In case of the modified Benjamin–Ono equation, the study on solitary wave solutions lead us to conclude that interaction process ended with annihilation of one of the two waves. The experiment on the Benjamin equation showed one more example of the effect of competing dispersion. As the amplitude increased, traveling wave solutions of wavelength 4π developed additional oscillations, and later connected up with a branch of solutions with wavelength $\pi/5$.

Future work on the SpecTraVVave package will be focused on development of its functionality and broadening the range of problems that can be studied. Possible extensions may include implementation of algorithms based on the Petviashvili method [4, 5] and generalization to systems of equations.

5. Appendix: Computing initial guesses from Stokes expansion.

$$u_t + [f(u)]_x + \mathcal{L}u_x = 0, \tag{5.1}$$

The goal of this section is to explain how the idea of Stokes's approximation works in providing the initial data (guess) on wave and phase velocity for solving (5.1) numerically.

We will consider $\mathcal{L}$ being linear and self-adjoint Fourier multiplier operator, and a function f that has degree of zeros $p \geq 2$:

$$\widehat{\mathcal{L}u}(k) = \alpha(k) \cdot \widehat{u}(k),$$
$$\langle \mathcal{L}u, v\rangle_{L^2(0,L)} = \langle u, \mathcal{L}v\rangle_{L^2(0,L)},$$
$$p = \min_{k\in\mathbb{N}} f^{(k-1)}(0) = 0 \text{ and } f^{(k)}(0) \neq 0$$

Consider equation (5.1) and its solution in the form $u(x,t) = \phi(x-ct)$, which is a traveling wave solution. Inserting $\phi(x-ct)$ into (5.1) leads to the equation

$$-c\phi' + f'(\phi)\phi' + \mathcal{L}\phi' = 0,$$

which can be integrated to give

$$-c\phi + f(\phi) + \mathcal{L}\phi = B, \quad B = \text{const}. \tag{5.2}$$

Consider $B = 0$ in equation (5.2), and expansions of ϕ and c:

$$\phi = \xi = \varepsilon\xi_1 + \varepsilon^2\xi_2 + \dots, \tag{5.3}$$

$$c = c_0 + \varepsilon c_1 + \varepsilon^2 c_2 + \dots. \tag{5.4}$$

The next step is to insert (5.3) and (5.4) to (5.2) and write out the terms at powers of ε. The function $f(\phi)$ is expanded around zero and, therefore, will appear only in ε^p terms. Thus, the term at the first power of ε reads

$$\varepsilon: \quad -c_0\xi_1 + \mathcal{L}\xi_1 = 0, \tag{5.5}$$

Hence, c_0 is an eigenvalue of the operator $\mathcal{L}$, regarded as defined on L-periodic functions. Taking the Fourier transform of (5.5) gives:

$$-c_0\widehat{\xi_1}(k) + \alpha(k)\widehat{\xi_1}(k) = 0. \tag{5.6}$$

Equation (5.6) has two trivial solutions: either $\xi_1(k) \equiv 0$ or $\alpha(k) \equiv c_0$. If we assume non-trivial ξ_1 and $\alpha(k) \neq \text{const}$, the following solves the problem

$$\widehat{\xi_1}(k) = 2\pi\delta(k - k_0), \quad \text{and} \quad c_0 = \alpha(k_0), \tag{5.7}$$

for some $k_0 \in \mathbb{R}$. Since ξ_1 is the first-order approximation to ϕ, the corresponding wave number should be equal to 1. The L-periodicity condition entails that $k_0 = 2\pi/L \cdot 1$. The spatial variable x has to be scaled to $x' = L/2\pi x$, accordingly. From the solutions in (5.7) we have

$$\xi_1(x') = e^{ik_0x'} = \cos(k_0x') + \sin(k_0x'). \tag{5.8}$$

Considering the projection onto the space $\mathcal{S}_N$, we are led to choose $\xi_1(x') = \cos(k_0x')$. For further analysis, let us define an operator $\mathcal{A}$,

$$\mathcal{A} := -c_0\mathcal{E} + \mathcal{L},$$

where $\mathcal{E}$ is the identity operator. The operator $\mathcal{A}$ inherits the property of being self-adjoint from $\mathcal{L}$. Moreover, it follows from (5.5) that $\mathcal{A}\xi_1 = 0$ and $\xi_1 \in \ker(\mathcal{A})$. If $p > 2$ then $f''(0) = 0$ and the terms at ϵ^2 are:

$$\mathcal{A}\xi_2 - c_1\xi_1 = 0. \tag{5.9}$$

Taking scalar multiplication of the latter with ξ_1, one obtains

$$\langle\xi_1, \mathcal{A}\xi_2\rangle_{L^2(0,L)} = c_1\|\xi_1\|^2_{L^2(0,L)}, \quad \langle\xi_1, \mathcal{A}\xi_2\rangle_{L^2(0,L)} = \langle\mathcal{A}\xi_1, \xi_2\rangle_{L^2(0,L)} = \langle 0, \xi_2\rangle_{L^2(0,L)} = 0.$$

As a result, one has $c_1\|\xi_1\|^2_{L^2(0,L)} = 0$ and, hence, $c_1 = 0$. Repeating the same argument, it becomes clear that $c_k = 0$ for any $k \leq p-1$. Besides that, ξ_2 is in the kernel of $\mathcal{A}$, so it may be assumed to be proportional to ξ_1. The terms at order ε^p are:

$$\mathcal{A}\xi_p - c_{p-1}\xi_1 + \frac{f^{(p)}(0)}{p!}\xi_1^p = 0. \tag{5.10}$$

Let us denote for brevity

$$f_p := \frac{f^{(p)}(0)}{p!}.$$

Pairing (5.10) with ξ_1 (and assuming $\|\xi_1\|_{L^2(0,L)} = 1$) gives

$$c_{p-1} = f_p \cdot \langle\xi_1^p, \xi_1\rangle_{L^2(0,L)}, \tag{5.11}$$

which gives us the value of c_{p-1}. It only remains to solve the following problem numerically in order to obtain ξ_p:

$$\mathcal{A}\xi_p = c_{p-1}\xi_1 - f_p\xi_1^p \tag{5.12}$$

For the last equation to be solved, the operator $\mathcal{A}$ has to be invertible. It is also required that $\langle \xi_1, \xi_p \rangle_{L^2(0,L)} = 0$. Therefore the solution is sought in the space orthogonal to $\ker(\mathcal{A})$. Since $\mathcal{A}$ is still a Fourier multiplier operator, one can take the Fourier transform of (5.12) to find

$$\widehat{\mathcal{A}}(k)\widehat{\xi_p}(k) = c_{p-1}\widehat{\xi_1}(k) - f_p\widehat{\xi_1^p}(k),$$
$$\widehat{\xi_p}(k) = \widehat{\mathcal{A}}(k)^{-1}\left(c_{p-1}\widehat{\xi_1}(k) - f_p\widehat{\xi_1^p}(k)\right).$$

Taking the inverse Fourier transform of $\widehat{\xi_p}(k)$ gives ξ_p. Since only even solutions of the problem are considered the cosine part of the Fourier transforms will be required. It is sufficient to use ξ_1 and c_0 as the initial guesses for the Newton method. However, it should be noted that for different values of p the pair of parameters ξ_p and c_{p-1} are computed in different ways.

(a) If $p = 2$, then ξ_2 is computed from (5.12), but c_{p-1} here becomes zero. Therefore one has to consider the next level of the expansion ε^p.
(b) For odd values of p the parameter c_{p-1} can be computed from (5.11) and ξ_p from (5.12).
(c) For even values of $p \geq 4$ the parameter ξ_p can be computed, but c_{p-1} may not be non-zero in general. In such cases a different strategy of fixing the initial guess should be used.

6. Appendix: Presentation of SpecTraVVave and its workflow

6.1. **Overview.** There are several classes in the SpecTraVVave package. An overview of the program is shown in Figure 12. The workflow begins with defining a flux function f and the Fourier multiplier function α to set up an equation. The traveling wave solution is characterized by the wavelength L and a boundary condition $\Omega(c, a, \phi_N, B)$. These parameters are fixed for a given problem. The defined equation is then discretized. The `Discretization` object contains all required elements such as grid points, wave-numbers and the discrete linear operator.

The initial guess and the equation's residual are passed from the `Discretization` to the `Solver` object. The `Navigation` object is responsible for finding good initial guesses for c and a that are passed to the `Solver` object. The `Solver` object applies Newton's method to find a solution to system of equations (2.4).

The new solution is sent back to the `Discretization` and `Navigation` objects, where variables get updated. All computed solutions are stored for further analysis. This finishes one iteration. For the next iteration the updated variables are used and a new solution is found. The process may be continued as long as the Jacobian of the problem is non-singular.

6.2. **Class Description.** We present an overview of the classes used in SpecTraVVave package. Note that, since the package is under continuous modification and development, we describe here only the basic classes and functions the package. We refer to the package repository [41] for up-do-date tutorials and installation instructions.

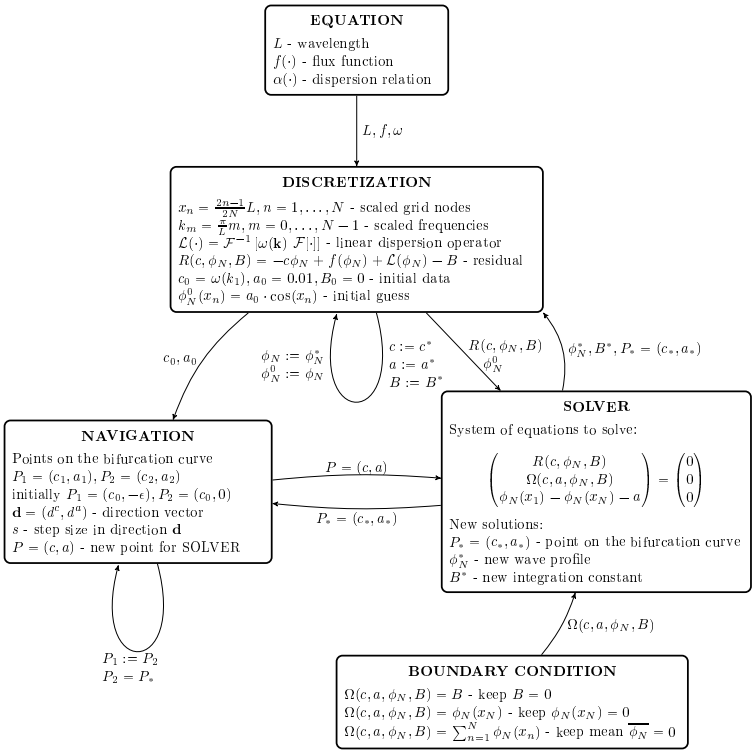

FIGURE 12. Overview of the SpecTraVVave package.

The `Equation` class is the general class for all model equations. Its only role is to store a parameter L, the wavelength:

```
class Equation(object):
    def __init__(self, L):
        self.length = L
```

A subclass of the `Equation` class has to implement two functions, `compute_kernel` and `flux`.

The KdV model equation

$$u_t + \frac{3}{2}uu_x + u_x + \frac{1}{6}u_{xxx} = 0$$

with $f(u) = \frac{3}{4}u^2$ and $\widehat{\mathcal{L}u}(k) = (1 - \frac{1}{6}k^2)\widehat{u}(k)$ is presented in the program as a subclass of the `Equation` class:

```
class KDV(Equation):
    def compute_kernel(self, k):
        return 1-1/6*k*k

    def flux(self, u):
        return 3/4*u*u
```

One can then create an object of the class `KDV` with the command:

```
kdv = KDV(L=np.pi)
```

The solver will compute only a half of a solutions profile. The full wavelength of the solutions of the defined equation will be equal to 2π.

In order to find solutions with specific features, boundary conditions are introduced as separate classes. For instance, the boundary condition specifying a constant of integration is implemented as follows:

```
class Const(object):
""" The boundary condition under which the constant of integration
(B) is always set to zero. """
    def __init__(self, level=0):
        self.level = level

    def enforce(self, wave, variables, parameters):
    """ Enforces the Const boundary condition. """
        return np.hstack([variables[0] - self.level])

    def variables_num(self):
    """ The number of additional variables that are required to
                                        construct
    the Const boundary condition. """
        return 1
```

A `Const` boundary condition object is created as follows:

```
boundary_condition = Const()
```

The next step is to create an object of `Discretization` class, which is initialized with a model equation such as `kdv_model` and the number of grid points. The main parts of the class are the following:

```
class Discretization(object):
    def __init__(self, model_equation, grid_size):
        self.equation = model_equation
        self.size = grid_size

    def operator(self, u):
        u_ = scipy.fftpack.dct(u, norm='ortho')
        Lv = self.fourier_multiplier()*u_
        result = scipy.fftpack.idct(Lv, norm='ortho')
        return result

    def residual(self, u, wavespeed, const_B):
        residual = - wavespeed*u + self.equation.flux(u)
                                        + self.operator(u) - const_B
        return  residual
```

The call `Discretization.operator(u)` computes $\mathcal{L}u$ as the inverse transform of a transformed convolution

$$\mathcal{L}u = \mathcal{F}^{-1}[\widehat{\mathcal{L}u}(k)] = \mathcal{F}^{-1}\left[\alpha(k)\cdot\widehat{u}(k)\right].$$

The result of the call `Discretization.residual(u, wavespeed, const_B)` is then used in the `Solver` class. An object of the `Solver` class is initialized with an object of the `Discretization` class, and a boundary condition object.

```
class Solver(object):
    def __init__(self, discrete_problem, boundary_condition):
        self.discretization = discrete_problem
        self.boundary = boundary_condition

    def solve(self, guess_wave, parameter_anchor, direction):
    """ Runs a Newton solver on a system of nonlinear equations once.
    Takes the residual(vector) to solve. parameter_anchor
    is the initial guess for (c,a) values and it is taken from the
    Navigation class. """
        size = len(guess_wave)
        self.discretization.size = size

        def residual(vector):
        """ Contructs a system of nonlinear equations. First part,
        main_residual, is from given wave equation; second part,
        boundary_residual, comes from the chosen boundary conditions.
                                                """
        . . .
        return np.hstack([main_residual, boundary_residual,
                                            amplitude_residual])
    . . .
    return new_wave, new_boundary_variables, new_parameter
```

Some omitted parts in the above script are substituted by '. . .' sign. Each iteration on a `Solver` object is run from a `Navigation` object, which takes the `Solver` object for initialization.

```
class Navigation(object):
""" Runs the Solver and stores the results. """

    def __init__(self, solver_object, size=32):
    self.solve = solver_object.solve # function to run Newton method
    self.size = size # size for navigation
    . . .
    def run_solver(self, current_wave, pstar, direction):
        new_wave, variables, p3 = self.solve(current_wave, pstar,
                                            direction)
        return new_wave, variables, p3
```

All the above classes can be modified and developed further, new classes may be defined as well.

6.3. **Detailed Workflow.** The workflow with the package consists of three basic steps:

(1) Once the necessary classes have been imported in the current namespace, generate all necessary objects:

```
equation = KDV(L=np.pi)
boundary_condition = Const()
discretization = Discretization(equation, grid_size=64)
solver = Solver(discretization, boundary_condition)
navigator = Navigation(solver)
```

(2) Choose a number of iterations, i.e., the number of solutions to compute, and run the solver:

```
n_iter = 50
navigator.run(n_iter)
```

(3) All computed solutions are stored in `navigation_object`

```
last_computed = -1
wave_profile = navigator[last_computed]['solution']
wave_speed = navigator[last_computed]['current'][0]
wave_amplitude = navigator[last_computed]['current'][1]
```

For up-to-date instructions on how to run the code, we refer the reader to the code repository `https://github.com/olivierverdier/SpecTraVVave`.

Acknowledgments. The authors would like to thank Mats Ehrnström and Erik Wahlén for fruitful discussions on the subject of the current paper. This research was supported by the Research Council of Norway on grant no. 213474/F20 and by the J C Kempe Memorial Fund on grant no. SMK-1238.

References

[1] Abdelouhab, L.; Bona, J. L.; Felland, M. Saut, J.-C.; *Nonlocal models for nonlinear dispersive waves*. Physica D **40**,360-392 (1989).

[2] Albert, J. P.; Bona, J. L.; Restrepo, J.M.; *Solitary-wave solutions of the Benjamin equation*. SIAM J. Appl. Math. **59**,2139–2161 (1999).

[3] Álvarez, J.; Durán, A.; *A numerical scheme for periodic travelling-wave simulations in some nonlinear dispersive wave models*. J. Comput. Appl. Math. **235**, 1790–1797 (2011).

[4] Álvarez, J.; Durán, A.; *An extended Petviashvili method for the numerical generation of traveling and localized waves*. Commun. Nonlinear Sci. Numer. Simul. **19**, 2272–2283 (2014).

[5] Álvarez, J.; Durán, A.; , *Petviashvili type methods for traveling wave computations: I. Analysis of convergence*. J. Comput. Appl. Math. **266**, 39–51 (2014).

[6] Álvarez, J.; Durán, A.; *Corrigendum to "Petviashvili type methods for traveling wave computations: I. Analysis of convergence*, [J. Comput. Appl. Math. 266 (2014) 39–51]. J. Comput. Appl. Math. **277**, 215–216 (2015).

[7] Benjamin, T.B .; *Internal Waves of permanent form in fluids of great depth*. J. Fluid Mech. **29**, 559–592 (1967).

[8] Benjamin, T. B.; *The stability of solitary waves*. Proc. Roy. Soc. London A 328, 153-183 (1972).

[9] Benjamin, T. B.; *A new kind of solitary wave*. J. Fluid Mech. **245**, 401–411 (1992).

[10] Bona, J. L.; Dougalis, V.A.; Karakashian, O. A.; McKinney, W.R.; *Conservative, high-order numerical schemes for the generalized Korteweg–de Vries equation*, Philos. Trans. Royal Soc. London Ser. A, **351**, 107–164 (1995).

[11] Bona, J. L.; Kalisch, H.; *Singularity formation in the generalized Benjamin–Ono equation*. Discrete Contin. Dyn. Syst. **11**, 779–785 (2004).

[12] Bona, J. L.; Souganidis, P. E.; Strauss, W. A.; *Stability and instability of solitary waves of Korteweg–de Vries type*. Proc. R. Soc. Lond. A **411**, 395-412 (1987).

[13] Borluk, H.; Kalisch, H.; Nicholls, D. P.; *A numerical study of the Whitham equation as a model for steady surface water waves*. J. Comput. Appl. Math. **296**, 293–302 (2016).

[14] Bridges, T. J.; *Superharmonic instability, homoclinic torus bifurcation and water-wave breaking*. J. Fluid Mech. **505**, 153-162 (2004).

[15] Chen, H.; *Existence of periodic travelling-wave solutions of nonlinear, dispersive wave equations*. Nonlinearity **17**, 2041–2056 (2004).

[16] Chen, H.; Bona, J. L.; *Existence and asymptotic properties of solitary-wave solutions of Benjamin-type equations*. Adv. Diff. Eq. **3**, 51-84 (1998).

[17] Chen, R. M.; Walsh, S.; *Continuous dependence on the density for stratified steady water waves*. Arch. Ration. Mech. Anal. **219**, 741–792 (2016).

[18] Choi, W.; Camassa, R.; *Fully nonlinear internal waves in a two-fluid system*. J. Fluid Mech. **396**, 1-36 (1999).

[19] Courtenay Lewis, J.; Tjon, J. A.; *Resonant production of solitons in the RLW equation*. Phys. Lett. A **73**, 275–279 (1979).

[20] de Frutos, J.; Sanz-Serna, J. M.; *An easily implementable fourth-order method for the time integration of wave problems*. J. Comp. Phys. **103**, 160–168 (1992).

[21] Doedel, E. J.; Champneys, A. R.; Fairgrieve, T. F.; Kuznetsov, Y.A.; Sandstede, B. and Wang, X.-J.; *AUTO97 : Continuation and bifurcation software for ordinary differential equations*, available at `http://indy.cs.concordia.ca/auto/`, Department of Computer Science and Software Engineering, Concordia University, Montreal, Canada, 1997.

[22] Dougalis, V. A.; Duran, A.; Mitsotakis, D.; *Numerical solution of the Benjamin equation*. Wave Motion **52**, 194–215 (2015).

[23] Ehrnström, M.; Kalisch, H.; *Traveling waves for the Whitham equation*. Differential Integral Equations **22**, 1193–1210 (2009).

[24] Ehrnström, M., Kalisch, H.; *Global bifurcation for the Whitham equation*. Math. Mod. Nat. Phenomena **8**, 13–30 (2013).

[25] Ehrnström, M.; Wahlén, E.; *On Whitham's conjecture of a highest cusped wave for a nonlocal dispersive equation*. arXiv:1602.05384 (2016).

[26] Fornberg, B.; Whitham, G. B.; *A numerical and theoretical study of certain nonlinear wave phenomena*. Phil. Trans. Roy. Soc. A **289**, 373–404 (1978).

[27] Führer, C.; Solem, J. E.; Verdier, O.; Computing with Python: An introduction to Python for science and engineering, Pearson (2014).

[28] Grujić, Z.; Kalisch, H.; *Gevrey regularity for a class of water-wave models*. Nonlinear Analysis **71**, 1160–1170 (2009)

[29] Hur, V. M.; *Breaking in the Whitham equation for shallow water waves*. arXiv:1506.04075 (2015).

[30] Hur, V. M.; Johnson, M.; *Modulational instability in the Whitham equation of water waves*. Studies in Applied Mathematics **134**, 120–143 (2015).

[31] Hur, V. M.; Tao, L.; *Wave breaking for the Whitham equation with fractional dispersion*. arXiv:1410.1570, 2014.

[32] Kalisch, H.; *Error analysis of a spectral projection of the regularized Benjamin-Ono equation*. BIT Numerical Mathematics **45**, 69–89 (2005).

[33] Kalisch, H.; *Derivation and comparison of model equations for interfacial capillary-gravity waves in deep water*. Math. Comput. Simulation **74**, 168–178 (2007).

[34] Kalisch, H.; Bona, J. L.; *Models for internal waves in deep water*. Discrete and Continuous Dynamical Systems **6**, 1–20 (2000).

[35] Kato, T.; *On the Cauchy problem for the (generalized) Korteweg–de Vries equation*. Studies in applied mathematics, 93–128, Adv. Math. Suppl. Stud., **8** (Academic Press, New York, 1983).

[36] Keller H. B.; *Numerical solution of bifurcation and nonlinear eigenvalue problems*. Applications of Bifurcation Theory, Rabinowitz, P. H., Academic Press, (1977), pp. 359–384.

[37] Lannes, D.; Saut, J.-C.; *Remarks on the full dispersion Kadomtsev–Petviashvli equation*. Kinet. Relat. Models **6**, 989–1009 (2013).

[38] Martel, Y.; Merle, F.; *Blow up in finite time and dynamics of blow up solutions for the L2-critical generalized KdV equation*. J. Amer. Math. Soc. **15**, 617–664 (2002).

[39] Martel, Y.; Pilod, D.; *Construction of a minimal mass blow up solution of the modified Benjamin-Ono equation*. arXiv:1605.01837 (2016).

[40] Moldabayev, D.; Kalisch, H.; Dutykh, D.; *The Whitham Equation as a model for surface water waves*. Phys. D **309**, 99–107 (2015)

[41] Moldabayev, D.; Verdier, O.; Kalisch, H.; *SpecTraVVave*, available at `https://github.com/olivierverdier/SpecTraVVave`.

[42] Nguyen, N. T.; Kalisch, H.; *Orbital stability of negative solitary waves*. Mathematics and Computers in Simulation **80**, 139-150 (2009).

[43] Ono, H.; *Algebraic Solitary Waves in Stratified Fluids*. J. Phys. Soc. of Japan **39**, 1082-1091 (1975).

[44] Pelinovsky, D. E.; Stepanyants, Y. A.; *Convergence of Petviashvili's iteration method for numerical approximation of stationary solutions of nonlinear wave equations*. SIAM J. Numer. Anal. **42**, 1110–1127 (2004).

[45] Pérez, F.; Granger, B. E.; *IPython: A System for Interactive Scientific Computing*, Computing in Science and Engineering, vol. 9, no. 3, pp. 21-29, May/June 2007. URL: `http://ipython.org`

[46] Petviashvili, V.I.; *Equation of an extraordinary soliton*, Sov. J. Plasma Phys. **2**, 257–258 (1976).

[47] Remonato, F.; Kalisch, H.; *Numerical bifurcation for the capillary Whitham equation*, Physica D: Nonlinear Phenomena, 343, 51–62 (2017).

[48] Sanford, N.; Kodama, K.; Carter, J. D.; Kalisch, H.; *Stability of traveling wave solutions to the Whitham equation*. Phys. Lett. A **378**, 2100–2107 (2014).

[49] Sherratt, J. A.; *Numerical continuation methods for studying periodic travelling wave (wavetrain) solutions of partial differential equations*. Appl. Math. Comp. **218**, 4684–4694 (2012).

[50] Walsh, S.; *Steady stratified periodic gravity waves with surface tension I: Local bifurcation*. Discrete Contin. Dyn. Syst. **34**, 3241–3285 (2014).

[51] Walsh, S.; *Steady stratified periodic gravity waves with surface tension II: global bifurcation*. Discrete Contin. Dyn. Syst. **34**, 3287–3315 (2014).

[52] Whitham, G. B.; *Variational methods and applications to water waves*. Proc. Roy. Soc. London A, **299**, 6–25 (1967).

[53] Whitham, G. B.; Linear and Nonlinear Waves. Wiley, New York, (1974).

Henrik Kalisch
Department of Mathematics, University of Bergen, P.O. Box 7800, 5020 Bergen, Norway
E-mail address: `henrik.kalisch@math.uib.no`

Daulet Moldabayev
Department of Mathematics, University of Bergen, P.O. Box 7800, 5020 Bergen, Norway
E-mail address: `daulet.moldabayev@math.uib.no`

Olivier Verdier
Department of Mathematics and Statistics, University of Umea, Sweden.
Department of Computing, Mathematics and Physics, Western Norway University of Applied Sciences, Norway
E-mail address: `olivier.verdier@gmail.com`

Paper D

Explicit solutions for a long-wave model with constant vorticity[1]

Benjamin Segal, Daulet Moldabayev, Henrik Kalisch, Bernard Deconinck

D

[1] Accepted for publication in the *European Journal of Mechanics / B Fluids*

Explicit Solutions for a Long-Wave Model with Constant Vorticity

Benjamin Segal*, Daulet Moldabayev†, Henrik Kalisch† and Bernard Deconinck*

Abstract

Explicit parametric solutions are found for a nonlinear long-wave model describing steady surface waves propagating on an inviscid fluid of finite depth in the presence of a linear shear current. The exact solutions, along with an explicit parametric form of the pressure and streamfunction give a complete description of the shape of the free surface and the flow in the bulk of the fluid. The explicit solutions are compared to numerical approximations previously given in [1], and to numerical approximations of solutions of the full Euler equations in the same situation [31]. These comparisons show that the long-wave model yields a fairly accurate approximation of the surface profile as given by the Euler equations up to moderate waveheights. The fluid pressure and the flow underneath the surface are also investigated, and it is found that the long-wave model admits critical layer recirculating flow and non-monotone pressure profiles similar to the flow features of the solutions of the full Euler equations.

1 Introduction

Background vorticity can have a significant effect on the properties of waves at the surface of a fluid [19,24,26,30,32,35]. In particular, in the seminal paper of Teles da Silva and Peregrine [31], it was found that the combination of strong background vorticity and large amplitude leads to a number of unusual wave shapes, such as narrow and peaked waves and overhanging bulbous waves. In the present contribution, we continue the study of a simplified model equation which admits some of the features found in [31]. The equation, which has its origins in early work of Benjamin [3], has the form

$$\left(Q+\frac{\omega_0}{2}u^2\right)^2\left(\frac{du}{dx}\right)^2=-3\left(\frac{\omega_0^2}{12}u^4+gu^3-(2R-\omega_0 Q)u^2+2Su-Q^2\right), \tag{1}$$

where we denote the volume flux per unit span by Q, the momentum flux per unit span and unit density corrected for pressure force by S, and the energy density per unit span by R. The gravitational acceleration is g and the constant vorticity is $-\omega_0$. The total flow depth as measured from the free surface to the rigid bottom is given by the function $u(x)$.

Equation (1) was recently studied in [1]. It was found that solutions of this equation exhibit similar properties as solutions of the full Euler equations displayed in [31]. In particular, in [1] an expression for the pressure was developed, and it was shown that the pressure may become non-monotone in the case of strong background vorticity. Indeed, it was shown in [1] that if

*Department of Applied Mathematics, University of Washington, Seattle, WA 98195-2420, USA
†Department of Mathematics, University of Bergen, Postbox 7800, 5020 Bergen, Norway

$|\omega_0|$ is big enough, the maximum fluid pressure at the bed is not located under the wavecrest. Such behavior is usually only found in transient problems (cf. [33]). Moreover in some cases, the pressure near the crest of the wave may be below atmospheric pressure.

The purpose of the present work is two-fold. First, we develop a method by which equation (1) can be solved *exactly*. The resulting solutions are compared to the the numerical approximations found in [1] and to some of the solutions of the full Euler equations from [31]. Secondly, more features of the solutions of (1) are discussed. Using a similar analysis as in [1], the streamfunction is constructed, and it is found that solutions of (1) may feature recirculating flow and pressure inversion. These features may have an impact on the study of sediment resuspension. Indeed, while it is generally accepted that the main mechanism for sediment resuspension is turbulence due to flow separation in the presence of strong viscous shear stresses [7,27,29], the strongly non-monotone pressure profiles exhibited by the solutions of (1) may represent a more fundamental mechanism for particle suspension than the viscous theory.

The geometric setup of the problem is explained as follows. Consider a background shear flow $U_0 = \omega_0 z$, where ω can be positive or negative (cf. Figure 1). Superimposed on this background flow is wave motion at the surface of the fluid. One may argue that the wave motion itself introduces variations into the shear flow due to the Stokes drift [16, 25]. However for very long waves, the Stokes drift can be compared to the Stokes drift in the KdV equation [5], and it becomes negligible in the long-wave limit. Moreover, as observed by a number of authors [3, 31, 32], a linear shear current can be taken as a first approximation of more realistic shear flows with more complex structures.

If it is assumed that the free surface describes a steady periodic oscillatory pattern, then the flow underneath the free surface can be uniquely determined [10, 23], even in the presence of vorticity. Thus for the purpose of studying periodic traveling waves, one may use a reference frame moving with the wave. This change of reference frame leads to a stationary problem in the fundamental domain of one wavelength. The incompressibility guarantees the existence of the streamfunction ψ and if constant vorticity $\omega = -\omega_0$ is stipulated, the streamfunction satisfies the Poisson equation

$$\Delta\psi = \psi_{xx} + \psi_{zz} = \omega_0, \text{ in } 0 < z < \eta(x) = \psi|_{z=\eta}. \tag{2}$$

As explained in [2, 4], the three parameters Q, S and R are defined as follows. If $\psi = 0$ on the streamline along the flat bottom, then Q denotes the total volume flux per unit width given by

$$Q = \int_0^\eta \psi_z dz\,. \tag{3}$$

Thus Q is the value of the streamfunction ψ at the free surface. The flow force per unit width S is defined by

$$S = \int_0^\eta \left\{ \tfrac{P}{\rho} + \psi_z^2 \right\} dz, \tag{4}$$

and the energy per unit mass is given by

$$R = \frac{1}{2}\psi_z^2 + \frac{1}{2}\psi_x^2 + g\eta \text{ on } z = \eta(x)\,. \tag{5}$$

Finally, the pressure can be expressed as

$$P = \rho\Big(R - gz - \frac{1}{2}(\psi_x^2 + \psi_z^2) + \omega_0\psi - \omega_0 Q\Big), \tag{6}$$

It is well known that the quantities Q and S do not depend on the value of x [4]. Using the fact that S is a constant, the derivation of the model equation (1) can be effected by assuming that the waves are long, scaling z by the undisturbed depth h_0, x by a typical wavelength L, and expanding in the small parameter $\beta = h_0^2/L^2$. This yields (1) as an approximate model equation describing the shape of the free surface. In order to distinguish from the free surface η in the full Euler description, we call the unknown of equation (1) u which is an approximation of η. The derivation of (1) was given in [1, 4], where it was shown that (1) is expected to be valid as an approximate model equation describing waves on the surface of the shear flow if the wavelength is long compared to the undisturbed depth of the fluid. On the other hand, a detailed analysis of the derivation explained in [1, 4] shows that there are no assumptions on the amplitude of the waves. Thus at least formally, the model (1) can be expected to model waves of intermediate amplitude.

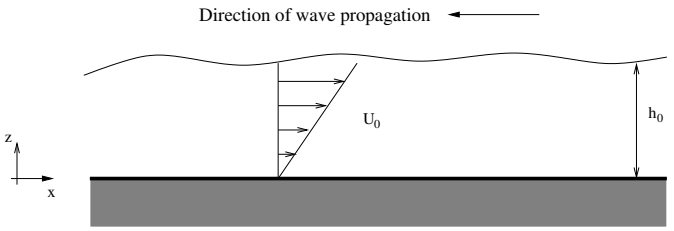

Figure 1: This figure shows the background shear flow $U_0 = \omega_0 z$. In the figure, ω_0 is positive, and the waves which are superposed onto this background current propagate to the left.

2 Explicit solutions

In order to obtain solutions of (1) given in explicit form, we apply the change of variables

$$\frac{dy}{ds} = \frac{du}{dx}\left(Q + \frac{\omega_0}{2}u^2\right),$$

$$y(s) = u(x).$$

This gives us a new equation for $y(s)$ in the form

$$\left(\frac{dy}{ds}\right)^2 = -3\left(\frac{\omega_0^2}{12}y^4 + gy^3 - (2R - \omega_0 Q)y^2 + 2Sy - Q^2\right), \tag{7}$$

and the relation

$$\frac{ds}{dx} = \frac{1}{Q + y^2\omega_0/2}. \tag{8}$$

Integrating (8) we have

$$x(s) = \int^s \left(Q + \frac{\omega_0}{2}y^2\right) d\xi - x_1. \tag{9}$$

where x_1 is a constant of integration, written explicitly for convenience. We want to solve (7) for $y(s)$ and plug our solution into (9). We notice that in the variables y and $\frac{dy}{ds}$ the equation describes an elliptic curve of genus one [14]. Hermite's Theorem [34, p. 394] states that for a uniform solution to exist we need $\int ds$ to be an abelian integral of the first kind. This condition

is indeed satisfied and we proceed with using a birational transformation to put (7) in the standard Weierstraß form

$$\left(\frac{dy_0}{dx_0}\right)^2 = 4y_0^3 - g_2 y_0 - g_3, \tag{10}$$

where the transformation is given as

$$x_0 = -\frac{24(-2\sqrt{12}Q^2y^2\omega_0 - \sqrt{12}Qgy^3 + 4\sqrt{12}QRy^2 + 4\sqrt{12}Q^3 - 6\sqrt{12}QSy + 8Q^2\frac{dy}{ds} - 4\frac{dy}{ds}Sy)}{y^3},$$

$$y_0 = \frac{4(-Qy^2\omega_0 + 2Ry^2 + \frac{dy}{ds}\sqrt{12}Q + 6Q^2 - 6Sy)}{y^2}, \tag{11}$$

and g_2 and g_3 are the lattice invariants

$$g_2 = -768QR\omega_0 + 768R^2 - 1152Sg,$$

$$g_3 = 2048Q^3\omega_0^3 - 6144Q^2R\omega_0^2 - 6912Q^2g^2 + 6144QR^2\omega_0 - 4608QSg\omega_0 + 2034S^2\omega_0^2 - 4096R^3 + 9216RSg.$$

It is well known that the solution to (10) is $y_0(x_0) = \wp(x_0 + c_0; g_2, g_3)$, where $\wp$ is the Weierstraß P function and c_0 is an arbitrary constant [6, 14]. We invert the birational transformation to determine the exact solution to (7) as

$$y(s) = \frac{A + B\wp'((s+c_0)/4; g_2, g_3) + C\wp((s+c_0)/4; g_2, g_3)}{\wp^2((s+c_0)/4; g_2, g_3) + D\wp((s+c_0)/4; g_2, g_3) + E},$$

with

$$A = -288Q^2g - 96Q\omega_0 S + 192RS,$$
$$B = \sqrt{12}Q,$$
$$C = -24S,$$
$$D = 8Q\omega_0 - 16R,$$
$$E = 64Q^2\omega_0^2 - 64QR\omega_0 + 64R^2.$$

This gives us $u(x(s))$ in the form

$$u(x(s)) = \frac{A + B\wp'((s+c_0)/4; g_2, g_3) + C\wp((s+c_0)/4; g_2, g_3)}{\wp^2((s+c_0)/4; g_2, g_3) + D\wp((s+c_0)/4; g_2, g_3) + E}, \tag{12}$$

as a function of the parameter s. If we express $x(s)$ as a function of s, then we have a parametric representation for $u(x)$, the surface elevation. From (9) we have

$$x(s) = Qs - x_1 + \frac{\omega_0}{2}\int^s y^2(\xi)d\xi. \tag{13}$$

Expanding and simplifying $y(s)^2$ gives

$$y^2 = \frac{4B\wp^3 + C^2\wp^2 + (2AC - B^2g_2)\wp + (A^2 - B^2g_3)}{(\wp^2 + D\wp + E)^2} + \frac{2AB - 2BC\wp}{(\wp^2 + D\wp + E)^2}\wp', \tag{14}$$

making use of the shorthand $\wp = \wp((s+c_0)/4; g_2, g_3)$ and $\wp' = \wp'((s+c_0)/4; g_2, g_3)$. Plugging (14) into (13) and integrating gives

$$x(s) = Qs - x_1 + \omega_0 B \left[\frac{8(2A - CD)\arctan\left(\frac{D+2\wp}{\sqrt{-D^2+4E}}\right)}{(-D^2+4E)^{3/2}} + \frac{-4AD + 8CE + (-8A+4CD)\wp}{(D^2-4E)(\wp^2 + D\wp + E)} \right] + \frac{\omega_0}{2} \int^s \frac{4B\wp^3 + C^2\wp^2 + (2AC - B^2 g_2)\wp + (A^2 - B^2 g_3)}{(\wp^2 + D\wp + E)^2} d\xi. \tag{15}$$

To evaluate the integral in (15) we let

$$m_1 = -\frac{D}{2} - \frac{\sqrt{D^2 - 4E}}{2},$$

$$n_1 = -\frac{D}{2} + \frac{\sqrt{D^2 - 4E}}{2},$$

denote the roots of $\wp^2 + D\wp + E = 0$. The integrand can be split into its components

$$\frac{4B\wp^3 + C^2\wp^2 + (2AC - B^2 g_2)\wp + (A^2 - B^2 g_3)}{(\wp - m_1)^2(\wp - n_1)^2} = \frac{J(m_1, n_1)}{(\wp - m_1)^2} + \frac{K(m_1, n_1)}{\wp - m_1} + \frac{J(n_1, m_1)}{(\wp - n_1)^2} + \frac{K(n_1, m_1)}{\wp - n_1},$$

with

$$J(m_1, n_1) = \frac{A^2 - B^2 g_3 + 2ACm_1 - B^2 g_2 m_1 + C^2 m_1^2 + 4B^2 m_1^3}{D^2 - 4E},$$

$$K(m_1, n_1) = \frac{-2A^2 + 2B^2 g_3 - 2ACm_1 + B^2 g_2 m_1 + 4B^2 m_1^3 - 2ACn_1 + B^2 g_2 n_1 - 2C^2 m_1 n_1 - 12B^2 m_1^2 n_1}{(4E - D^2)^{3/2}}.$$

Letting

$$\alpha = \wp^{-1}(m_1),$$

$$\beta = \wp^{-1}(n_1),$$

and

$$x_1 = -c_0 Q + x_2,$$

where x_2 is another arbitrary constant, we express $x(s)$ as

$$x(s) = Q(s + c_0) - x_2 + \omega_0 B \left[\frac{8(2A - CD)\arctan\left(\frac{D+2\wp}{\sqrt{-D^2+4E}}\right)}{(-D^2+4E)^{3/2}} + \frac{-4AD + 8CE + (-8A+4CD)\wp}{(D^2-4E)(\wp^2 + D\wp + E)} \right] + 2\omega_0 \big[J(m_1, n_1) I_2((s+c_0)/4, \alpha) + K(m_1, n_1) I_1((s+c_0)/4, \alpha) + J(n_1, m_1) I_2((s+c_0)/4, \beta) + K(n_1, m_1) I_1((s+c_0)/4, \beta) \big], \tag{16}$$

where I_1 and I_2 come from [6] and [21] and are expressed as

$$I_1(u, \gamma) = \frac{1}{\wp'(\gamma)} \left[\log\left(\frac{\sigma(u-\gamma)}{\sigma(u+\gamma)}\right) + 2u\zeta(\gamma) \right],$$

$$I_2(u, \gamma) = \frac{\wp''(\gamma)}{\wp'^3(\gamma)} \log\left(\frac{\sigma(u+\gamma)}{\sigma(u-\gamma)}\right) - \frac{1}{\wp'^2(\gamma)} \left(\zeta(u+\gamma) + \zeta(u-\gamma)\right) - \left(\frac{2\wp(\gamma)}{\wp'^2(\gamma)} + \frac{2\wp''(\gamma)\zeta(\gamma)}{\wp'^3(\gamma)}\right) u.$$

Here ζ is the Weierstraß zeta function and σ is the Weierstraß sigma function. Thus we have $x(s)$ given in (16) and $u(x(s))$ given in (12) both as functions of s. This gives a parametric representation of our solution as a function of s

$$\begin{cases} y = u(x(s)), & \text{given in (12)}, \\ x = x(s), & \text{given in (16)}. \end{cases} \tag{17}$$

The approximation to the pressure given in [1] is

$$P = \rho\Bigg\{R - gz - \frac{1}{2}\left(\frac{Q}{u^2} + \frac{\omega_0}{2}\right)^2 (z^2u'^2 + u^2) + \frac{1}{2}\left(\frac{\omega_0}{6}u^3 - \frac{\omega_0}{2}z^2u - \frac{2}{3}\omega_0 z^3 - \frac{Q}{3}u + z^2\frac{Q}{u}\right) \times \left(2Q\frac{u'^2}{u^3} - u''\left(\frac{Q}{u^2} + \frac{\omega_0}{2}\right)\right)\Bigg\}. \tag{18}$$

This leads to a parametric representation of the pressure as a function of s

$$\begin{cases} y = P(u(x(s)), z), & \text{given in (18)}, \\ x = x(s), & \text{given in (16)}, \end{cases} \tag{19}$$

where z is the distance from the channel bed.

Finally, note that an expression for the streamfunction can be derived using the techniques of [1]. Since this was not done in [1], the derivation is outlined in the appendix for the sake of completeness. The expression for the streamfunction is

$$\psi = \frac{1}{2}z^2\omega_0 + z\left(\frac{Q}{u} - \frac{u\omega_0}{2} + \frac{Qu'^2}{3u} - \frac{Qu''}{6} - \frac{\omega_0 u^2 u''}{12}\right) - \frac{z^3}{6}\left(\frac{2Qu'^2}{u^3} - \frac{Qu''}{u^2} - \frac{\omega_0 u''}{2}\right), \tag{20}$$

which gives a parametric representation of the streamfunction as a function of s as

$$\begin{cases} y = \psi(u(x(s)), z), & \text{given in (20)}, \\ x = x(s), & \text{given in (16)}. \end{cases} \tag{21}$$

3 Matching the explicit solutions to previous works

First, we verify the explicit solutions found here and the numerical approximations given in [1] by comparing them to each other. Following the analysis of [1], we first note that (1) can be written in the form

$$u'^2 = \frac{\mathcal{G}(u)}{\mathcal{F}(u)}. \tag{22}$$

Letting Z_1, Z_2, m and M represent the roots of the numerator $\mathcal{G}$ on the right-hand side of (22) we write

$$\begin{aligned} \mathcal{G}(u) &= -3\left(\frac{\omega_0^2}{12}u^4 + gu^3 - (2R - \omega_0 Q)u^2 + 2Su - Q^2\right) \\ &= \frac{\omega_0^2}{4}(M - u)(u - m)(u - Z_1)(u - Z_2). \end{aligned} \tag{23}$$

By comparing the coefficients of (23) and assuming that Q, m, and M are given, the two additional roots Z_1 and Z_2 are found as (note that a small typo in [1] has been corrected here)

$$Z_1 = \tfrac{1}{2}\left\{-\left(\tfrac{12}{\omega_0^2}g + (M+m)\right) - \sqrt{\left(\tfrac{12}{\omega_0^2}g + (M+m)\right)^2 + \tfrac{48Q^2}{\omega_0^2 mM}}\right\},$$

$$Z_2 = \tfrac{1}{2}\left\{-\left(\tfrac{12}{\omega_0^2}g + (M+m)\right) + \sqrt{\left(\tfrac{12}{\omega_0^2}g + (M+m)\right)^2 + \tfrac{48Q^2}{\omega_0^2 mM}}\right\}.$$

The total head R and the flow force S are obtained as

$$R = \frac{\omega_0 Q}{2} - \frac{\omega_0^2}{24}\left(Z_1 Z_2 + mM + (M+m)(Z_1+Z_2)\right),$$

$$S = -\frac{\omega_0^2}{24}\left((M+m)Z_1 Z_2 + mM(Z_1+Z_2)\right).$$

Following the work in [1] there are two cases depending on the sign of ω_0. If $\omega_0 > 0$, then u'^2 has no singularities and there is a smooth periodic solution if $Z_2 < m < M$. If $\omega_0 < 0$, then u'^2 has two singularities and the parameter space is more restricted. To find the conditions for smooth solutions to exist, we let $\mathcal{F}(u)$ be expressed as

$$\mathcal{F}(u) = \left(Q + \frac{\omega_0}{2}u^2\right)^2 = \frac{\omega_0^2}{4}(u - A_+)^2(u - A_-)^2, \tag{25}$$

which reveals that the derivative is singular when u takes the values $A_+ = \sqrt{\frac{2Q}{-\omega_0}}$ and $A_- = -\sqrt{\frac{2Q}{-\omega_0}}$. In the case $\omega_0 < 0$, smooth solutions exist when $M < A_+$. To better understand this condition, we introduce the non-dimensional Froude number

$$F = \frac{\omega_0 M^2}{2Q}.$$

Substituting F for ω_0 we find four cases:

$$\begin{cases} 0 < F: & \text{smooth solutions exist is } Z_2 < m < M, \\ -1 < F < 0: & \text{smooth solutions exist,} \\ F = -1: & \text{limiting case of smooth solutions ceasing to exist,} \\ F < -1.1: & \text{smooth solutions do not exist but overhanging waves are possible.} \end{cases} \tag{26}$$

Only solutions of the first two cases above are seen in [1]. Below we show one representative example of each of the cases. As in [1], we use the parameters

$$g = 9.81;\ \rho = 1;\ m = 1.1;\ Q = 1.2\sqrt{g};\ h_0 = \sqrt[3]{g^{-1}Q^2};\ \omega_0 = \frac{2QF}{M^2}. \tag{27}$$

For the following figures, we use the following parameters:

$$\begin{cases} 0 < F: & M = 1.3 \text{ and } F = 1.15, \\ -1 < F < 0: & M = 1.7 \text{ and } F = -0.3, \\ F = -1: & M = 1.7 \text{ and } F = -1, \\ F < -1.1: & M = 1.7 \text{ and } F = -1.1. \end{cases}$$

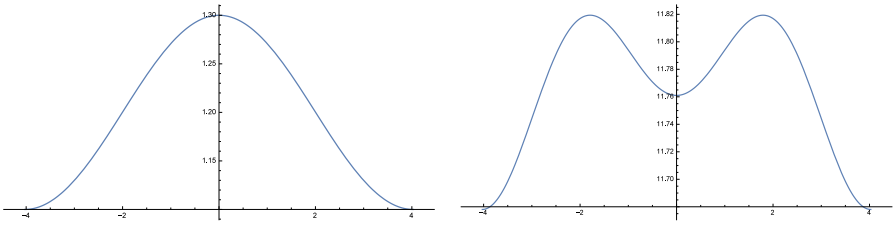

(a) (b)

Figure 2: (*a*) $u(x)$ as a function of x. (*b*) $P(u(x), 0)$ as a function of x.
$0 < F$, $M = 1.3$, $F = 1.15$, and $-1/2 \leq s \leq 1/2$. Smooth solutions exist.

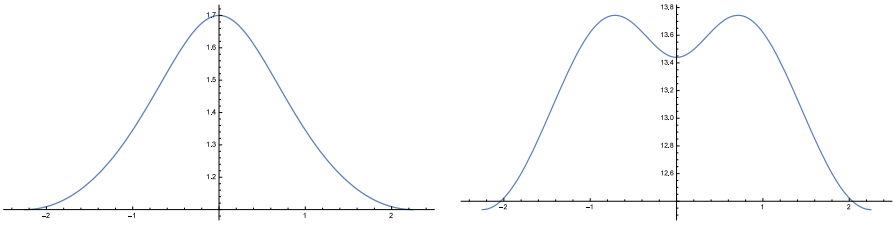

(a) (b)

Figure 3: (*a*) $u(x)$ as a function of x. (*b*) $P(u(x), 0)$ as a function of x.
$-1 < F < 0$, $M = 1.7$, $F = -0.3$, and $-1/2 \leq s \leq 1/2$. Smooth solutions exist.

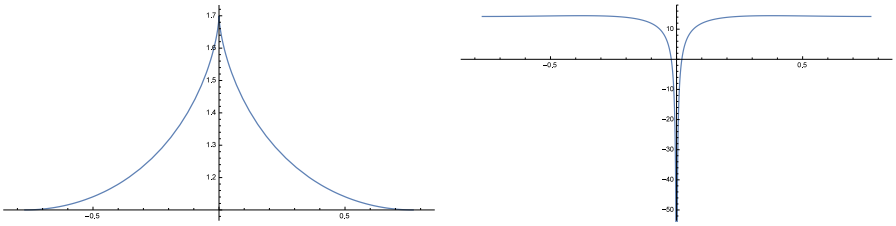

(a) (b)

Figure 4: (*a*) $u(x)$ as a function of x. (*b*) $P(u(x), 0)$ as a function of x.
$F = -1$, $M = 1.7$, $F = -1$, and $-1/2 \leq s \leq 1/2$. Cusp solution.

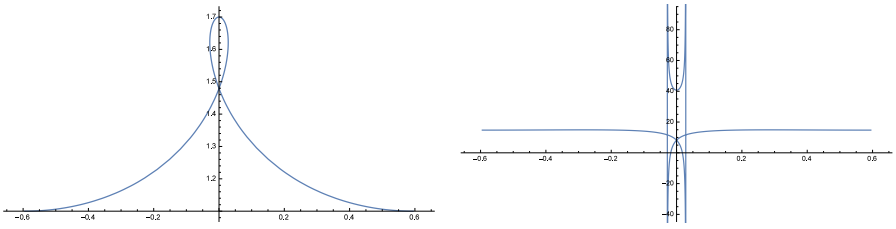

(a) (b)

Figure 5: (*a*) $u(x)$ as a function of x. (*b*) $P(u(x), 0)$ as a function of x.
$F < -1$, $M = 1.7$, $F = -1.1$, and $-1/2 \leq s \leq 1/2$. Overhanging solutions.

Additionally, in order to obtain periodic solutions with $m < u(x) < M$ and with zero imaginary part, we need to set

$$c_0 = 4\omega_2(g_2, g_3), \tag{28}$$

where ω_2 is a Weierstraß half period corresponding to the lattice invariants g_2 and g_3 with non-zero imaginary part.

We produce plots of the explicit solutions for the various cases of (26) with the parameters given in (27), (28) and (32). Two plots for each case will be shown:

1. $u(x)$ as a function of x,
2. $P(u(x), 0)$ as a function of x.

Note that since our solutions are symmetric under spacial translations (varying x_2) we can shift the waves so they coincide with those in [1]. Figures 2 and 3 show two curves found in [1], and no visual difference can be detected between the explicit solutions and the numerical approximations of [1]. We notice that $x(s)$ is a monotone function of s as $F > -1$ decreases up until the critical value of $F = -1$. Beyond the critical point where $F = -1$, $x(s)$ is no longer monotone and as a result the solutions are no longer smooth. Figure 4 shows the limiting case of a cusped solution. Note that the evaluation of the pressure at the bottom under the wavecrest appears to yield extremely low and apparently non-physical values. Figure 5 shows a looped (or self-intersecting) solution which is allowed in equations (10) and (11), but not possible in (1). Since it was assumed in the derivation that the free surface is a single-valued function of x, the solution shown in Figure 5 is beyond the physical validity of the equation.

Next we investigate whether the solutions of (1) are close to the solutions of the full Euler equations with a background shear flow found in [31]. Figure 6 and 7 show a sequence of large waveheight solutions with waveheight $H = 1.2$, and for the set of parameters $g = 9.81, \rho = 1.0, h_0 = 1.0$. Note also that by rearranging the variables, we can make the self-intersecting solution look like an overhanging solution. Even though the curves shown in Figure 7 look similar to the free surface profiles shown in Figure 6 of [31], strictly speaking, the curves in Figure 7 do not represent solutions of (1).

We can also set our solutions to be 2π periodic. For this we need to examine the periods of $x(s)$ and $u(s)$. Let ω_1 be the Weierstraß half period corresponding to the lattice invariants g_2 and g_3 with non-zero real part. We note that

$$u(s + T_u) = u(s),$$

where

$$T_u = 8\omega_1,$$

denotes the period of $u(x)$, since both $\wp((s + c_0)/4; g_2, g_3)$ and $\wp'((s + c_0)/4; g_2, g_3)$ are periodic of period $8\omega_1$. Next we notice that

$$x(s + T_u) = x(s) + T_x,$$

where

$$T_x = QT_u + 2\omega_0 \left[J(m_1, n_1)J_2(\alpha) + K(m_1, n_1)J_1(\alpha) + J(n_1, m_1)J_2(\beta) + K(n_1, m_1)J_1(\beta) \right],$$

with

$$J_1(\gamma) = \frac{1}{\wp'(\gamma)} \left(-4\zeta(\omega_1)\gamma + 4\omega_1\zeta(\gamma) \right),$$

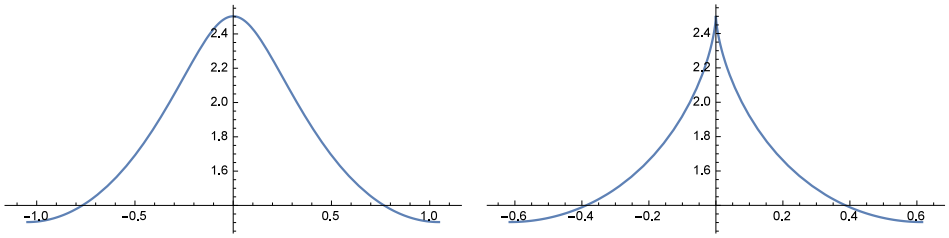

(a) (b)

Figure 6: $u(x)$ as a function of x: (a) smooth solution $F = -0.5$, (b) peaked solution $F = -1.0$.

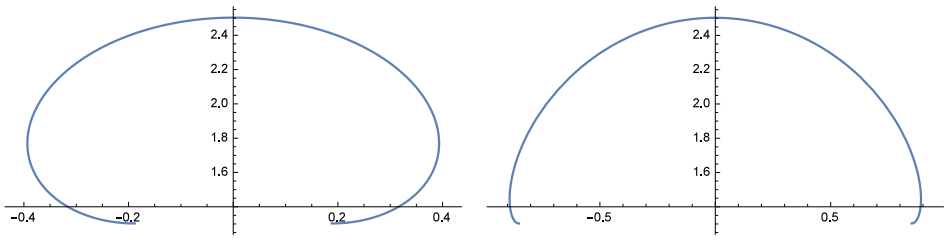

(a) (b)

Figure 7: $u(x)$ as a function of x: (a) overhanging solution $F = -2.0$, (b) overhanging solution $F = -3.0$.

and

$$J_2(\gamma) = \frac{\wp''(\gamma)}{\wp'^3(\gamma)} 4\zeta(\omega_1)\gamma - \frac{4\zeta(\omega_1)}{\wp'^2(\gamma)} - 2\omega_1 \left(\frac{2\wp(\gamma)}{\wp'^2(\gamma)} + \frac{2\wp''(\gamma)\zeta(\gamma)}{\wp'^3(\gamma)} \right).$$

This was determined by noting that

$$I_1(u + 2\omega_1, \gamma) = I_1(u, \gamma) + J_1(\gamma),$$

$$I_2(u + 2\omega_1, \gamma) = I_2(u, \gamma) + J_2(\gamma),$$

which we see from [28]:

$$\zeta(u + 2\omega_1) = \zeta(z) + 2\zeta(\omega_1),$$

$$\sigma(u + 2\omega_1) = -e^{2\zeta(\omega_1)(u+\omega_1)}\sigma(z).$$

Here T_x gives an analytical expression for the wavelength of the solution. If we wanted to force our solutions to be 2π periodic, we could simply rescale x by $2\pi/T_x$ and u by $2\pi/T_x$ as this is the scaling symmetry of (1).

In order to better compare our results with those in [1], we would like to have the peak of the wave at $x = 0$. To achieve this we determine the value of s for which $u(s)$ is at a peak and call this value T_s. Taking (11) we have

$$\wp((T_s + c_0)/4, g_2, g_3) = \frac{4(-QM^2\omega_0 + 2RM^2 + 6Q^2 - 6SM)}{M^2},$$

where we plugged in $y = M$ and $dy/ds = 0$ to be at the peak of the wave. This gives

$$T_s = 4\wp^{-1}\left(\frac{4(-QM^2\omega_0 + 2RM^2 + 6Q^2 - 6SM)}{M^2}, g_2, g_3 \right) - c_0.$$

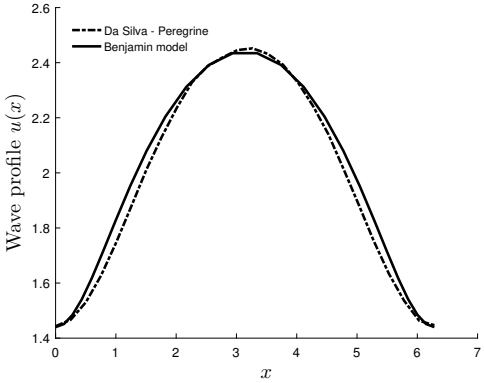

Figure 8: Comparing approximate solutions of the full Euler equations (dashed curve) to exact solutions of (1) (solid curve). The waves have waveheight $H = 1$ and wavelength 2π. The problem is normalized with $g = 1$ and $h_0 = 1$, and the background vorticity is $\omega_0 = -3$.

Thus for solutions with the peak at $x = 0$, we rewrite (17), (19), and (21) as

$$\begin{cases} y = u(T_u(s - T_s)), & \text{given in (12)}, \\ x = x(T_u(s - T_s)), & \text{given in (16)}, \end{cases} \tag{29}$$

$$\begin{cases} y = P(u(T_u(s - T_s)), z), & \text{given in (18)}, \\ x = x(T_u(s - T_s)), & \text{given in (16)}. \end{cases} \tag{30}$$

$$\begin{cases} y = \psi(u(T_u(s - T_s)), z), & \text{given in (20)}, \\ x = x(T_u(s - T_s)), & \text{given in (16)}. \end{cases} \tag{31}$$

Additionally, we set

$$\begin{aligned} x_2 = T_u\Bigg(& Q(\tilde{s} + c_0) + \omega_0 B \Bigg[\frac{8(2A - CD)\arctan\left(\frac{D + 2\wp((\tilde{s}+c_0)/4)}{\sqrt{-D^2+4E}}\right)}{(-D^2 + 4E)^{3/2}} \\ & + \frac{-4AD + 8CE + (-8A + 4CD)\wp((\tilde{s} + c_0)/4)}{(D^2 - 4E)(\wp((\tilde{s} + c_0)/4)^2 + D\wp((\tilde{s} + c_0)/4) + E)} \Bigg] \\ & + 2\omega_0 \big[J(m_1, n_1) I_2((\tilde{s} + c_0)/4, \alpha) + K(m_1, n_1) I_1((\tilde{s} + c_0)/4, \alpha) \\ & + J(n_1, m_1) I_2((\tilde{s} + c_0)/4, \beta) + K(n_1, m_1) I_1((\tilde{s} + c_0)/4, \beta) \big] \Bigg), \end{aligned} \tag{32}$$

where $\tilde{s} = T_u(0 - T_s)$. This x_2 is chosen so that when $s = 0$, $x = 0$. Additionally, note that we scale s by T_u. The scaling of s is so that as s ranges from $-1/2$ to $1/2$, we plot exactly one period of wavelength T_x.

We compare some wave profiles presented in Fig. 6 of by Teles da Silva and Peregrine [31] with solutions of same parameters computed by the current explicit method. Note that in [31], the parameters g and h_0 were normalized, so that we need to choose $g = 1$ and $h_0 = 1$.

We first present a comparison of a traveling wave of waveheight $H = 1$ and vorticity $\omega_0 = -3$. In order to get a good match with the plot from Fig. 6 of [31], we selected $m = 1.44, M =$

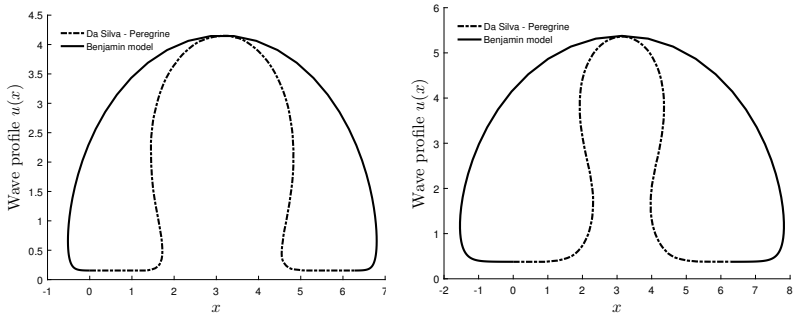

(a) (b)

Figure 9: Comparing approximate solutions of the full Euler equations (dashed curve) to exact solutions of (1) (solid curve). The problem is normalized with $g = 1$, $h_0 = 1$ and wavelength 2π. The background vorticity is $\omega_0 = -3$. (a) waveheight $H = 4$. (b) waveheight $H = 5$.

$2.44, Q = 0.09$ Figure 8 shows an explicit solution of (1) compared to a solution of the full Euler equations shown in Fig. 6 in [31]. Even though the waveheight-depth ratio of 1/2 is not very small, the profiles match fairly closely.

Comparing higher-amplitude waves is more difficult since the solutions shown in [31] with wave-height larger than 1 are overhanging. Setting all parameters correctly yields the comparison shown in Figure 9. As can be seen, the wavelength matches, and the solutions of (7),(8) are also overhanging, but look very different nevertheless. One may conclude from this last comparison, that if solutions of (7),(8) are not single-valued, and therefore are beyond the validity of (1), they will not in general represent the physical reality of the surface-water wave problem.

4 Pressure contours and streamlines

In this section, we explore the flow underneath the surface as predicted by (1), with the help of the expression (18) for the pressure and (20) for the streamfunction.

First, pressure contours and streamlines are reviewed for positive Froude numbers F. This case corresponds to the case labelled 'upstream' in [31]. As mentioned in that work, it is in this case that a critical layer is possible. Examining figures 10-15, it appears that as the strength of the vorticity increases, first, the pressure becomes non-monotone (Figure 11). In other words, the pressure strongly departs from hydrostatic pressure, the bottom pressure is maximal under the sides of the wave (not the crest), and this goes hand in hand with the development of closed streamlines (Figure 12). For large enough Froude numbers, a critical layer (i.e., a closed circulation) develops in the interior of the fluid domain (Figure 13). In the extreme case of $F = 3$, pressure inversion occurs as regions of high pressure are above regions of low pressure in the fluid column (Figure 15).

For negative Froude numbers, the flow corresponds to the downstream case [31]. In this case non-monotone pressures also develop, but no critical layer occurs in the fluid domain. Figures 19 and 20 show strongly non-monotone pressures. Apparently, as the shape of the free surface approaches a cusped profile, non-physical features appear in the description of the flow.

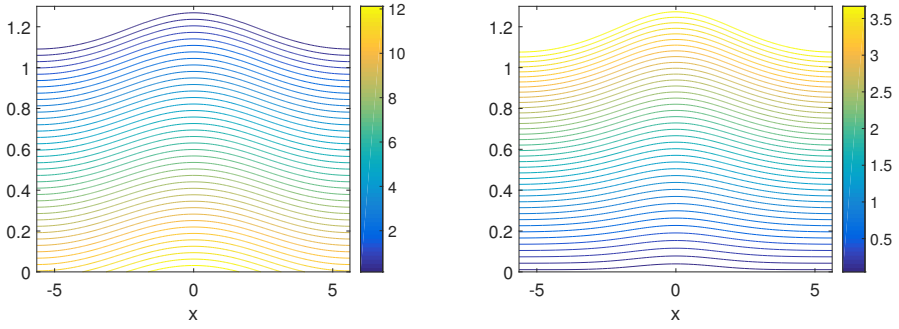

Figure 10: Traveling wave with $m = 1.1$, $M = 1.3$, and $F = 0.2$. Left: pressure contours. Right: streamlines.

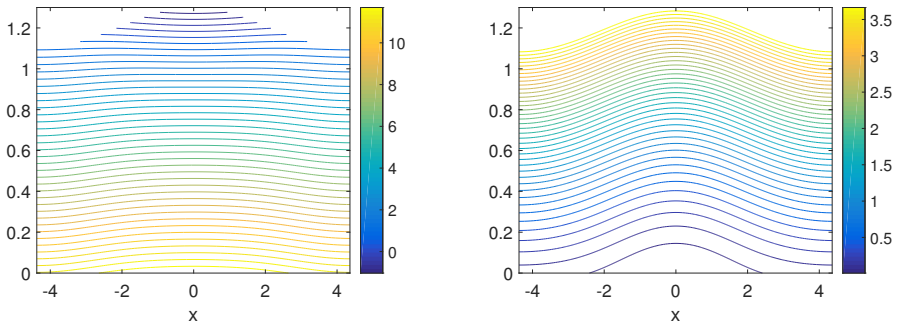

Figure 11: Traveling wave with $m = 1.1$, $M = 1.3$, and $F = 0.9$. Left: pressure contours. Right: streamlines.

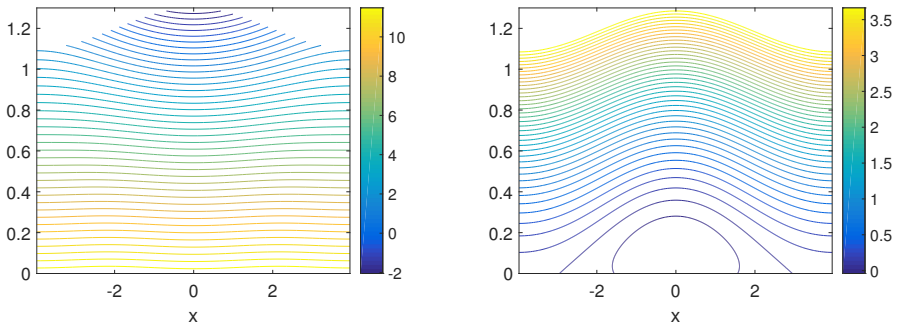

Figure 12: Traveling wave with $m = 1.1$, $M = 1.3$, and $F = 1.2$. Left: pressure contours. Right: streamlines.

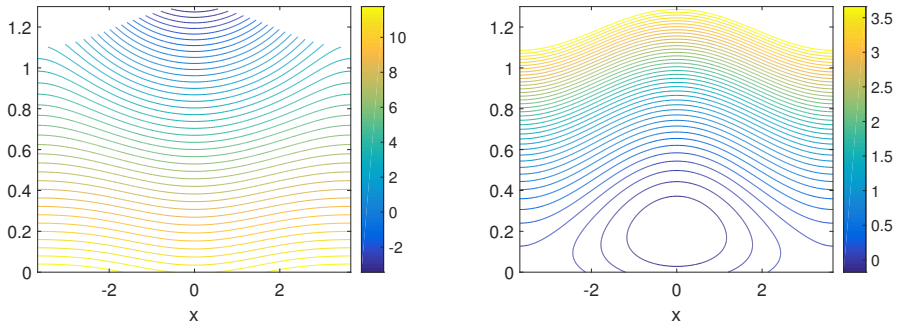

Figure 13: Traveling wave with $m = 1.1$, $M = 1.3$, and $F = 1.5$. Left: pressure contours. Right: streamlines. Pressure highly non-monotone, critical layer appears.

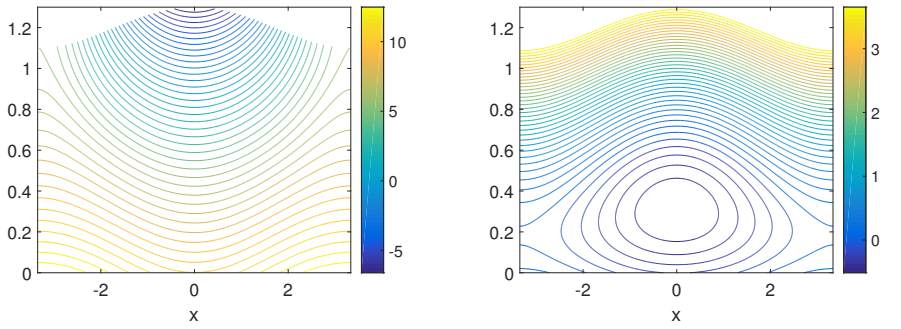

Figure 14: Traveling wave with $m = 1.1$, $M = 1.3$, and $F = 2.0$. Left: pressure contours. Right: streamlines.

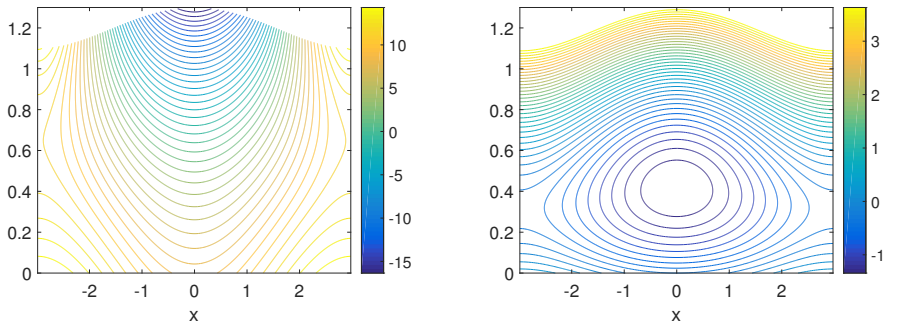

Figure 15: Traveling wave with $m = 1.1$, $M = 1.3$, and $F = 3.0$. Left: pressure contours. Right: streamlines. Pressure inversion: high pressure above low pressure.

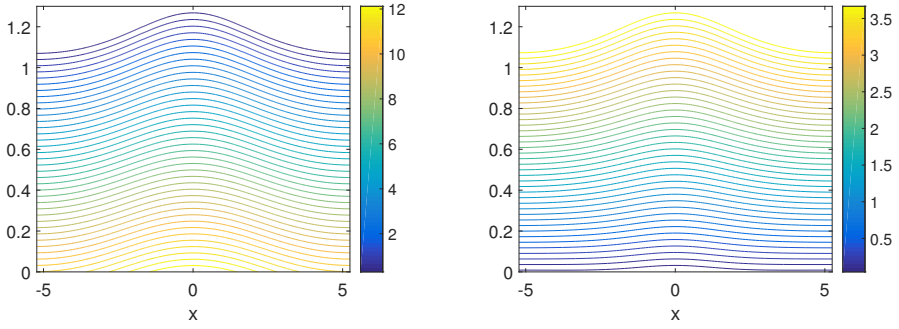

Figure 16: Traveling wave with $m = 1.1$, $M = 1.3$, and $F = -0.001$. Left: pressure contours. Right: streamlines.

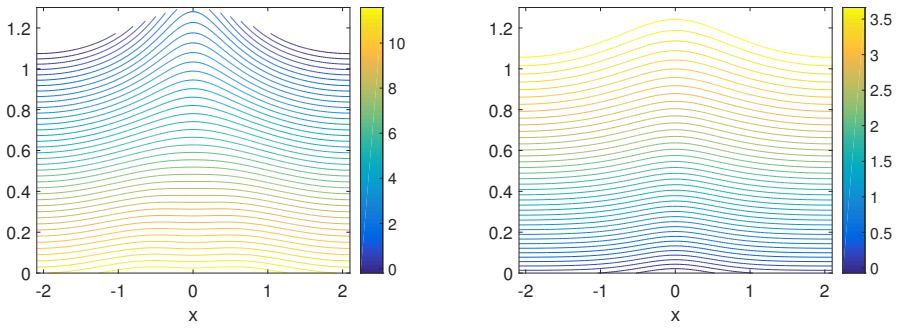

Figure 17: Traveling wave with $m = 1.1$, $M = 1.3$, and $F = -0.5$. Left: pressure contours. Right: streamlines.

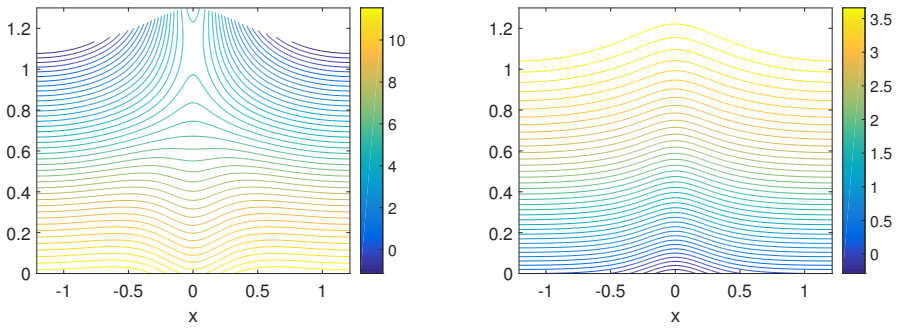

Figure 18: Traveling wave with $m = 1.1$, $M = 1.3$, and $F = -0.7$. Left: pressure contours. Right: streamlines.

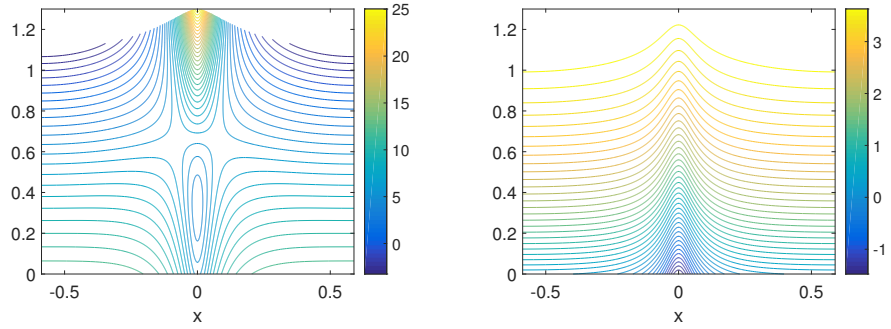

Figure 19: Traveling wave with $m = 1.1$, $M = 1.3$, and $F = -0.9$. Left: pressure contours. Right: streamlines.

5 Conclusion

The nonlinear differential equation (1) is known to be a model for steady surface water waves on a background shear flow. The equation has been found to admit solutions given explicitly in terms of a parametric representation featuring the Weierstraß P, zeta and sigma functions. This representation is a convenient tool for obtaining a variety of wave profiles without having to resort to numerical approximation. In connection with the reconstruction of the pressure underneath the surface explained in [1], and the reconstruction of the streamfunction detailed in the appendix, a complete description of the flow can be obtained.

The exact solutions of (1) have been compared to wave profiles obtained from full Euler computations in [31], and fair agreement was found for regular waves. On the other hand, overhanging waves were found not to agree with the full Euler solutions. This is not surprising since the parametric representation enables the description of multi-valued profiles which transcends the collection of solutions of (1).

With a view towards the flow in the fluid column below the wave, a number of wave shapes with increasing strength of vorticity were exhibited. It was found in the case of steady waves propagating upstream that the flow underneath the waves may feature critical layers and non-monotone pressure profiles. In the case of waves propagating downstream, the development of cusped surface profiles goes hand in hand with unrealistic pressure profiles apparently conflicting with the long-wave approximation which is the basis for the model (1). Building on the results of this paper, future work may focus on detailed comparisons of the fluid flow as described by the methods of the current work to numerical approximations of the flow governed by the Euler equations with background vorticity. Such a study will cast more light on the limitations of the current model, especially as regarding the ability to describe properties of the flow in the bulk of the fluid.

Acknowledgments

This research was supported in part by the Research Council of Norway under grant 213474/F20 and by the National Science Foundation under grant NSF-DMS-1008001. Any opinions, findings, and conclusions

or recommendations expressed in this material are those of the authors and do not necessarily reflect the views of the funding sources.

A Reconstruction of the streamfunction

We want to reconstruct the streamfunction $\psi(x,z)$ using the solutions u of the differential equation (1). This is done by using the ansatz

$$\psi = \frac{1}{2}z^2\omega_0 + zf - \frac{1}{3!}z^3 f'', \tag{33}$$

for the streamfunction and the identity

$$Q = \frac{1}{2}u^2\omega_0 + \zeta f - u^3\frac{1}{6}f'',$$

both of which are valid to second order in the long-wave parameter $\beta = h_0^2/\lambda^2$, where h_0 is the undisturbed depth of the fluid, and λ is the wavelength. To obtain an expression for f in terms of ζ, one has to invert the operator $1 - \frac{1}{6}\zeta^2\partial_{xx}$, leading to

$$\left[1 - \frac{1}{6}\zeta^2\partial_{xx}\right]^{-1}\left(\frac{Q}{\zeta} - \frac{1}{2}\zeta\omega_0\right) = f.$$

In order to bring out the difference in scales between the undisturbed depth h_0 and the wavelength L, we use the scaling

$$\tilde{x} = \frac{x}{L}, \quad \tilde{z} = \frac{z}{h_0}, \quad \tilde{\zeta} = \frac{\zeta}{h_0}, \quad \tilde{\psi} = \frac{1}{c_0 h_0}\psi, \quad \tilde{\omega}_0 = \frac{h_0}{c_0}\omega_0,$$

In addition, Q is scaled as

$$\tilde{Q} = \frac{Q}{h_0 c_0}.$$

In non-dimensional variables, the expression for ψ is

$$\tilde{\psi} = \frac{1}{2}\tilde{z}^2\tilde{\omega}_0 + \tilde{z}\tilde{f} - \frac{\beta}{3!}\tilde{z}^3\tilde{f}'' + \mathcal{O}(\beta^2).$$

The function $\tilde{f}$ is written as

$$\begin{aligned}\tilde{f} &= \left[1 + \frac{\beta}{6}\tilde{u}^2\partial_{\tilde{x}}^2 + \mathcal{O}(\beta^2)\right]\left(\frac{\tilde{Q}}{\tilde{u}} - \frac{1}{2}\tilde{u}\omega_0\right) + \mathcal{O}(\beta^2).\\ &= \frac{\tilde{Q}}{\tilde{u}} - \frac{1}{2}\tilde{u}\tilde{\omega}_0 + \frac{\beta}{3}Q\frac{(\tilde{u}')^2}{\tilde{u}} - \frac{\beta}{6}Q\tilde{u}'' - \frac{\beta}{12}\omega_0\tilde{u}^2\tilde{u}'' + \mathcal{O}(\beta^2).\end{aligned}$$

The second derivative is

$$\tilde{f}'' = 2\frac{\tilde{Q}}{\tilde{u}^3}(\tilde{u}')^2 - \frac{\tilde{Q}}{\tilde{u}^2}\tilde{u}'' - \frac{1}{2}\omega_0\tilde{u}'' + \mathcal{O}(\beta).$$

Putting these together, we find the streamfunction in terms of $\tilde{u}$:

$$\begin{aligned}\tilde{\psi} &= \frac{1}{2}\tilde{z}^2\tilde{\omega}_0 + \tilde{z}\left[\frac{\tilde{Q}}{\tilde{u}} - \frac{1}{2}\tilde{u}\tilde{\omega}_0 + \frac{\beta}{3}Q\frac{(\tilde{u}')^2}{\tilde{u}} - \frac{\beta}{6}Q\tilde{u}'' - \frac{\beta}{12}\omega_0\tilde{u}^2\tilde{u}''\right]\\ &\quad -\frac{\beta}{3!}\tilde{z}^3\left[2\frac{Q}{\tilde{u}^3}(\tilde{u}')^2 - \frac{Q}{\tilde{u}^2}\tilde{u}'' - \frac{\omega_0}{2}\tilde{u}''\right] + \mathcal{O}(\beta^2).\end{aligned}$$

References

[1] A. Ali and H. Kalisch, *Reconstruction of the pressure in long-wave models with constant vorticity* Eur. J. Mech. B Fluids **37** (2013), 187–194.

[2] A. Ali and H. Kalisch, *On the formulation of mass, momentum and energy conservation in the KdV equation*, Acta Appl. Math. **133** (2014), 113–131.

[3] T. B. Benjamin, *The solitary wave on a stream with an arbitrary distribution of vorticity*, J. Fluid Mech. **12** (1962), 97–116.

[4] T. B. Benjamin and M. J. Lighthill, *On cnoidal waves and bores*, Proc. Roy. Soc. London Ser. **A 224** (1954), 448–460.

[5] H. Borluk and H. Kalisch, *Particle dynamics in the KdV approximation*, Wave Motion **49** (2012), 691–709.

[6] P.F. Byrd and M.D. Friedman, Handbook of elliptic integrals for engineers and scientists, vol. 67. (Springer Berlin, 1971).

[7] T.L. Clarke, B. Lesht, R.A. Young, D.J.P. Swift and G.L. Freeland, *Sediment resuspension by surface-wave action: An examination of possible mechanisms*, Marine Geology, **49** (1982) 43–59

[8] T. Colin, F. Dias and J.-M. Ghidaglia, *On rotational effects in the modulations of weakly nonlinear water waves over finite depth*, Eur. J. Mech. B Fluids **14** (1995), 775–793.

[9] A. Constantin, M. Ehrnström and E. Wahlén, *Symmetry of steady periodic gravity water waves with vorticity*, Duke Math. J. **140** (2007), 591–603.

[10] A. Constantin and J. Escher, *Symmetry of steady periodic surface water waves with vorticity*, J. Fluid Mech. **498** (2004) 171–181.

[11] A. Constantin and W. Strauss, *Exact steady periodic water waves with vorticity*, Comm. Pure Appl. Math. **57** (2004), 481–527.

[12] A. Constantin and W. Strauss, *Pressure beneath a Stokes wave*, Comm. Pure Appl. Math. **63** (2010), 533–557.

[13] A. Constantin and E. Varvaruca, *Steady periodic water waves with constant vorticity: regularity and local bifurcation*, Arch. Ration. Mech. Anal. **199** (2011), 33–67.

[14] R. Conte and M. Musette, The Painlevé Handbook (Springer Science & Business Media, 2008).

[15] W. Choi, *Strongly nonlinear long gravity waves in uniform shear flows*, Phys. Rev. E **68** (2003), 026305.

[16] L. Debnath Nonlinear Water Waves (Academic Press, 1994).

[17] S.H. Doole, *The pressure head and flowforce parameter space for waves with constant vorticity*, Quart. J. Mech. Appl. Math. **51** (1998), 61–72.

[18] S.H. Doole and J. Norbury, *The bifurcation of steady gravity water waves in (R, S) parameter space* J. Fluid Mech. **302** (1995), 287–305.

[19] M. Ehrnström and G. Villari, *Linear water waves with vorticity: rotational features and particle paths*, J. Differential Equations **244** (2008), 1888–1909,

[20] M. Ehrnström, J. Escher and E. Wahlén, *Steady water waves with multiple critical layers*, SIAM J. Math. Anal. **43** (2011), 1436–1456.

[21] I. Gradshteyn and I. Ryzhik, Table of Integrals, Series and Products, 5th edn (Academic Press, New York, 1994).

[22] V. M. Hur, *Exact solitary water waves with vorticity*, Arch. Ration. Mech. Anal. **188** (2008), 213–244.

[23] H. Kalisch, *A uniqueness result for periodic traveling waves in water of finite depth*, Nonlinear Anal. **58** (2004), 779–785.

[24] J. Ko and W. Strauss, *Large-amplitude steady rotational water waves*, Eur. J. Mech. B Fluids **27** (2008), 96–109.

[25] P.K. Kundu and I.M. Cohen, Fluid Mechanics, 4th edition (Academic Press, 2008)

[26] Y. Li and S.Å. Ellingsen, *Ship waves on uniform shear current at finite depth: wave resistance and critical velocity*, J. Fluid Mech. **791** (2016), 539–567.

[27] C.C. Mei, S.-J. Fan and K.-R. Jin, *Resuspension and transport of fine sediments by waves*, J. Geophys. Res. Oceans **102** (1997), 15807–15821.

[28] F.W.J. Olver, D.W. Lozier, D.F. Boisvert and C.W. Clark, Eds. NIST Handbook of Mathematical Functions, (Cambridge University Press, New York, 2010).

[29] J.S. Ribberink and A.A. Al-Salem, *Sediment transport in oscillatory boundary layers in cases of rippled beds and sheet flow*, J. Geophys. Res. Oceans **99** (1994), 12707–12727.

[30] R. Thomas, C. Kharif and M. Manna, *A nonlinear Schrdinger equation for water waves on finite depth with constant vorticity* Phys. Fluids **24** (2012), 127102.

[31] A.F. Teles da Silva and D.H. Peregrine, *Steep, steady surface waves on water of finite depth with constant vorticity*, J. Fluid Mech. **195** (1988), 281–302.

[32] J. Touboul, J. Charland, V. Rey and K. Belibassakis, *Extended mild-slope equation for surface waves interacting with a vertically sheared current*, Coastal Engineering **116** (2016), 77–88.

[33] J. Touboul and E. Pelinovsky, *Bottom pressure distribution under a solitonic wave reflecting on a vertical wall*, Eur. J. Mech. B Fluids **48** (2014), 13–18.

[34] G. Valiron and J. Glazebrook, The Geometric Theory of Ordinary Differential Equations and Algebraic Functions (Math Sci Press, 1984).

[35] J.-M. Vanden-Broeck, *Periodic waves with constant vorticity in water of infinite depth*, IMA J. Appl. Math. **56** (1996), 207–217.

[36] E. Wahlén, *Steady water waves with a critical layer*, J. Differential Equations **246** (2009), 2468–2483.

[37] E. Wahlén, *Hamiltonian long-wave approximations of water waves with constant vorticity*, Phys. Lett. A **372** (2008), 2597–2602.